FINAL REPORT

High Resolution Delineation of Contaminant Concentrations, Biogeochemical Processes, and Microbial Communities in Saturated Subsurface Environments

SERDP Project ER-2419

FEBRUARY 2020

Dr. Andrew Jackson
Texas Tech

Dr. Paul B. Hatzinger
Aptim Federal Services

Distribution Statement A
This document has been cleared for public release

SERDP
DOD ▪ EPA ▪ DOE

Page Intentionally Left Blank

This report was prepared under contract to the Department of Defense Strategic Environmental Research and Development Program (SERDP). The publication of this report does not indicate endorsement by the Department of Defense, nor should the contents be construed as reflecting the official policy or position of the Department of Defense. Reference herein to any specific commercial product, process, or service by trade name, trademark, manufacturer, or otherwise, does not necessarily constitute or imply its endorsement, recommendation, or favoring by the Department of Defense.

Page Intentionally Left Blank

REPORT DOCUMENTATION PAGE

Form Approved
OMB No. 0704-0188

The public reporting burden for this collection of information is estimated to average 1 hour per response, including the time for reviewing instructions, searching existing data sources, gathering and maintaining the data needed, and completing and reviewing the collection of information. Send comments regarding this burden estimate or any other aspect of this collection of information, including suggestions for reducing the burden, to Department of Defense, Washington Headquarters Services, Directorate for Information Operations and Reports (0704-0188), 1215 Jefferson Davis Highway, Suite 1204, Arlington, VA 22202-4302. Respondents should be aware that notwithstanding any other provision of law, no person shall be subject to any penalty for failing to comply with a collection of information if it does not display a currently valid OMB control number.
PLEASE DO NOT RETURN YOUR FORM TO THE ABOVE ADDRESS.

1. REPORT DATE *(DD-MM-YYYY)*
01/02/2020

2. REPORT TYPE
SERDP Final Report

3. DATES COVERED *(From - To)*
5/19/2014 - 5/19/2019

4. TITLE AND SUBTITLE
High Resolution Delineation of Contaminant Concentrations, Biogeochemical Processes, and Microbial Communities in Saturated Subsurface Environments

5a. CONTRACT NUMBER
14-C-0019

5b. GRANT NUMBER

5c. PROGRAM ELEMENT NUMBER

5d. PROJECT NUMBER
ER-2419

5e. TASK NUMBER

5f. WORK UNIT NUMBER

6. AUTHOR(S)
Dr. W. Andrew Jackson
Texas Tech University

Dr. Paul B. Hatzinger
Aptim Federal Services

7. PERFORMING ORGANIZATION NAME(S) AND ADDRESS(ES)
Texas Tech University
10th and Akron
Lubbock, TX 79409

8. PERFORMING ORGANIZATION REPORT NUMBER
ER-2419

9. SPONSORING/MONITORING AGENCY NAME(S) AND ADDRESS(ES)
Strategic Environmental Research and Development Program (SERDP)
4800 Mark Center Drive, Suite 16F16
Alexandria, VA 22350-3605

10. SPONSOR/MONITOR'S ACRONYM(S)
SERDP

11. SPONSOR/MONITOR'S REPORT NUMBER(S)
ER-2419

12. DISTRIBUTION/AVAILABILITY STATEMENT
DISTRIBUTION STATEMENT A. Approved for public release: distribution unlimited.

13. SUPPLEMENTARY NOTES

14. ABSTRACT
The ability to predict contaminant (e.g. chlorinated volatile organic compounds (CVOCs)) fate and transport in aquifers is often limited by the intrinsic heterogeneity associated with the flow field, contaminant distribution, and coupled biotic and abiotic reactions. Processes occurring in low permeability zones are particularly important, as studies have demonstrated that contaminants residing in such materials can sustain groundwater plumes and impede overall contaminant attenuation. While the importance of identifying these processes in heterogeneous media has been well documented, previously there has been no costeffective tool for providing high resolution profiling of coupled contaminant, biogeochemical, and microbiological characteristics at the cm-scale. The primary objective of this SERDP research was to develop and demonstrate a High-Resolution Passive Profiler (HRPP) as a fine-scale delineation tool for the saturated subsurface. Focus was placed on discerning contaminant, microbiological, and biogeochemical differences between low permeability and high permeability zones within heterogeneous or stratified media.

15. SUBJECT TERMS
High Resolution Delineation, Contaminant Concentrations, Biogeochemical Processes, Microbial Communities, Saturated Subsurface Environments

16. SECURITY CLASSIFICATION OF:			17. LIMITATION OF ABSTRACT	18. NUMBER OF PAGES	19a. NAME OF RESPONSIBLE PERSON
a. REPORT	b. ABSTRACT	c. THIS PAGE			Andrew Jackson
UNCLASS	UNCLASS	UNCLASS	UNCLASS	139	19b. TELEPHONE NUMBER *(Include area code)* 806-742-2801(x230)

Page Intentionally Left Blank

LIST OF FIGURES iii
LIST OF TABLES viii
1 EXECUTIVE SUMMARY 1
1.1 Introduction 1
1.2 Objectives 2
1.3 Technical Approach 3
1.4 Results and Discussion 4
1.5 Implications for Future Research and Benefits 10
2 OBJECTIVES 12
3 BACKGROUND 13
3.1 Contaminant Distribution in High and Low Permeability Zones 13
3.2 Microbiological and Biogeochemical Differences in High and Low Permeability Zones 13
3.3 Site Characterization for Subsurface Remediation 14
3.4 Existing Techniques for Subsurface Site Characterization 17
3.5 Background on Passive Sampling 18
3.6 Mass Transfer Related to Passive Sampling 24
4 MATERIALS AND METHODS 28
4.1 Development and Validation of the Use of HRPP to Determine In Situ Transport Parameters at High Resolution 28
4.2 Development and Validation of HRPP Micro-Biotraps To Evaluate CSIA of Adsorbed CVOCs and Microbial Community Structure and Activity. 35
4.3 Development of an HRPP Capable of Direct Drive Insertion in Shallow Aquifers. 38
4.4 Field Demonstrations 41
5 RESULTS AND DISCUSSION 56
5.1 Development and Validation of the Use of HRPP to Determine In-Situ Transport Parameters at High Resolution 56
5.2 Development and Validation of HRPP Micro-biotraps to Evaluate CSIA of Adsorbed CVOCs and Microbial Community Structure and Activity. 63
5.3 Development and Field Validation of a HRPP Capable of Insertion in Shallow Aquifers. 74
6 CONCLUSIONS AND IMPLICATIONS FOR FUTURE RESEARCH/IMPLEMENTATION 113
7 LITERATURE CITATIONS 115

8 APPENDICES 118

LIST OF FIGURES

Figure 1.1. Conceptual model of standard sampling from wells compared to the proposed deployable HRPP 2

Figure 1.2. General design of the HRPP including five cells sets over four-foot length, coarse stainless-steel mesh, fine nylon mesh, and 0.45 µm membrane attached with cover plate and screws. HRPP was manufactured from 2.5" stainless steel rod and was threaded on each end to allow it to be coupled to other HRPP units or a direct drive device 4

Figure 1.3. Relationship between pore velocity and measured HRPP Br^- k_m value based on lab scale flow boxes studies. Verification of relationship overlaid as "X" symbols using full scale HRPP samplers and mesoscale two-layer flow box system for 10 and 60 cm/day velocity through sand layer and negligible flow in clay layer 5

Figure 1.4. (Left Panels) Depth distributions of CVOCs measured by HRPP, vertical discrete wells (SMLS 1), standard wells (SPW 3-1,2), soil cores, and MIP at one location. Right Panels) The $\delta^{13}C$ of VC and *cis*-DCE based on well water, in well Biotraps, and HRPP micro-biotraps.. 7

Figure 1.5. Estimates of groundwater pore velocity based on HRPP and passive flux meters compared to qualitative results from HPT at one location and overall site average based on pumping tests. 8

Figure 1.6 Example distributions of microbial populations based on HRPP micro-biotraps, in well Biotraps, and well water..... 8

Figure 1.7. Concentration Distribution across groundwater transect. A) Concentrations based on sampled well water; B) Concentrations based on depth averaged HRPP concentrations. 9

Figure 1.8. Concentration with depth based on HRPP samples across groundwater transect..... 10

Figure 3.1. Vertical plane X-Z model domain for 2D passive sampler equilibration (Harper et al 1997) 21

Figure 3.2. Boundary conditions for the case of constant solute supply (left) and solute supply limited by diffusion through sediment (right)..... 22

Figure 3.3. Model domain of 2D diffusion through soil into a horizontal sample cell. 24

Figure 3.4. Laminar (left) and turbulent (right) flow in a pipe 25

Figure 3.5. Momentum diffusivity (left) and molecular or mass diffusivity (right)..... 26

Figure 4.1. Conceptual schematic of stirred-tank bottle study to determine k_m of bromide for membrane resistance only. Bottles filled with bromide and beaker filled with DDI water..... 29

Figure 4.2. Dimensions, 3D view, and side view of laboratory flow box system. 30

Figure 4.3. Velocity HRPP cross-section in sediment and laboratory flow box setup..... 30

Figure 4.4. Lab scale passive sampler design: three sets of four cells with varying cell volume to opening area ratios (V/A)..... 31

Figure 4.5. Example curve fit to determine k_m from four cell volume to opening area ratios (V/A)..... 32

Figure 4.6. Sampler was tested at three orientations to flow: perpendicular to flow (left), parallel to flow (center), and 180º away from flow (right). 32

Figure 4.7. Large flow box system with clay on bottom half and sand on top half. 34

Figure 4.8. Four-foot sampler design with five sets of velocity cells 35

Figure 4.9. Photograph of HRPP unit packed with different media (left photograph) and HRPP and Bipotrap being lowered into monitoring well at Fort Dix, NJ (right photograph). 36

Figure 4.10. Sectional view of flow with two layers of differing hydraulic conductivities. Dark precipitates are visible at the oxic/anoxic interface. 37

Figure 4.11. Small scale HRPPs after removal from layered flow cell. 38

Figure 4.12. HRPP prototype 1. 39

Figure 4.13. HRPP design modifications: 1) inset cover plates; 2) capable of coupling multiple four-foot sections; 3) fewer velocity cells; 4) smaller microbial/CSIA cells. 40

Figure 4.14. General design of the HRPP-B including five cells sets over four-foot length, coarse stainless steel mesh, fine nylon mesh, and 0.45 µm membrane attached with cover plate and screws. 41

Figure 4.15. Installment depths (feet BGS) of well screens and HRPPs at Fort Dix site. Note: Ground surface elevation (GSE) varies between the two HRPP locations. GSE at HRPP-1 is used as reference for this figure. 42

Figure 4.16. Cross-section of Fort Dix well and HRPP depths/locations showing plume concentrations of TCE and *cis*-DCE. 43

Figure 4.17. Aerial view of HRPP and well spacing at Fort Dix site. 43

Figure 4.18. Photographs of: 1) prototype samplers (HRPP-P1) being installed at Fort Dix in September of 2015 (upper left); 2) HRPP-P1 being sampled (upper right); and 3) sampler after insertion (bottom center). 45

Figure 4.19. Alameda site stratigraphy and HRPP insertion depths. 46

Figure 4.20. Alameda DNAPL source zone and location of wells, MIP/HPT, soil cores, and HRPPs. 47

Figure 4.21. Alameda cross-section of well and HRPP grouping by location. Note: Horizontal dimensions are visual approximation, not to exact scale. 48

Figure 4.22. Beaverdam Road Landfill at the BARC site. Contours of the TCE plume are provided. Figure from BMT (2017). The shallow geology of the BDRLF site consists of 20 to 30 ft of alluvial Quartenary river terrace deposits that are underlain by the lower Cretaceous Arundel Clay Formation, which itself is estimated to be more than 30 m thick (BMT, 2017). The layered geology includes silty sands (SM), silts and fine sands, clayey silts (ML), and clays (CL) (Figure A). 51

Figure 4.23. Typical soil boring at the BDRLF site. Figure from BMT (2017). 52

Figure 4.24. Location of the biowall at the BDRLF site. The inset shows transect wells installed to monitor biowall performance. Figure from Schanzle (2018). 53

Figure 4.25. General locations for deployment of HRPPs at the BDRLF site. The circles in red demarcated A, B, C, and D represent likely locations for installing HRPPs. Figure modified from Schanzle (2018). 54

Figure 4.26. Cross section of site illustrating deployment depths. 55

Figure 5.1. Chloride (Cl^-) and Br^- concentration in the HRPP equilibration cells as a function of time for pore velocities of 0, 4, 16, and 100 cm/d. 57

Figure 5.2 Mass transfer coefficients for bromide in the small flow box. (a) k_m values for sampler orientation perpendicular to flow; (b) comparative k_m values for orientation parallel to flow and 180° away from flow. Error bars indicate standard deviations of triplicate measurements. 57

Figure 5.3. Mass transfer coefficients for bromide in the small flow box are independent of time. 58

Figure 5.4. Relation between the mass transfer coefficient of Br^- as an equilibrium reporter and Cl^- as a model species equilibrating with the HRPP. The mass transfer coefficient for TCE at a pore velocity of 64 cm/d is represented by the star symbols. The solid line is a 1:1 line for comparison. 59

Figure 5.5. Measured k_m (bromide) in the big, two-layer flow box system for 10 and 60 cm/day velocity through the sand and negligible flow in the clay compared to lab-scale k_m vs. velocity results. 60

Figure 5.6. Conceptual schematic of 2D quasi-steady state analytical model for a flat sheet undergoing diffusion in the z direction and advection in the x direction. 60

Figure 5.7. Experimental mass transfer coefficients for bromide plotted against 2D quasi-steady state analytical model (Equation5.9)..... 62

Figure 5.8. Sensitivity analysis of 2D quasi-steady state analytical model or (a) porosity, ϕ, of 0.15, 0.37, and 0.75, and (b) membrane impedance, D_m/δ of 0.1, 3, and 10. 63

Figure 5.9 Dissolved Oxygen (DO) in two soil layers of differing hydraulic conductivities. The lower permeability layer had been exposed to TCE, a dechlorinating culture, and emulsified oil. 69

Figure 5.10. TCE, DCE, and VC in a lower permeability layer that had been exposed to TCE, a dechlorinating culture, and emulsified oil. 69

Figure 5.11. TCE, DCE, and VC in a lower permeability layer. 70

Figure 5.12. Gene copies of Dehalobacter spp. (DHBt), Dehalococcoides spp. (DHC), Desulfitobacterium spp. (DSB), and Sulfate Reducing Bacteria (APS) as measured by QuantArray-Chlor. Only intervals with detections are indicated. 71

Figure 5.13. Gene copies of epoxyalkane transferase (EtnE), phenol hydroxylase (PHE), toluene monooxygenase 2 (RDEG), soluble methane monooxygenase (sMMO) as measured by QuantArray-Chlor. Only intervals with detections are indicated. 72

Figure 5.14. Carbon isotope composition (as δ13C) of TCE in the HRPPs ("Peepers") and co-located water ("Aqueous")..... 73

Figure 5.15. Carbon isotope composition (as δ13C) of TCE, cDCE, and VC in the anaerobic sediment layer as collected by HRPP ("Peepers") and co-located water ("Aqueous"). 73

Figure 5.16. Fort Dix geochemical indicators (chloride, sulfate) detected by HRPP-1 and HRPP-2 compared to well water from MAG 4, MAG 66, and MAG 112. 75

Figure 5.17. Fort Dix CVOCs (cis-DCE, vinyl chloride) detected by HRPP-1 and HRPP-2 compared to well water from MAG 4, MAG 66, and MAG 112. 76

Figure 5.18. Fort Dix HRPP-1 and HRPP-2 total eubacteria, sulfate-reducing bacteria, and methanogens compared to well water and bio-traps from MAG 4, MAG 66, and MAG 112. 78

Figure 5.19. Fort Dix HRPP-1 and HRPP-2 reductive dechlorination microbial data compared to well water and bio-traps from MAG 4, MAG 66, and MAG 112. 80

Figure 5.20. Fort Dix HRPP-1 and HRPP-2 aerobic cometabolic microbial data compared to well water and bio-traps from MAG 4, MAG 66, and MAG 112. 82

Figure 5.21. Fort Dix HRPP-1 and HRPP-2 CSIA for cis-DCE and vinyl chloride compared to well water and Biotraps from MAG 4, MAG 66, and MAG 112. 83

Figure 5.22. HRPP-1 and HRPP-2 estimated velocities based on mass transfer of bromide. Note: HRPP-2 data points lay on top of HRPP-1 data points at depths 22 and 23 feet BGS. 84

Figure 5.23. Alameda geochemical indicators (chloride, sulfate, phosphate) detected by HRPP-3,4,5 compared to nearby monitoring wells. 86

Figure 5.24. Alameda CVOC concentrations (cis-DCE, vinyl chloride) detected by HRPP-3,4,5 compared to monitoring well concentrations, MIP-PID, MIP-ECD, and soil cores. 87

Figure 5.25. Alameda HRPP-3 and HRPP-5 total eubacteria, sulfate-reducing bacteria, and methanogens compared to monitoring well water and Biotraps in wells. 89

Figure 5.26. Alameda HRPP-3 and HRPP-5 reductive dechlorination microbial data compared to monitoring well water and Biotraps in wells. 90

Figure 5.27. Alameda HRPP-4 and HRPP-5 reductive dechlorination microbial data compared to monitoring well water and Biotraps in wells. 91

Figure 5.28. Alameda HRPP-3,4,5 CSIA for cis-DCE and vinyl chloride compared to monitoring well water and Biotraps in wells. 92

Figure 5.29. Alameda HRPP-3,4,5 velocity estimates based on mass transfer of a conservative tracer compared to passive flux meters in wells, hydraulic head site average, MIP-EC, and HPT. 93

Figure 5.30. Concentration distributions of VOCs and geochemical indicators, CSIA of CVOCs, and pore velocity at location MW6, BARC site. 97

Figure 5.31. Microbial Distribution at the upgradient MW6 site. Small solid symbols represent HRPP micro-biotrap, large open symbols represent in well Bio-traps, and solid lines represent well water. 98

Figure 5.32 Concentration distributions of VOCs and geochemical indicators, CSIA of CVOCs, and pore velocity at location BW6, BARC site. 101

Figure 5.33. Microbial Distribution at the upgradient MW6 site. Small solid symbols represent HRPP microbio-trap, large open symbols represent in well Biotraps, and solid lines represent well water. 102

Figure 5.34. Concentration distributions of VOCs and geochemical indicators, CSIA of CVOCs, and pore velocity at location BW6, BARC site. 104

Figure 5.35. Microbial Distribution at the upgradient MW6 site. Small solid symbols represent HRPP microbio-trap, large open symbols represent in well Bio-traps, and solid lines represent well water. 105

Figure 5.36. Concentration Distribution across groundwater transect. A) Concentrations based on sampled well water; B) Concentrations based on depth averaged HRPP concentrations; C) Concentrations based on maximum HRPP concentrations. 109

Figure 5.37. Concentration of CVOCs with depth based on HRPP samples across groundwater transect. 110

Figure 5.38. Concentration of geochemical indicators with depth based on HRPP samples across groundwater transect. 111

Figure 5.39. Pore Velocity with depth based on HRPP samples across groundwater transect. . 112

LIST OF TABLES

Table 4.1 Area/Volume ratios utilized in laboratory flow box experiments. 31

Table 4.2 Area/Volume ratios of velocity cells for second iteration HRPP design (Alameda, CA field trial). 40

Table 4.3 Analytical Parameters and Laboratories. 45

Table 4.4 Timeline of sampling activities in Alameda, California. 49

Table 5.1 Quantarray data from the MAG-70 Well at Fort Dix. 64

Table 5.2 Quantarray data from the MAG-112P Well at Fort Dix. 66

Table 5.3 Quantarray data from the WP022MW357 Well at Kelly AFB. 67

Table 5.4 δ^{13}C-TCE for Bio-sep beads and Ag coated GAC deployed at Ft. Dix and Kelley AFB in existing wells compared to standard Bio-traps deployed in the same wells. 68

LIST OF **ACRONYMS**

2D	2-dimensional
3D	3-dimensional
µg	Micrograms
µm	Micron
Ag	Silver
Ag-GAC	Silver-modified granular activated carbon
APS	Sulfate reducing bacteria
BARC	Beltsville Agricultural Research Center
BDRLF	Beaverdam Road Landfill site
BGS	below ground surface
Br^-	Bromide
C	Carbon
CH_4	Methane
cis-DCE	1,2-dichloroethylene
Cl^-	Chloride
cm	Centimeter
CSIA	Compound specific isotope analysis
CVOCs	Chlorinated Volatile Organic Compounds
DDI	Distilled deionized
DHC	*Dehalococcoides* spp.
DHBt	*Dehalobacter* spp.
DSB	*Desulfitobacterium* spp.
DNAPL	Dense nonaqueous phase liquid
DO	Dissolved Oxygen
DoD	Department of Defense
EC	Electrical conductivity
ECD	Electron Capture Detector
EPA	Environmental Protection Agency
EtnE	Epoxyalkane transferase
Fe^{+2}	Iron (II)/ferrous iron
Fe^{+3}	Iron (III)/ferric iron
Fe_T	Total iron
GAC	granular activated carbon
GORE	??
HPT	Hydraulic Profiling Tool
HRPP	High Resolution Passive Profiler
K_m	Mass transfer coefficient
L	Liter(s)
m	Meter
mg	Milligrams
MIP	Membrane Interface Probe
MIP-ECD	MIP-Electron capture detector

MiHPT	Combined MIP and HPT
MNA	Monitored natural attenuation
MTBE	Methyl *tert*-Butyl Ether
N	Nitrogen
N_2	Nitrogen gas
NJ	New Jersey
NO_2^-	Nitrite
NO_3^-	Nitrate
NPL	National Priority List
O_2	Oxygen
ORP	Oxidative reductive potential
P	Phosphorus
PCE	Tetrachloroethene
PDB	Passive diffusive bag
PFM	Passive Flux Meter
PHE	Phenol hydroxylase
PID	Photoionization Detector
POCIS	Polar organic chemical integrative samplers
PVC	Polyvinyl chloride
qPCR	Quantitative polymerase chain reaction
RCDM	Regenerated cellulose dialysis membrane
RDEG	Toluene monooxygenase 2
s	Second(s)
SERDP	Strategic Environmental Research and Development Program
sMMO	Soluble methane monooxygenase
SO_4^{2-}	Sulfate
SPMDs	Semi-permeable membrane devices
TCE	Trichloroethene
TeCA	Tetrachloroethane
TTU	Texas Tech University
TWs	Transect wells
TX	Texas
USDA	United States Department of Agriculture
V/SA	Volume/Surface Area
VC	Vinyl chloride
VCR	Vinyl chloride reductase
VOA	Volatile organic analysis
VOCs	Volatile organic compounds

ACKNOWLEDGMENTS

The project team included Dr. Andrew Jackson (Texas Tech University) who was responsible for leading the development of the direct insertion passive sampling tool, project coordination and reporting; and Dr. Paul Hatzinger (Aptim Federal Services) who led the field demonstration and development of the micro-biotraps. Our research team gratefully acknowledges the financial and technical support provided for this project by the Strategic Environmental Research and Development Program (SERDP). We thank Dr. Andrea Leeson for her guidance, and the support staff at Noblis for their administrative assistance. Major contributors to this work included Dr. Haley Schneider (TTU) who received her Ph.D. based on this work, Dr. Stephen Morse, who contributed to the structural analysis, and Uriel Garza-Rubalcava and Dr. Danny Reible (TTU) who made substantial contributions to the modeling effort, as well as Graig Lavorgna, Paul Hedman, and Mark Tucker who provided significant field support (Aptim Federal Services).

ABSTRACT

Introduction and Objectives- The ability to predict contaminant (e.g. chlorinated volatile organic compounds (CVOCs)) fate and transport in aquifers is often limited by the intrinsic heterogeneity associated with the flow field, contaminant distribution, and coupled biotic and abiotic reactions. Processes occurring in low permeability zones are particularly important, as studies have demonstrated that contaminants residing in such materials can sustain groundwater plumes and impede overall contaminant attenuation. While the importance of identifying these processes in heterogeneous media has been well documented, previously there has been no cost-effective tool for providing high resolution profiling of coupled contaminant, biogeochemical, and microbiological characteristics at the cm-scale. The primary objective of this SERDP research was to develop and demonstrate a *High-Resolution Passive Profiler* (HRPP) as a fine-scale delineation tool for the saturated subsurface. Focus was placed on discerning contaminant, microbiological, and biogeochemical differences between low permeability and high permeability zones within heterogeneous or stratified media.

Methodology-Our approach consisted of developing a direct drive HRPP designed to determine contaminant concentration, groundwater velocity, microbial community structure, and potential for abiotic/biotic contaminant degradation *in situ* at the cm-scale along a vertical profile. Laboratory studies were used to develop a new method to measure pore velocity and to demonstrate the ability of using micro-biotraps to measure the microbial community and perform compound specific isotope analysis on adsorbed CVOCs. Based on laboratory results, a full scale HRPP was designed, manufactured, and tested in the field. Based on initial field tests, new generations of HRPP were manufactured and field tested. A second field test evaluated HRPP performance against other methods of sub-surface site evaluation (vertical discrete wells, cores, Membrane Interface and Hydraulic Profiling Tools (MIP/HPT), and standard monitoring wells. A third field test was used to contrast site assessment results using standard monitoring wells and HRPP deployed along a contaminated groundwater transect at a site using a mulch bio-wall for treatment.

Results- A direct drive HRPP was developed that can be coupled together to evaluate vertical lengths ranging from 1.2 to 3.6 m and can be deployed down to ~9 m using direct drive devices. It produces co-located concentration profiles (~20 cm resolution) of CVOCs, geochemical indicators (e.g. Cl^-, NO_3^-, SO_4^{-2}, Fe, CH_4, ethene), microbial community, compound specific isotope analysis (CSIA) of CVOCs, and pore velocity (0-100 cm/d) even in low hydraulic conductivity media (e.g. clay). HRPP concentration profiles of these parameters were comparable to other traditional site assessment methods. However, the resolution achieved by the HRPP provides information on contaminant fate and transport that cannot be obtained by other methods.

Conclusions-During this SERDP project, we developed and validated a modified peeper design (HRPP) capable of providing information far beyond concentration data, including microbial numbers and activity, groundwater and contaminant flux, and contaminant degradation at cm-scale resolution. Samplers capable of producing such a holistic set of characterization parameters with

this level of resolution will be an enormous advantage over existing methods and should lead to higher fidelity site models, more tailored design of remediation activities, and improved remedial performance evaluations. Further, the tool allows monitoring and assessment of highly heterogenous contaminated formations that are presently hard to evaluate, particularly with respect to processes occurring in low permeability regions. The new tool can be deployed relatively easily, similar to other direct drive tools and can provide data to guide source zone assessment, well placement, rebound potential from low permeability zones, homogeneity and extent of bioaugmentation/stimulation efforts, or other remedial activities.

1 EXECUTIVE SUMMARY

1.1 Introduction

The ability to predict contaminant (e.g. chlorinated volatile organic compounds (CVOCs)) fate and transport in aquifers is often limited by the intrinsic heterogeneity associated with the flow field, contaminant distribution, and coupled biotic and abiotic reactions. Processes occurring in low permeability zones are particularly important, as studies have demonstrated that contaminants residing in such materials can sustain groundwater plumes and impede overall contaminant attenuation. While the importance of identifying these processes in heterogeneous media has been well documented, previously there has been no cost-effective tool for providing high resolution profiling of coupled contaminant, biogeochemical, and microbiological characteristics at the cm-scale. For example, the membrane interface probe (MIP) is only able to provide a semi-quantitative high-resolution vertical profile of contaminant concentration and the hydraulic profiling tool (HPT) can produce only a high-resolution vertical profile of aquifer permeability. High-resolution characterization recently has relied on tools such as multi-level discrete interval groundwater sampling devices. While these groundwater sampling tools are useful, they are not able to discern heterogeneity at a scale less than approximately 0.3 meters (m), and installation of the groundwater wells needed to apply this technology can be cost prohibitive. Passive Flux Meters (PFMs) must be inserted within existing groundwater wells, but can provide high-resolution vertical profiles of both the hydraulic and contaminant fluxes. The application of techniques to evaluate microbial communities *in situ*, such as Bio-Traps, suffer from similar constraints; only the microbial community in the "bulk" groundwater is represented. Thus, although all the aforementioned techniques provide valuable information, with the exception of the MIP and HPT, they all require the installation of groundwater wells, and only characterize conditions within the well bore (**Figure 1.1**). Thus, the ability to identify and measure these processes *in situ* is needed to provide sufficient plume characterization, and to ultimately facilitate improved estimates of contaminant fate and transport.

A single tool that can be cost-effectively and rapidly deployed to measure the parameters discussed above at the cm-scale would be an important advance in site assessment technology. Such a tool could also be easily employed to produce data for remedial design and to assess remedial technology effectiveness. Our approach was to develop a passive pore water sampling technology, the High Resolution Passive Profiler (HRPP), that meets the above objectives. The basic technology was based on diffusion samplers (peepers). Peepers have been used to determine the vertical distribution of soluble constituents in saturated sediments/material. In general, they consist of a solid rod or plate with cells milled along the length. The cells are initially filled with pure water separated from the sediment by means of an appropriate membrane. The water in each cell passively equilibrates with the sediment pore water due to diffusion and, once equilibrated, the sampler is removed, and the water evaluated for species of interest. The rate of equilibrium is a function of the cell characteristic length (volume/surface area), the diffusion coefficient of the species of interest, resistance of the membrane, temperature of the system, groundwater velocity, and porosity of the sediment. Peepers can be made with many different geometries and can achieve cm-scale sampling resolution and produce samples with detection limits similar to those for

groundwater sampling. The final resolution and sensitivity are functions of the cell volume required.

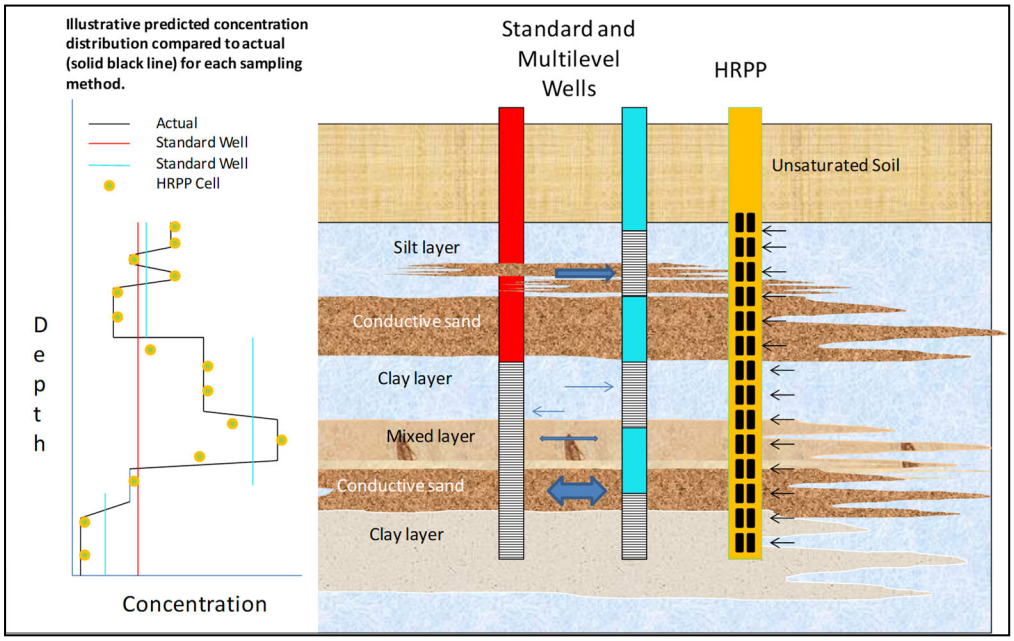

Figure 1.1. Conceptual model of standard sampling from wells compared to the proposed deployable HRPP

While the use of peepers to delineate the distribution of contaminants and geochemical indicators is well developed in very shallow sediments, marshes, and surface waters, significant development and validation was required to apply the method in deeper applications such as groundwater aquifers. Further, the standard peeper technology cannot produce information beyond concentration data such as: microbial numbers and activity, groundwater and contaminant flux, and contaminant degradation at cm-scale resolution. Development of samplers capable of producing such a holistic set of characterization parameters with this level of resolution would be an enormous advantage over existing methods.

1.2 Objectives

The overall goal of this research was to develop and demonstrate a direct drive High Resolution Passive Profiler (HRPP) as a fine-scale delineation tool for the saturated subsurface. Focus was placed on discerning contaminant, microbiological, and biogeochemical differences between low permeability and high permeability zones within heterogeneous or stratified media. Specific objectives in the design and application of the HRPP were as follows:

1. Directly measure groundwater and contaminant flux at the cm-scale.
2. Quantify biogeochemical conditions at the cm-scale.
3. Assess microbial community structure and activity at the cm-scale.
4. Assess effectiveness for quantifying contaminant and biogeochemical processes in heterogeneous saturated soils.

5. Determine the extent to which the newly developed HRPP can be used to improve conceptual site models.

1.3 Technical Approach

The project combined lab-based development efforts with three field demonstrations. Lab studies were performed to develop a relationship between pore velocity and the mass transfer of a conservative tracer. Initial experiments were conducted in small scale flow boxes under well-controlled hydraulic regimes and small-scale prototype sampling devices. These experiments were used to develop the basic correlation between the mass transfer of Br^- from the cells and pore velocity. The experiments evaluated the impact of equilibration time, velocity (0-100 cm/d), and sampler orientation with respect to flow direction. Additional experiments using a meso scale flow box were used to confirm the correlations developed for the full-size field samplers as well as the ability to measure velocity in layered systems with differing hydraulic conductivities.

Other laboratory experiments were used to demonstrate the ability of the samplers to use micro-biotraps (small compartments filled with Bio-Sep beads that serve as a matrix for bacterial growth) to measure the microbial community composition, as well as to conduct stable isotope analysis of adsorbed CVOCs to assess whether degradation is occurring in an aquifer. Small scale flow boxes consisting of two layers of differing hydraulic conductivity were equilibrated with trichloroethene (TCE), a culture of reductive dechlorinating bacteria and edible oil as a substrate. Once reductive dechlorination was documented consistently in the low permeability layer, prototype HRPP samplers were installed and allowed to equilibrate. Bio-Sep beads placed in the HRPP samplers were removed and sent for commercial analysis (Microbial Insights Knoxville, TN) of the microbial community using a qPCR array designed for assessing chlorinated solvent degrading communities in aquifers and $\delta^{13}C$ analysis of adsorbed CVOCs using compound specific isotope analysis (CSIA). Field experiments included initial testing of the micro-biotraps in wells at Fort Dix (NJ) and Kelley Air Force Base (TX) to measure microbial community abundance and CSIA of CVOCs as well as 3 field deployments of the full scale HRPP. Prototype HRPP samplers with micro-biotraps containing BioSep beads, activated carbon, and silver impregnated activated carbon, were equilibrated in wells. Adsorptive media were sent to Microbial Insights for microbial community analysis and CSIA of adsorbed CVOCs.

Full-scale field-deployable HRPPs were deployed at three CVOC sites. The general design of an HRPP is provided in Figure 1.1. After each field test, a review was conducted to evaluate the HRPP performance and usability. The results of each field test were used to optimize the design of the next generation. The HRPP design was based on: (1) incorporating the volume requirements established during laboratory and preliminary field tests for aqueous samples and Bio-Sep beads; (2) optimizing the volume/area ratios and spacing of the cells used to estimate groundwater velocity; and (3) improving structural integrity to prevent physical deformation of the structure HRPP during insertion. Each HRPP version (labeled A, B, and C) was capable of measuring concentrations of dissolved species in pore water, groundwater velocity, microbial community abundance and composition, and stable isotopic composition of CVOCs.

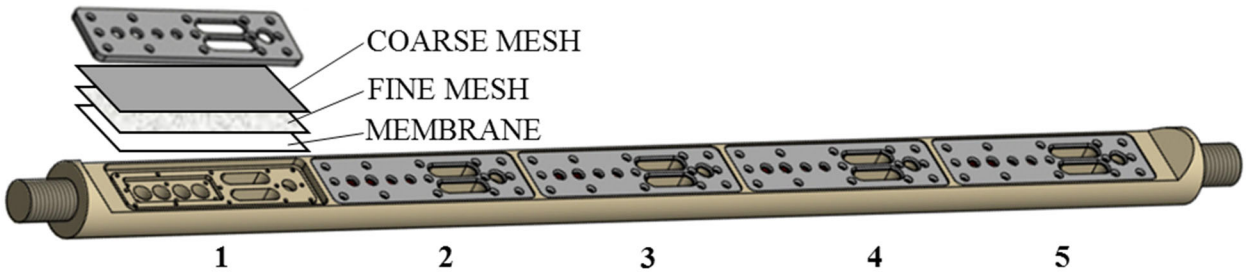

Figure 1.2. General design of the HRPP including five cells sets over four-foot length, coarse stainless-steel mesh, fine nylon mesh, and 0.45 µm membrane attached with cover plate and screws. HRPP was manufactured from 2.5" stainless steel rod and was threaded on each end to allow it to be coupled to other HRPP units or a direct drive device

The HRPPs were tested in three sequential field trials. The first field trial took place at Fort Dix near Trenton, New Jersey, in September 2015. Two HRPP-first generation (HRPP-A) samplers were installed and data were compared to nearby monitoring wells data and standard Bio-Traps. Design modifications were made to the HRPP, and the second generation (HRPP-B) was tested a year later at the former Alameda Naval Air Station in Alameda, California. HRPP-A and HRPP-B samplers were deployed at Alameda, and the resulting data were once again compared to nearby monitoring well data, standard Bio-Traps, data from a MIP/HPT deployment, and soil core data. Upon completion of the Alameda deployment, additional design changes were made and the new version (HRPP-C) was deployed at the USDA BARC site in Maryland. At the BARC site, HRPP-B and HRPP-C samplers were deployed along a contaminated groundwater flow transect across a biowall. Data from the HRPP were compared to well data and in well Bio-Traps.

1.4 Results and Discussion

1.4.1 Pore Velocity Estimation

Data from laboratory studies showed a strong correlation between the mass transfer of Br^- from the HRPP sampler and pore velocity. The technique used variation in specific surface area of HRPP velocity cells to produce variations in equilibrium with a single deployment interval. The variation in Br^- equilibrium with respect to specific surface area was used to determine the mass transfer coefficient (K_m) of Br^-. By evaluating the change in K_m with pore velocity in controlled experiments, we developed a relationship (**Figure 1.3**) to predict pore velocity from the measured Br^- K_m value. We also tested the impact of sampler orientation and equilibration time and found neither impacted the developed correlation. The technique is able to estimate pore velocity between 3-100 cm/d. Velocities below 3 cm/d cannot be differentiated from the zero-velocity case. After development of the K_m pore velocity relationship, we used large meso-scale flow boxes and tested the full-scale field deployable HRPP samplers. Samplers were directly inserted into the flow box that was packed with two layers (sand and sandy clay) of material with differing hydraulic conductivities. Using tracers, we measured the flow in each layer and compared the pore velocity to that measured by the HRPP. Predicted velocities in the sand and clay layer were indistinguishable from measured pore velocities in each layer (**Figure 1.3**).

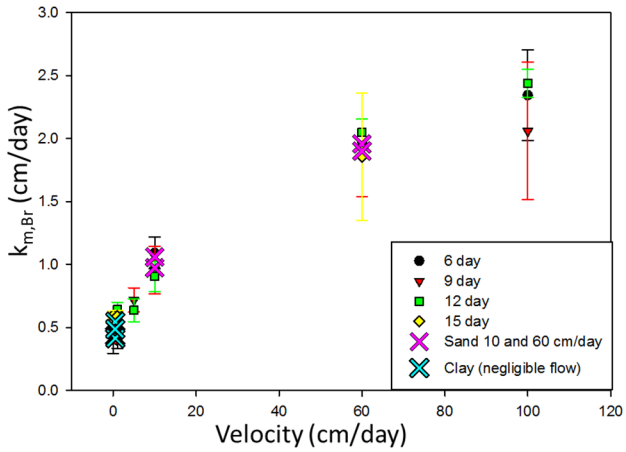

Figure 1.3. Relationship between pore velocity and measured HRPP Br^- k_m value based on lab scale flow boxes studies. Verification of relationship overlaid as "X" symbols using full scale HRPP samplers and mesoscale two-layer flow box system for 10 and 60 cm/day velocity through sand layer and negligible flow in clay layer

1.4.2 Microbial Community Analysis and CSIA of CVOCs Using HRPP

Results from multiple studies and sites supported the ability of the samplers to measure the relative densities of a variety of different bacteria, including many known to be involved in reductive dechlorination. Microbial community population abundances detected on Bio-Sep beads were similar to in-well standard Bio-Trap samplers (Microbial Insights, Knoxville, TN). While some small differences were observed, there was no systematic variation between micro-biotraps in the HRPP units and traditional Bio-Traps. The $\delta^{13}C$ values measured for chlorinated ethenes adsorbed on Bio-Sep beads emplaced in the HRPP units were also comparable (within ~1 ‰) to standard in-well Bio-Traps. These proof of concept studies were supported by laboratory studies that evaluated the microbial community and CSIA changes in a two-layer flow box in which reductive dechlorination was occurring. Micro-biotraps in protype HRPPs were able to measure changes in microbial populations with depth even though the total depth of both layers was < 60 cm. Populations of bacteria capable of reductive dechlorination were at higher abundance in the low permeability layer than more oxidized high permeability layer, while oxidative co-metabolic genes were more prevalent in oxic layers. The $\delta^{13}C$ values measured for chlorinated ethenes (TCE, *cis*-DCE, and VC) for both pore water and micro-biotraps were comparable.

1.4.3 Field Deployments

1.4.3.1 Fort Dix

Three generations of HRPP samplers (HRPP-A, B, and C) were sequentially field tested to validate the HRPP performance against traditional site assessment techniques, with the results of each field test used to update the design. The first-generation sampler (HRPP-A) was tested at Ft. Dix, NJ. This field test was primarily focused on evaluating the structural integrity of the sampler while being inserted using a direct-push (Geoprobe) sampler. HRPPs were successfully deployed down to ~8 m BGS. Samplers were able to produce concentration profiles of geochemical parameters and CVOCs (*cis*-DCE and VC were present) at high resolution (~20 cm). Concentrations of CVOCs were comparable to nearby wells, taking into consideration the relatively long well screens of the monitoring wells and distance between wells and HRPP locations. HRPP samplers were also successfully able to measure relevant microbial populations and stable isotope composition

of CVOCs (*cis*-DCE and VC). Generally, HRPP samplers were not only consistent with each other, but also with data from well water and Bio-Traps. HRPP samplers measured velocities ranging from 1 to 10 cm/day. The estimated average annual velocity across the site is 7.5 cm/day based on hydraulic gradient, a rate that is within the range of velocities estimated by HRPP. The similarities of measured velocities with depth for both HRPP at two different locations, as well as the similarity to the average site formation, support the ability of the HRPP to estimate velocity.

1.4.3.2 Former Alameda Naval Air Station

Two sets of 3 coupled HRPP-B samplers (3.7 m) and one HRPP-A sampler were installed in a source zone to a depth of ~ 8 m BGS at Alameda. Data from HRPPs were compared to HPT/MIP data, core extractions, standard monitoring wells (including deployment of Bio-Traps and passive flux meters), and multiple depth interval well screens (multi-level wells) taken at the time of insertion.

Geochemical Indicators- HRPP samplers produced consistent and reproducible Cl^- and SO_4^- concentration profiles at both locations. Profiles were similar to one of the depth discrete multi-level wells, but significant concentration differences were observed between multi-level wells at similar depths located within a few meters of each other. Thus, the site displayed significant local variability. In addition, standard monitoring well concentrations were generally different than both HRPP and multi-level wells. Observed variations were most likely due to well screens sampling from more hydraulic conductive zones and potentially vertical short circuiting.

CVOC Concentration Profiles-CVOC concentration profiles were remarkably similar to those produced by multi-level wells, HRPP samplers, and soil cores (**Figure 1.4**). All three methods produced concentration profiles that exhibit sharp peaks in *cis*-DCE and VC at 5.8 m BGS, with concentrations decreasing by orders of magnitude within <1 m. HRPP profiles also reflect an additional zone of elevated CVOC concentrations at ~ 4 m BGS (near the peak Cl^- and SO_4^{-2} concentration). This finding is reflected in soil cores but not well water, because no existing wells were screened across that depth interval. This shallower peak also coincides with a zone of low permeability sediment identified in field inspections of cores. Standard monitoring wells (SPW3-1, SPW3-2, and PEW 02) generally had concentrations that matched the average HRPP concentrations and vertical discrete well intervals over the depth the standard wells were screened. Overall, the CVOC concentrations captured with the HRPPs reproduce the same concentration profiles created by multilevel wells and soil core samples. CVOC concentrations captured with HRPPs also generally matched standard monitoring well concentrations, but the HRPPs had higher resolution capabilities and therefore created more complete concentration profiles than standard wells. There was generally poor agreement between qualitative MIP profiles and any other data sets.

The $\delta^{13}C$ of VC was consistent with depth for all HRPP micro-biotrap samples (~ -25 ± 2 ‰) (**Figure 1.4**). Values were also within the range of those measured in samples from well water and standard Bio-Traps. The $\delta^{13}C$ values from the water and Bio-Traps, however, were much more variable than observed with the HRPP micro-biotraps. $\delta^{13}C$ values of *cis*-DCE were not available for one of the HRPPs (HRPP-3) deployed at Alameda, due to an apparent analytical issue at the stable isotope laboratory. Values for the other HRPP (HRPP-3) were similar to local well water samples and in the range of some of the multilevel well samples, although as with VC, these values showed significant variability. Most importantly, the deployment showed that enough

CVOC can be captured in a 3-week deployment to conduct standard CSIA analysis, and that, excluding the anomalous *cis*-DCE data, the values are reasonable and consistent.

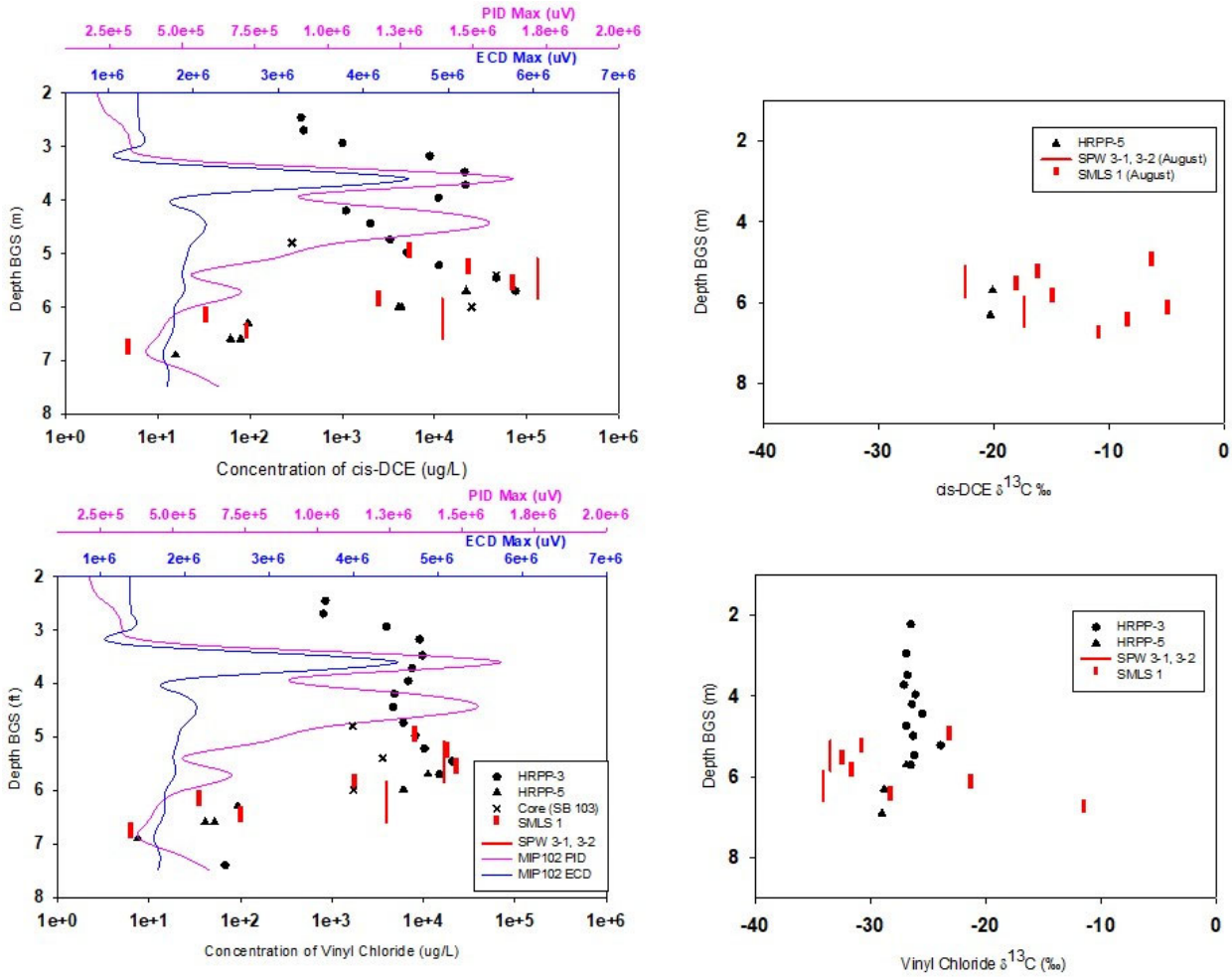

Figure 1.4. (Left Panels) Depth distributions of CVOCs measured by HRPP, vertical discrete wells (SMLS 1), standard wells (SPW 3-1,2), soil cores, and MIP at one location. Right Panels) The $\delta^{13}C$ of VC and *cis*-DCE based on well water, in well Biotraps, and HRPP micro-biotraps.

Velocity Results-Comparative velocity measurements at the Alameda site included an estimated average site velocity, MIP/HPT data, and passive flux meters installed in the standard monitoring wells (**Figure 1.5**). The site average velocity based on hydraulic head difference is 2 cm/day. The passive flux meters measured velocities of 3-8 cm/day, in various wells. HRPP velocity estimates ranged from 1 to 8 cm/day based on depth and location. In general, the HRPP intervals with lower velocities (1 cm/day) occurred at depths where the MIP/HPT indicated high pressure and high electrical conductivity, which both indicate a relatively low permeability soil. The HRPP velocity measurements were similar to those estimated by other methods (MIP/HPT, PFMs, etc.), whether qualitative or quantitative. The HRPP is not susceptible to interferences that can affect other methods of measuring velocity, such as high salinity for the MIP-EC.

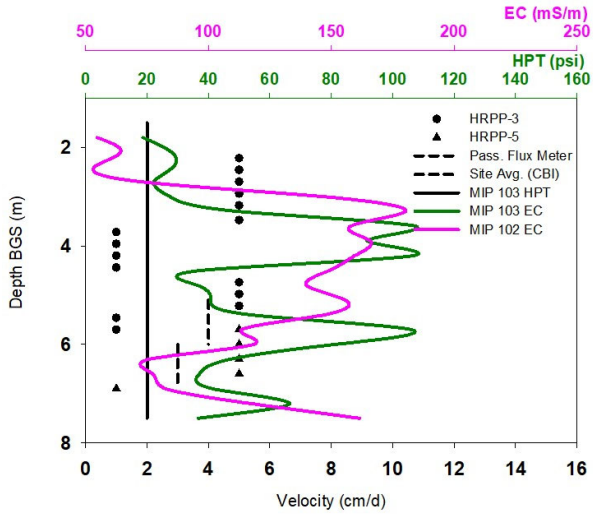

Figure 1.5. Estimates of groundwater pore velocity based on HRPP and passive flux meters compared to qualitative results from HPT at one location and overall site average based on pumping tests.

Microbial Community Analysis- HRPP micro-biotraps, well water, and in well Biotraps all generally detected similar species/genes (See **Figure 1.6 for examples**). There were no consistent patterns between the abundances (cells or genes) measured by each technique with well water abundances (cells or genes /ml) greater or lesser than in well Biotraps or micro-biotraps (cells or genes/bead) dependent on the specific species. The lack of consistent pattern suggests differences may reflect relative abundances in pore water compared to sediment. Overall, the HRPP micro-biotrap was capable of quantifying a wide suite of microbial species, and indicated population/gene differences in some instances that may reflect microbial communities in well water vs those present on the sediments that contact the HRPPs.

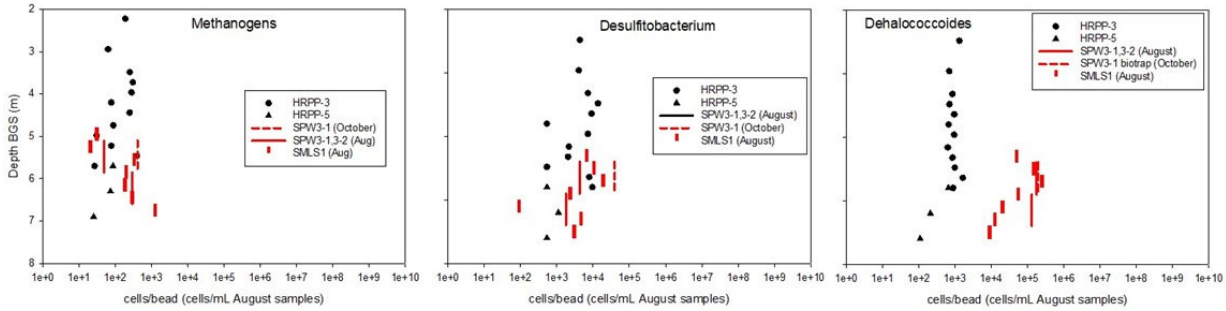

Figure 1.6 Example distributions of microbial populations based on HRPP micro-biotraps, in well Biotraps, and well water.

1.4.3.3 USDA BARC Site

HRPPs were placed along a groundwater transect near an old landfill and upgradient of a mulch biobarrier, within a mulch biobarrier, and then downgradient of the biobarrier into a small stream where plume discharge was hypothesized. In general, at individual sites along the contaminated groundwater transect, data were comparable between well samples (water and Bio-Traps) and HRPP discrete depth samples. Using either the HRPP depth averaged or maximum concentrations of Cl^-, CVOCs, and CH_4, the overall trend in concentration change as well as concentration along

the transect was very similar to well data (**Figure 1.7**). Based on HRPP data, compared to well water or well Bio-Traps, populations of bacteria capable of reductive dichlorination were generally higher and more species were present along the transect, supporting the observed continued reduction in CVOCs and increased presence of VC and ethene in the biowall. This difference may reflect bacteria present on sediments (HRPP) vs planktonic cells in groundwater (well water and standard Bio-Traps). HRPP depth-averaged porewater velocities ranged from 2 to 8 cm/d, which were similar to estimates from slug tests, pumping tests, and tracer tests. (2 to 5 cm/d). Conclusions based on average or maximum HRPP values would be similar to those for well water, except that CVOC degradation appeared to be more complete and there appears to be continued loss of CVOCs downgradient of the biowall.

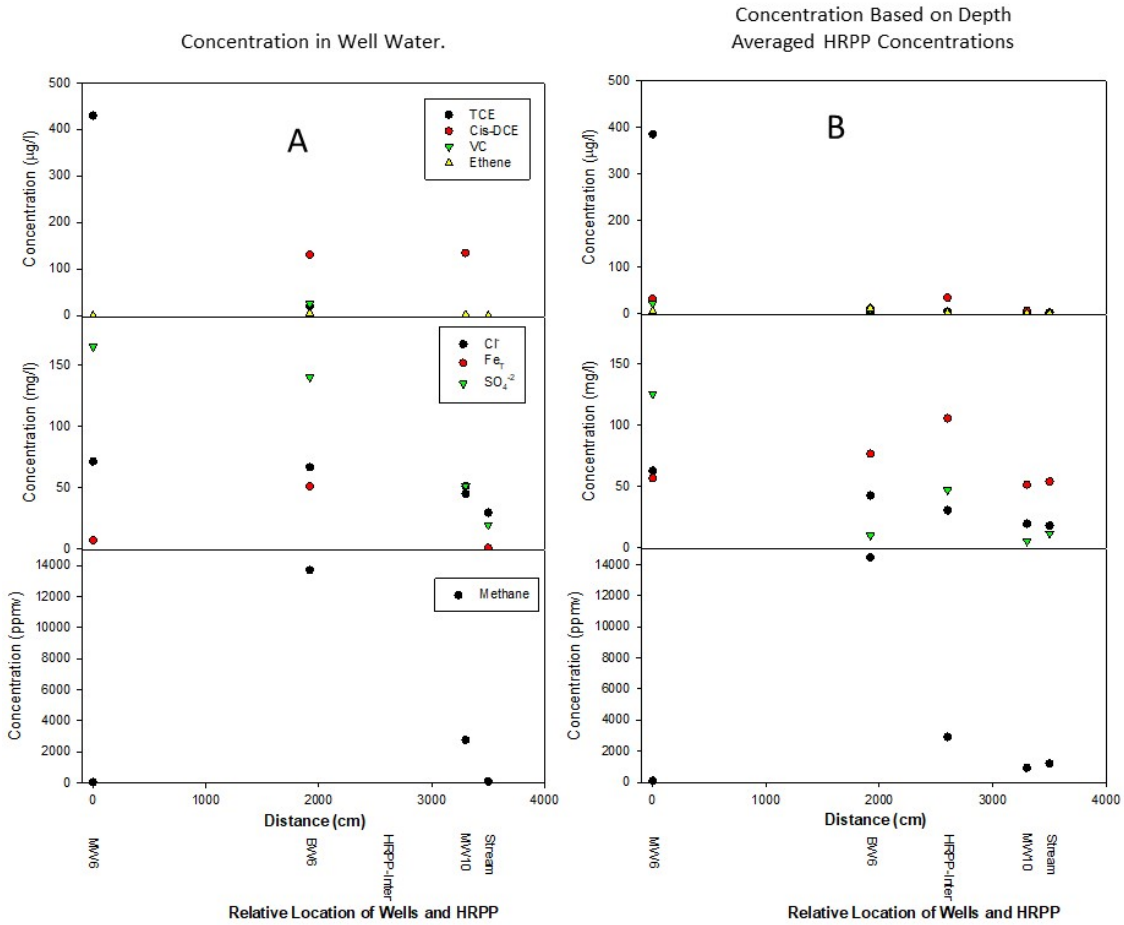

Figure 1.7. Concentration Distribution across groundwater transect. A) Concentrations based on sampled well water; B) Concentrations based on depth averaged HRPP concentrations.

However, while well data or HRPP data used to assess the efficacy of the mulch biowall for treating CVOCs generally leads to similar "gross" conclusions, there are also a number of important differences. In the upgradient area, data from well water only would not predict the large change in CVOC concentration with depth or in an observed clay layer (**Figure 1.8**). In the biowall, well data would predict *cis*-DCE breakthrough across the whole biowall depth rather than through a relatively small high permeability zone (**Figure 1.8**). Well data from the biowall would also predict

that reductive dechlorination is generally incomplete and bacteria capable of reducing *cis*-DCE are not present, while HRPP data supports a model of complete degradation except in the high permeability zone. The high velocity zone appears to exist across the transect downgradient of the biowall based on velocities with depth, profiles that largely overlap with presence of CVOCs downgradient of the biowall. Due to the assumption that well water represents the average concentration across the well screen, calculated fluxes at each location based on well water would be much higher than those based on depth discrete CVOC concentration and velocity profiles. Although CVOCs are present at depths below the stream and in adjacent wells, no CVOCs appear to be upwelling into stream water; this observation could not be supported from well data alone, given the concentrations of *cis*-DCE in MW10. Thus, the HRPP data provided new insights into the behavior of the plume and its level of treatment at the BARC site.

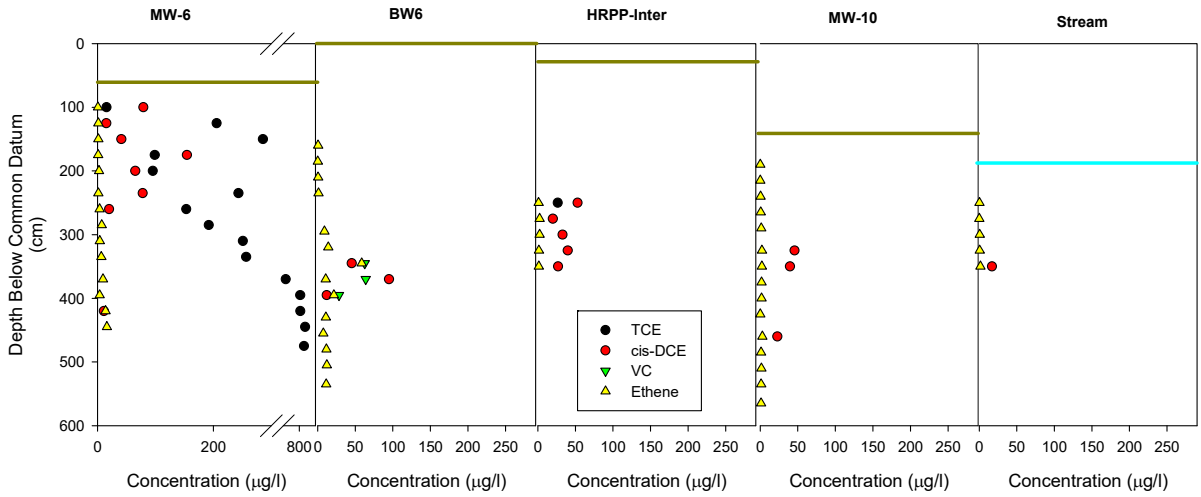

Figure 1.8. Concentration with depth based on HRPP samples across groundwater transect.

1.5 Implications for Future Research and Benefits

During this SERDP project, we developed and validated a modified peeper design (HRPP) capable of providing information far beyond concentration data, including microbial numbers and activity, groundwater and contaminant flux, and contaminant degradation at dm-scale resolution. Samplers capable of producing such a holistic set of characterization parameters with this level of resolution will be an enormous advantage over existing methods and should lead to higher fidelity site models, more tailored design of remediation activities, and improved remedial performance evaluations. Further, the tool allows monitoring and assessment of difficult contaminated formations such as thin layers of high or low permeability and clay layers that cannot currently be adequately evaluated. The new tool can be relatively easily deployed similar to other direct drive tools and can provide data to guide source zone assessment, well placement, rebound potential from low permeability zones, homogeneity and extent of bioaugmentation/stimulation efforts, or other remedial activities.

The HRPP tool is currently ready for commercialization. The application of the tool could easily be provided by any number of consultants or field service companies. Commercialization will most likely be dependent on establishing the benefits of the HRPP with site managers and regulators, who can then encourage its use to improve site characterization, site conceptual

models and impact of remedial activities. At the time of this writing, the NAVY was further evaluating the tools capabilities, additional demonstrations through the ESTCP program would also facilitate its adoption by further demonstrating its utility.

2 OBJECTIVES

The overall goal of this project is to develop and demonstrate a direct drive High Resolution Passive Profiler (HRPP) as a fine-scale delineation tool for the saturated subsurface. Focus is placed on discerning contaminant, microbiological, and biogeochemical differences between low permeability and high permeability zones within heterogeneous or stratified media. Specific objectives in the design and application of the HRPP are as follows:

1. Directly measure groundwater and contaminant flux at the cm-scale.

2. Quantify biogeochemical conditions at the cm-scale.

3. Assess microbial community structure and activity at the cm-scale.

4. Assess effectiveness for quantifying contaminant and biogeochemical processes in heterogeneous saturated soils.

5. Determine the extent to which the newly developed HRPP can be used to improve conceptual site models.

3 BACKGROUND

The ability to predict contaminant fate and transport in aquifers is often limited by the intrinsic heterogeneity associated with the flow field, contaminant distribution, and coupled biotic and abiotic reactions. An aquifer flow field is a complex structure composed of high permeability materials such as sand and gravel mixed with low permeability materials such as clay and silt. It is common for screened groundwater wells to be installed to monitor contaminant concentrations and geochemical conditions in aquifers. Contaminant concentrations and geochemical conditions present in groundwater wells often reflect only the most permeable portions of the aquifer and may, therefore, misrepresent contaminant distribution and dominant chemical and biological processes in the bulk aquifer. Contaminant concentrations and biogeochemical processes often differ significantly between high and low permeability zones. Therefore, the ability to delineate subsurface environments beyond the use of wells is necessary to provide sufficient plume characterization, and to ultimately facilitate estimates of contaminant fate and transport.

3.1 Contaminant Distribution in High and Low Permeability Zones

There is often a difference in contaminant concentration between high and low permeability zones. Contaminant attenuation tends to occur more quickly in high permeability material than in low permeability material. Both laboratory (Sale et al., 2008; Haggerty et al., 2004) and field (Feehley and Zheng, 2000) studies have demonstrated that contaminants residing in low permeability materials can sustain groundwater plumes and impede overall contaminant attenuation. Dense non-aqueous phase liquids (DNAPLs) tend to accumulate above low permeability clay or silt lenses, allowing the DNAPL source to diffuse from the high permeability zone into the low permeability zone. Once the source is depleted or removed from the high permeability zone, the accumulated DNAPL in the low permeability zone causes a shift in the concentration gradient so that the contaminant diffuses back out into the high permeability zone (Sale et al., 2008). Back diffusion from the low permeability zone acts to sustain the life of the groundwater plume past the point of source removal, impacting the time and remediation efforts required to improve down gradient water quality (Liu and Ball, 2002; Chapman and Parker, 2005).

3.2 Microbiological and Biogeochemical Differences in High and Low Permeability Zones

Contaminant concentrations in aquifers are affected by coupled abiotic and biotic processes, which can differ substantially between high and low permeability zones. Differences in mineralogy between a sandy zone and a silty or clayey zone affect the abiotic and biotic contaminant transformation processes that take place (Stucki 2006). Clay minerals such as smectite and dithionite have the ability to transform chlorinated organic compounds abiotically. For example, pentachloroethane degrades to tetrachloroethene via a dehydrochlorination reaction

when exposed to reduced smectite surfaces (Cervini-Silva 2000). Dechlorination of thrichloroethene occurs in the presence of dithionite, and the dechlorination process is enhanced in a heterogeneous system of dithionite and smectite (Nzengung et al. 2001). Abiotic contaminant transformation potential can depend on the biotic processes taking place. For example, the reduction of iron (often by means of iron reducing bacteria) encourages transformation of chlorinated organics by clay mineral surfaces (Gorby et al. 1994). Therefore, the presence or absence of iron-reducing bacteria in saturated clays can indirectly affect the ability of the clay to degrade chlorinated organic compounds.

Several studies have shown that microbial biomass and activity in aquifers are related to soil grain size (Albrechsten and Winding, 1992; Amellal et al., 2001; Musslewhite et al., 2007; Cozzarelli et al., 1999). However, how degradative organisms and relevant microbial communities shift on a centimeter scale in an aquifer, and how the shifts are correlated to geology, is presently unknown.

3.3 Site Characterization for Subsurface Remediation

Subsurface site characterization is a complex process that requires several inputs. Physical, chemical, and biological factors combine to create a unique system for any individual site. The purpose of characterizing a contaminated site is to determine what contaminants are there, where the contaminants are spatially located, where the contaminants are going, and what, if anything, is happening to the contaminants under current conditions. Site characterization can then be used to determine what steps, if any, need to be taken by engineers to promote remediation of the site.

Key physical, chemical, and biological parameters of a contaminated site include geology, permeability, geochemistry, pH, contaminant concentrations, compound specific isotope analysis (CSIA), redox potential, carbon:nitrogen:phosphorous (C:N:P) ratio, enumeration of microbial communities, and microbial kinetics and activity. Subsurface site characterization typically consists of a description of the vadose zone as well as the saturated zone. The focus of this research effort is the delineation of aquifers, so only characterization of the saturated zone is discussed in detail in this report.

3.3.1 Contaminant Concentrations, Location, and Origin

One of the first steps of site characterization is to determine what contaminants are present. Environmental contaminants are numerous and diverse, as are the chemical properties and health risks associated with each contaminant. Knowing what contaminants are present provides an understanding of health hazards and how the contaminants will behave in the environment.

In addition to contaminant identification, determining contaminant concentrations and locations is a priority. Contaminant location becomes relevant when assessing transport and risk of drinking water contamination. Concentration levels are a primary concern because the concentration of a contaminant determines its toxicity to humans, animals, and the environment. Contamination of an aquifer often leads to the formation of a groundwater plume, in which the

most concentrated levels of contaminant are near the source area, and concentrations dilute as the contaminant spreads further from the source area. In order to approximate the spatial scope of the contaminated plume, multiple samples are collected from the source area and the surrounding area.

Concentrations are not only used to spatially delineate a plume, but also to assess the potential for natural attenuation. The ability of microorganisms to effectively remove contaminants is partially dependent upon concentration. Many organic contaminants are readily degraded under aerobic conditions; however, heavy loadings of contaminants can exhaust the natural oxygen supply of groundwater, in which case aerobic degradation of the contaminants cannot be sustained (EPA Site Characterization, 1991).

In addition to identification and location of contaminants, the origin of contamination is important. The origin of a contaminated plume is relevant in determining who is responsible for remediation of the site. Compound specific isotope analysis can help determine the source(s) of contamination through the measure of isotopic ratios of a contaminant. Isotopic ratios depend on the starting material, manufacturing process, and degradation of a contaminant, so contaminants from different sources have different isotopic footprints. The isotopic ratios change in a systematic way during the course of degradation, and CSIA is capable of measuring such changes. Further applications of CSIA are discussed in the following section.

3.3.2 Contaminant Migration and Attenuation

Once contaminants and concentrations are located and identified, it is necessary to determine what is happening to contaminants under current site conditions and where the contaminants are likely to be transported. The transportation of contaminants depends heavily on the hydrogeology of an aquifer. Hydrogeology covers a broad scope of the physical structure of the subsurface including stratigraphy, lithology, and structural geology. Stratigraphy defines the heterogeneous soil composition of aquifers (e.g. sands, silts, clays, and gravels). Understanding the stratigraphy of a contaminated site is important for site characterization because it helps to determine where and how the contaminated plume will travel. Contaminants are more likely to travel quickly through high permeability zones (sands and gravels) of an aquifer, so stratigraphy provides a sort of framework of the groundwater flow system. Lithology includes individual physical characteristic of unconsolidated deposits such as mineralogy, organic carbon content, grain size and shape, and compaction level. Lithology helps to determine the sorption of contaminants as well as where contaminants are likely to be stored and cause back-diffusion. Through grain size analysis, lithology provides location of high and low permeability zones in an aquifer. A relationship between soil permeability and grain size distribution is given by Hazen's equation:

$$K_p = c(d_{10})^2 \qquad \text{Eq. 3.1}$$

Where K_p is permeability, c is Hazen's empirical coefficient (0 to 1.5, depending on literature source), and d_{10} is the diameter of the 10-percentile grain size of the soil.

The final component of geology is structural geology. Structural geology of a site includes features such as folds, faults, fractures, and interconnected voids. Hydrogeology ties in stratigraphy, lithology, structural geology, and how water moves through the elements of geology. By understanding the hydrogeology of a site, one can predict the direction(s) and rate(s) of groundwater flow and implement a remediation strategy that is appropriate for the system.

In addition to where the contaminants are going, it is important to examine what happens to contaminants under natural conditions. If natural attenuation is occurring to an effective extent, monitored natural attenuation (MNA) can be considered as a remediation strategy. If natural attenuation is occurring, but not to an extent that is considered effective, remediation strategies such as the injections of substrates or biological cultures may be considered to promote an increase in degradation. Several parameters can be used to predict the occurrence and effectiveness of natural attenuation including CSIA, microbial enumeration, redox conditions, nutrient and substrate availability, pH, and temperature. CSIA is commonly performed on pore water samples containing CVOCs to clarify issues regarding the source(s) of the contaminant, but it is also effective in determining the potential for biodegradation and the extent to which the contaminant is being degraded abiotically or biotically under current conditions. Indicators of biodegradation such as daughter products of chlorinated solvents can be detected through CSIA to determine if biodegradation is likely occurring. An example is the detection of *cis*-DCE and vinyl chloride at a TCE contaminated site. CSIA can also be useful in detecting clues of abiotic degradation in situations where in situ chemical oxidation/reduction or nanoscale iron has been implemented. While it is a strong indicator, CSIA is not a conclusive method to determine the occurrence of biodegradation and/or abiotic degradation, so it is often used in conjunction with other lines of evidence.

Studies have shown that diverse microbial communities exist in aquifers regardless of the type of soil media in the aquifer or the known input of organics (Ghiorse and Balkwill 1983, Ghiorse and Balkwill 1985, Beeman and Sulfita 1987, Webster et al 1985). When characterizing a site, it is important to enumerate microbial populations that are naturally present in order to determine if the targeted contaminant is a reasonable candidate for natural or amended biodegradation. In addition to microbial enumeration, modern analysis methods are capable of quantifying functional genes involved in the degradation of targeted contaminants. Chlorinated solvents, such as TCE, have multiple potential pathways for degradation. The quantification of populations such as *Dehalococcoides, Dehalobacter, Dehalogenimonas,* and *Desulfitobacterium* reflects the potential for reductive dechlorination. The quantification of functional genes, such as certain monooxygenases and dioxygenases, reflects the potential for degradation through several anaerobic and aerobic (co)metabolic pathways.

Biodegradation does not solely depend on the presence of the appropriate bacterial populations. Nutrient content and redox conditions are both factors that affect microbial activity. As previously mentioned, many organic contaminants are readily degraded by bacteria under aerobic respiration but are not as effectively degraded in other states (nitrate reduction, iron reduction, sulfate reduction, and methanogenesis). Different bacterial populations perform optimally to degrade contaminants under different redox conditions, so characterizing redox

conditions in a groundwater plume is key to choosing an effective remediation strategy. In addition to appropriate substrate and redox conditions, lack of nutrient availability of carbon, nitrogen, and phosphorous can be a factor that limits microbial growth, so the C:N:P ratio of a site can also be modified to promote biodegradation.

Temperature and pH of a site can have mild effects on microbial activity and abiotic reactions. The pH of groundwater can impact subsurface geochemical processes such as adsorption of organics, oxidation-reduction reactions, and biodegradation. Adsorption is affected by pH because physical and chemical bonding processes are strongly influenced by hydrogen ions (EPA Site Characterization, 1991). As pH increases, redox systems tend to become more reducing (ZoBell 1946). The types of bacteria present at a contaminated site are impacted by pH, so consequently the potential for biodegradation is affected (Baas-Becking et al. 1960). Many types of bacteria have growth optimums at a pH range of six to eight. However, microbial growth can still occur at extremely high or low pH for limited types of bacteria. Temperature affects the potential for biodegradation in the way that an increase in temperature (within an optimum range of approximately 10ºC to 30ºC) generally causes an increase in microbial growth (Dragun, 1988). As a result, there can be mild seasonal effects on the rate of bioremediation for contaminated soils.

3.4 Existing Techniques for Subsurface Site Characterization

Common techniques for delineating subsurface conditions include monitoring wells, sediment cores, borehole logging, and geophysical methods such as surface resistivity, electromagnetic surveys, seismic reflection, ground-penetrating radar, and magnetometer surveys. These techniques provide evidence regarding stratigraphic profiling, location of buried objects, distribution of contaminants, and indigenous microbial populations as well as soil properties such as porosity, permeability, moisture content, and grain size. Subsurface site characterization is a complex process, so no single tool is adequate for fully characterizing a site. Surveying and analytical techniques are combined like pieces of a puzzle to assemble a detailed picture of the subsurface.

3.4.1 Techniques for Determining Stratigraphy and Soil Properties

Geophysical methods such as electrical resistivity, electromagnetic conductivity, seismic reflection, ground-penetrating radar, and magnetometers contribute to stratigraphic profiling. Electrical resistivity delineates contrasts in lithology and the presence of groundwater based on electrical potential differences between electrodes. Water is highly conductive, whereas most soil materials are resistive. Therefore, the depth to the water table and local stratigraphy can be deduced from electrical resistivity measurements. Electromagnetic conductivity can provide much of the same stratigraphic information as electrical resistivity. Electromagnetic conductivity methods do not require the installation of electrodes and can be performed by one person, so they are typically more time and cost efficient than electrical resistivity methods.

Ground-penetrating radar provides similar information to the other geophysical techniques, but it is only suitable for delineating stratigraphy at shallow depths. Electromagnetic conductivity, ground-penetrating radar, and magnetometers can all be applied to detect the location of buried objects such as tanks and drums. Magnetometers are used specifically to detect metallic containers and iron-bearing rock. The use of geophysical methods can be limited due to bulkiness of equipment or limitations in urban environments such as subsurface utilities and pipelines.

Borehole logging is a term used for a variety of tests performed by lowering tools into boreholes. Borehole logging is useful for determining soil properties such as clay/shale content, porosity, hydraulic conductivity, grain size, moisture content, and the location of fractures and void spaces. Additionally, estimates of the direction and velocity of groundwater flow can be made from borehole logs. Types of borehole logging include caliper, resistivity, neutron, gamma, and sonic logging. Borehole logging is performed by creating an impulse or disturbance and measuring the response of the geologic system.

3.4.2 Techniques for Delineating Contaminants and Microbial Populations

Monitoring wells are widely used for sampling contaminated groundwater. General monitoring well design consists of a cased borehole that is capped at a certain depth and screened over one or more intervals. The screened intervals allow groundwater to flow into the well for collection and analysis. In addition to contaminant concentrations, microbial populations can be sampled in monitoring wells through Bio traps. Multilevel wells are often used in highly stratified sites to pull groundwater samples from multiple layers. Unfortunately, it is difficult to determine precise differences in contamination between sediment layers due to mixing within the well. Monitoring wells also tend to disproportionately represent conditions in highly permeable layers due to the inclination of groundwater to flow more readily through sands and gravels as opposed to clays and silts.

Electrical resistivity and electromagnetic conductivity can provide information on the quality of groundwater as well as its location, however, they cannot detect what specific contaminants are present. When using electrical resistivity and electromagnetic conductivity, contaminant plumes often appear as highly conductive regions due to the conductivity of solutes. A membrane interface probe (MIP) is a cone penetrometer system that pushes a probe into the ground and records CVOCs and petroleum product concentrations at desired depths up to about 100 feet below ground surface. A MIP investigation is not typically used instead of monitoring wells, but rather as a precursor to determine the best location(s) for placement of wells.

3.5 Background on Passive Sampling

Passive samplers are designed to obtain groundwater samples with minimal disturbance to the surrounding environment. The first commercially available passive sampler design was implemented in the late 1990s with the use of the passive diffusive bag (PDB), which acquires samples by equilibrating with groundwater in a monitoring well. Since the PDB, passive

sampling has evolved to include not only equilibrium samplers but also sorptive samplers, which incorporate sorptive media to accumulate analytes over time. Like any technology, passive samplers have important benefits as well as limitations. Research over the past decade in modeling passive sampler equilibration has led to enhanced passive sampler designs as well as an improved understanding of passive sampler equilibration dynamics.

3.5.1 Applicability of Passive Sampling

Equilibrium samplers are passive samplers that include no sorptive materials and simply collect contaminant concentrations by equilibrating with monitoring well water. The efficiency of equilibrium samplers is based on the assumption that the well water is representative of contaminant concentrations in the surrounding saturated sediment. The two major types of equilibrium samplers are PDBs and regenerated cellulose dialysis membrane (RCDM) samplers.

PDB samplers are the most simplistic equilibrium sampler design, consisting of a polyethylene tube filled with deionized water and closed at both ends. PDB samplers are best applied in sampling volatile organic compounds (CVOCs) and should not be used for collecting inorganic or semi-volatile organic compounds. PDBs are deployed by attaching a weight to the bottom of the bag and lowering it into the monitoring well. Deployment times for PDBs can vary depending on the contaminants of concern and the temperature of the groundwater. In a laboratory study, PDB concentrations of benzene, cis-1,2-dichloroethene, tetrachlorethene, trichloroethene, toluene, naphthalene, 1,2-dibromoethane, and total xylenes equilibrated with surrounding aqueous concentrations in 48 hours at 21ºC (Vroblesky, 2001). Lower temperatures can cause longer equilibration times for some compounds. RCDM samplers are very similar in design and function to PDBs. The tubing of RCDMs is typically made of regenerated cellulose as opposed to the polyethylene used for PDBs. The key advantage of RCDMs over PDBs is the ability to sample both inorganic and organic contaminants.

Sorptive samplers, or integrative samplers, are another type of passive sampler design which incorporates sorptive media to accumulate contaminants over time. Common types of sorptive samplers include semi-permeable membrane devices (SPMDs), GORE sorber modules, and polar organic chemical integrative samplers (POCIS). SPMDs are designed to mimic the bioaccumulation of contaminants in the fatty tissues of living organisms.

SPMDs are designed similarly to PDBs, except the tubular membrane bag is filled with a high molecular weight lipid rather than deionized water. Analytes are recovered from the SPMD by submersing the sampler in an organic solvent, causing contaminants to diffuse out into the solvent while lipids remain inside the tubing. SPMDs can have deployment times ranging from days to months, but an average deployment time is one month.

GORE sorber modules are packets of sorbent encased in a thin tube of expanded polytetrafluoroethylene membrane. The hydrophobic membrane only allows vapor migration of contaminants to reach the sorbent material, so Henry's Law is used to determine concentrations across phases. GORE sorbers can be used in the vadose zone, the saturated zone, and monitoring wells to detect a wide range of analytes depending on the sorbent packets contained within the sampler.

POCIS consist of a solid sorbent material between two microporous polyethersulfone membranes and are meant to mimic the respiratory exposure to contaminants by living organisms. Like SPMDs, POCIS can be deployed from weeks to months but are typically deployed for one month.

Peeper samplers encompass a wide range of passive sampler designs that vary in size, shape, and purpose. Generally, peeper samplers have a rigid structure with one or more openings covered by a membrane and are used to sample pore water. The rigid body material and membrane material chosen depend on the contaminants of concern. Peeper samplers can be inserted into saturated sediments at very shallow depths (1-3 meters) via a specially designed corer or direct push. Peepers are typically used to collect water samples at the groundwater/surface water interface or to collect water samples in groundwater monitoring wells.

3.5.2 Theoretical Modeling of Passive Equilibrium Dialyzers (Peepers)

While the first commercial passive sampler was not available until the late 1990s, the first experimental investigation of dialysis sampler equilibration was conducted by Hesslein in 1976 in river sediments (Hesslein 1976). Hesslein determined the following: (1) equilibration with sediment pore water requires more time than equilibration in open water; (2) species diffusivity is dependent not only on temperature, salinity, and molecular size, but also on sediment porosity and tortuosity. Hesslein rationalized extended equilibration times in sediments versus open water by concluding that in sediments the interstitial water layer directly adjacent to the membrane is depleted of solute fluxing into the cell more quickly than it is replenished by solute diffusing through the soil.

Soil porosity and tortuosity are correlated to species diffusivity and are therefore correlated to the time required to replenish the interstitial water layer. The impact of soil porosity and tortuosity on passive sampler equilibration is discussed more quantitatively in later investigations of equilibration dynamics (Harper et. al 1997 and Webster et. al 1998). The following one-dimensional model has been used to describe three-dimensional problems for the sake of simplicity (Berner 1980):

$$\frac{\partial C}{\partial t} = D_{eff}\frac{\partial^2 C}{\partial z^2} + \left(\frac{\partial D_{eff}}{\partial z} + \frac{D_{eff}}{\emptyset}\frac{\partial \emptyset}{\partial z}\right)\frac{\partial C}{\partial z} \qquad \text{Eq. 3.2}$$

Where C is the dissolved pore water concentration of solute, D_{eff} is the effective sediment diffusion coefficient, ϕ is the soil porosity, z is the vertical distance below the sediment/water interface, and t is time. The equation can be simplified to:

$$\frac{\partial C}{\partial t} = D_{eff}\frac{\partial^2 C}{\partial z^2} \qquad \text{Eq. 3.3}$$

if porosity and diffusion coefficient are considered to change negligibly with depth. The 1D model is acceptable in simplified cases where horizontal homogeneity is assumed and edge effects are ignored. However, in reality the sampler is of finite volume and is surrounded by an "infinite" volume of sediment, which can lead to significant edge effects due to vertical diffusion beyond the edges of the finite sampler. When edge effects are considered, a two-dimensional model is necessary. Harper et. al examined the following three cases of peeper equilibration using a 2D model: (1) solute concentrations in the interstitial water layer are constantly resupplied by desorption from soil; (2) solute concentrations are resupplied only by diffusion; (3) solute concentrations are resupplied by partial desorption from soil and diffusion (Harper et. al 1997). Solute transport for the first and second cases can be modeled over the same domain by the same set of equations using different initial and boundary conditions. The domain for all three scenarios is represented by a vertical plane as shown in **Figure 3.1.**

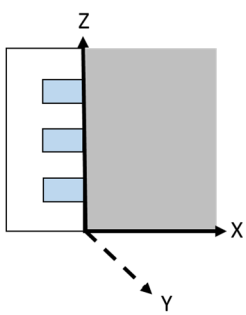

Figure 3.1. Vertical plane X-Z model domain for 2D passive sampler equilibration (Harper et al 1997)

The solute transport equation for the constant resupply and diffusion only cases is the 2D equivalent of Berner's 1D molecular diffusion model:

$$\frac{\partial C}{\partial t} = D\nabla^2 C \qquad \text{Eq. 3.4}$$

where $\nabla^2 C$ is the second spatial derivative of concentration and D is the appropriate diffusion coefficient (free ion diffusion coefficient, D_w, in peeper cells and effective sediment diffusion coefficient, D_{eff}, in sediment). The sediment diffusion coefficient, D_{eff}, is related to sediment porosity and tortuosity and is defined by Equations 3.5 and 3.6:

$$\tau = 1 - 2\ln(\emptyset) \qquad \text{Eq. 3.5}$$

$$D_{eff} = \frac{D_w}{\tau} \qquad \text{Eq. 3.6}$$

where τ is soil tortuosity (Webster et. al 1998). The first case examined by Harper et. al is the steady resupply of solute, which results in constant concentration gradients in the interstitial water layer and is defined by the boundary conditions in **Figure 3.2**. The initial condition for the first case is C_0=0, where C_0 is the initial concentration of solute.

The second case examined by Harper et. al is the supply of solute through diffusion only, which is defined by the boundary conditions in **Figure 3.2**. The initial conditions for the second case are C_0=0 in the sampler cells and C_0=1 in the sediment.

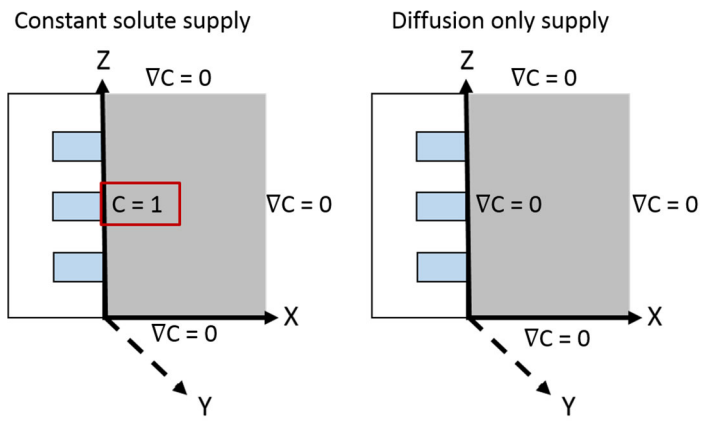

Figure 3.2. Boundary conditions for the case of constant solute supply (left) and solute supply limited by diffusion through sediment (right).

For the third case, in which solute is partially resupplied by desorption and partially by diffusion, Equations 3.7 and 3.8 are used:

$$\frac{\partial C}{\partial t} = -k_1 C + k_{-1} C_p C_s + D\nabla^2 C + R \qquad \text{Eq. 3.7}$$

$$\frac{\partial C_s}{\partial t} = \frac{k_1 C}{C_p} - k_{-1} C_s \qquad \text{Eq. 3.8}$$

where k_1 and k_{-1} are the soil desorption and sorption rate constants, respectively, C_p is the concentration of soil particles (particle mass/pore water volume), C_s is the concentration of solute sorbed to the solid phase, and R is an optional term that accounts for a vertical pore water concentration profile. The initial concentration of solute sorbed to the solid phase, $C_{s,0}$, is calculated by Equation 3.9:

$$C_{s,0} = K_d C_0 \qquad \text{Eq. 3.9}$$

where K_d is the distribution coefficient between the sorbed phase and dissolved phase. The initial conditions and boundary conditions for the partial resupply case are the same as those for the diffusion only case, with additional conditions put in place for C_s. There is an additional initial condition of $C_{s,0}=K_d$ due to the initial condition of $C_0=1$ in the sediment. There is also a boundary condition of $\nabla C_s=0$ at all four domain boundaries in addition to the previous boundary condition of $\nabla C=0$ at all boundaries.

The three models in Harper et. al determined that the constantly supplied case equilibrates the fastest, the diffusion only case equilibrates the slowest, and the partially resupplied case falls in between the other two, yet closer to the diffusion only case. Therefore, the partial resupply case is determined to be the most accurate in predicting equilibration times with an average time of 2-3 weeks, which is in agreement with other equilibration studies (Webster et. al 1998, Carignan 1984).

The equilibration time of passive samplers depends largely upon the size and orientation of the sample cells. Cells that are orientated with the membrane side facing horizontally tend to mix more efficiently and equilibrate more quickly than cells orientated with the membrane side facing upward or downward (Webster et. al 1998). Shallow cells, or cells with a larger area to volume ratio, tend to equilibrate more quickly than deeper cells. The area to volume relationship is described as the F factor of the cell and is represented by the following equation:

$$F = \frac{V}{A} \qquad \text{Eq. 3.10}$$

where A is the membrane covered area of the cell and V is the volume of the cell. When the cell is orientated horizontally it can be assumed that the cell is mixed instantaneously (Webster et. al 1998). When instantaneous mixing is assumed and transfer across the membrane is the time limiting step, the following equation can be used to describe equilibration dynamics within the cell:

$$C_{cell} = C_{sed}\left(1 - e^{\frac{-k_m t}{F}}\right) \qquad \text{Eq. 3.11}$$

where C_{cell} is the concentration inside the cell, C_{sed} is the concentration in the sediment, k_m is the membrane permeation speed, and t is time. In low permeability soils, the limiting step is likely to be solute diffusion through the soil as opposed to transfer across the membrane. Webster et. al employed a 2D model to investigate the case in which solute is transported to the cell by diffusion only, similar to the intention of one of the models previously discussed by Harper et. al. Equations 3.12 and 3.13 describe 2D diffusion of solute through the sediment using the model domain in **Figure 3.3**:

$$\frac{\partial C_b}{\partial t} = \emptyset D_{eff} \frac{\partial^2 C}{\partial x^2} + \frac{\emptyset D_s}{y} \frac{\partial}{\partial y} y \frac{\partial C}{\partial y} \qquad \text{Eq. 3.12}$$

$$C = \frac{C_b}{\emptyset} \qquad \text{Eq. 3.13}$$

where C_b is the bulk concentration of solute in the sediment and C is the pore water concentration of solute.

There are zero flux boundary conditions at S_f, concentrations remain constant at C0 along surfaces S_c, and at the membrane surface Equation 3.14 is applied:

$$flux = k_m(C - C_{cell}) \qquad \text{Eq. 3.14}$$

with initial conditions of $C=C_0$ and $C_{in}=0$. The model simulation predicts equilibration times between 20-30 days for a range of F factors; this prediction is similar to the equilibration times predicted by Harper et. al and also compares well with the typical deployment time of one month for most passive samplers.

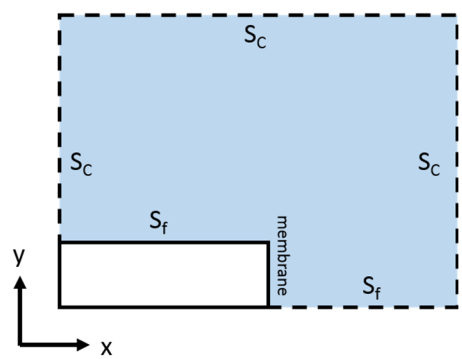

Figure 3.3. Model domain of 2D diffusion through soil into a horizontal sample cell.

3.6 Mass Transfer Related to Passive Sampling

3.6.1 Impact of Dimensionless Numbers on Mass Transfer Coefficient

The Reynolds number (Re) is a dimensionless number used in fluid dynamics to determine whether fluid flow is laminar or turbulent. It effectively evaluates the influence of momentum forces versus the influence of viscous forces for a given fluid in a given system, as can be seen by the relationship in Equation 3.15.

$$Re = \frac{momentum\ force}{viscous\ force} = \frac{\rho v L}{\mu} \qquad \text{Eq. 3.15}$$

where ρ is the fluid density, v is the fluid velocity, L is a characteristic length based on the geometry of the system under consideration, and μ is the dynamic viscosity of the fluid. Low Reynolds numbers (Re< 2000) indicate that viscous forces are dominant, causing the flow to be laminar. Laminar flow occurs because shear viscous forces work to dampen tendencies for momentum transfer that cause turbulence (**Figure 3.4**). High Reynolds numbers (Re> 4000) indicate that momentum forces are dominant, causing the flow to be turbulent. Turbulent flow occurs when transverse exchange of momentum is allowed through erratic fluid movement. Reynolds numbers between 2000 and 4000 indicate the transition range from laminar to turbulent flow.

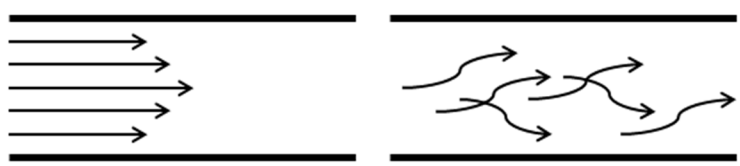

Figure 3.4. Laminar (left) and turbulent (right) flow in a pipe

The Schmidt number (Sc) is a dimensionless quantification of the ratio of momentum diffusion to molecular diffusion. It is analogous to the Prandtl number for heat transfer. There are slightly different definitions for the Schmidt number in laminar flow and in turbulent flow, as can be seen in the two relationships in Equations 3.16 and 3.17.

$$Sc_{laminar} = \frac{diffusion\ of\ momentum}{diffusion\ of\ mass} = \frac{\mu}{\rho D} \qquad \text{Eq. 3.16}$$

$$Sc_{\ turbulent} = \frac{eddy\ viscosity}{eddy\ diffusivity} = \frac{v_t}{K_{eddy}} \qquad \text{Eq. 3.17}$$

where D is the mass diffusivity of a given species in a given fluid, v_t is eddy viscosity, and K_{eddy} is eddy diffusivity. The necessity for different Schmidt correlations in laminar and turbulent flow conditions is due to the differing behavior of adjacent fluid layers in laminar and turbulent flow.

The Schmidt number is more intuitively understood under laminar flow conditions. Momentum diffusivity is the component of diffusion in a fluid that is caused by shear stresses between fluid layers with different velocities. Due to the no-slip condition, fluid flowing along a flat wall has a velocity of zero. The velocity gradually increases with distance from the wall. It follows that a velocity gradient is formed, and flow can be conceptualized as a series of fluid layers that build out from the no-slip wall with increasing velocities. Between each velocity layer shear force is acting in the direction of flow to speed up the slower layer as well as against the flow to slow down the faster layer (**Figure 3.5**). The diffusion of momentum that results from the shear forces is the momentum diffusivity in the numerator of the Schmidt number.

Molecular diffusivity is more straightforward than momentum diffusivity. Molecular diffusivity is also commonly referred to as mass diffusivity, and it is the rate at which a given species diffuses through a substance (such as water) due to an existing concentration gradient (**Figure 3.5**). Momentum typically diffuses much more quickly than mass in liquids, resulting in Schmidt numbers on the order of 10^3. Momentum and mass diffuse at approximately the same rate in gases, so the Schmidt number is typically 1.

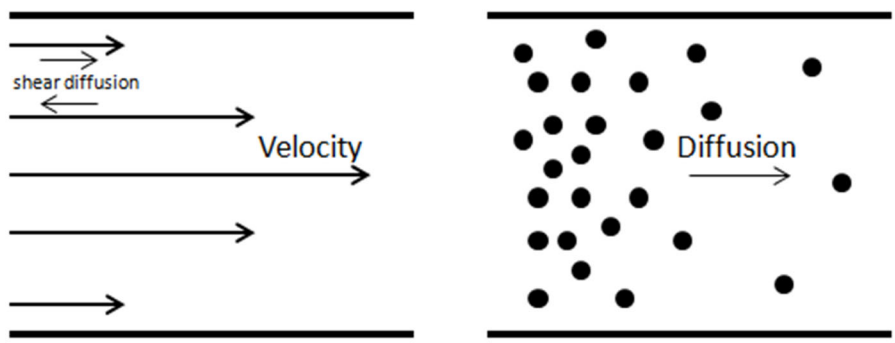

Figure 3.5. Momentum diffusivity (left) and molecular or mass diffusivity (right).

The product of the Reynolds and Schmidt numbers is the Peclet number. The Peclet number relates advective and diffusive transport through Equation 3.18:

$$Pe = (Re)(Sc) = \frac{advective\ transport}{diffusive\ transport} = \frac{vL}{D} \qquad \text{Eq. 3.18}$$

At high Peclet numbers, advection and dispersion dominate over molecular diffusion, and at low Peclet numbers diffusive transport governs mass transport.

The Reynolds, Schmidt, and Peclet numbers are related to heat or mass transfer through the Ranz-Marshall equation, which was derived for heat transfer to a single sphere (Ranz and Marshall 1952). Heat transfer through conduction and mass transfer through diffusion are analogous processes, so the Ranz-Marshall equation has been translated in the literature from the Nusselt number (Nu) for heat transfer to the Sherwood number (Sh) for mass transfer. The Sherwood number is related to the mass transfer coefficient, k, through the Ranz-Marshall based relationships shown in Equations 3.19, 3.20 and 3.21:

$$Nu = 2.0 + 0.6\, Re^{1/2} Pr^{1/3} \qquad \text{Eq. 3.19}$$

$$Sh = 2.0 + 0.6\, Re^{1/2} Sc^{1/3} \qquad \text{Eq. 3.20}$$

$$Sh = \frac{L_c k}{D} = \frac{rate\ of\ mass\ transfer}{rate\ of\ diffusion} \qquad \text{Eq. 3.21}$$

where k is the convective mass transfer rate and L_c is a characteristic length dependent upon the geometry of the system. The Ranz-Marshall equation provides a basis for the understanding of mass transfer, but empirical correlations are often necessary to derive Sherwood relationships for different geometries (e.g. flow through a packed bed rather than a single sphere).

This research concerns liquid mass transfer in a diluted packed bed, so it is relevant to understand how a range of Peclet numbers affects Sherwood correlations in porous media. Nusselt numbers, and therefore Sherwood numbers, in packed beds should be higher than those for a single sphere based on theoretical consideration of Equations 3.22 and 3.23 (Martin 1977):

$$Nu_{sphere} = 2 + F_{Nu} \frac{\sqrt{Pe/_4}}{\sqrt[6]{Pr}} \qquad \text{Eq. 3.22}$$

$$Nu_{packed\ bed} = [1 + 1.5(1 - \emptyset)]Nu_{sphere} \qquad \text{Eq. 3.23}$$

where F_{Nu} is a factor based on Reynolds number, Prandtl number, and free stream turbulence. Experimentally determined Sherwood numbers in packed beds at high Peclet numbers (Pe>200) have been found to be higher than theoretical Ranz-Marshall values for a single sphere (Martin 1977). However, experiments conducted in packed beds at low Peclet numbers (<100) yield results that indicate Sherwood numbers orders of magnitude lower than the theoretical value for a single sphere (Kunu and Suzuki 1967, Martin 1977, Rexwinkel et al. 1997). Kunu and Suzuki and Martin suggest particle size in the packed beds as a factor in decreasing Sherwood numbers for the same Peclet number. Both studies site that smaller particles result in lower Sherwood numbers. Beyond particle size, there is little consistent agreement on what causes extremely low Sherwood numbers at low Peclet numbers. Rexwinkel et. al suggests that the low Sherwood number results are potentially caused by misinterpretation of experimental results, arguing that radial concentration profiles should be considered to avoid wrongful application of plug flow models (1997).

4 MATERIALS AND METHODS

4.1 Development and Validation of the Use of HRPP to Determine In Situ Transport Parameters at High Resolution.

4.1.1 Development of a Method to Measure Pore Velocity

Overview- We used a passive diffusion, or peeper, sampler that enabled us to experimentally correlate pore velocity with the measured rate of mass transfer across the sampler membrane. The experiments generally consisted of inserting HRPP samplers in containers filled with saturated sediment and well-defined flow. The loss of a conservative tracer (Br^-) from the samplers was measured after a defined time period, and data was used to estimate the mass transfer coefficient of Br^-. By varying velocity in the flow boxes, a relationship between the mass transfer coefficient and velocity was developed.

The samplers were designed to measure velocity after a single deployment of the sampler. The change in the concentration due to transport of a conservative tracer into and out of a sample cell can be modeled based on Equations 4.1 and 4.2 respectively (Webster et al. 1998):

$$into \quad C = C_0\left(1 - e^{-\frac{k_m t}{V/A}}\right) \qquad - \qquad \text{Eq. 4.1}$$

$$out \quad C = C_0 e^{-\frac{k_m t}{V/A}} \qquad \text{Eq. 4.2}$$

where C is the concentration of a conservative tracer (bromide) inside the sample cell at time t, C_0 is the initial concentration of bromide inside the sampler, k_m is the measured mass transfer coefficient across the membrane, V is the volume of the sample cell, and A is the area of the opening of the sample cell. The only unknown variable in Equations 4.1 and 4.2 is k_m, which was solved for by equipping the sampler with multiple cells of varying specific surface area, (volume to opening area ratios (F=V/A)). After developing the experimental relationship between the mass transfer coefficient and velocity, a model based on basic transport parameters was developed to validate/explain the observed relationship.

4.1.1.1 Determination of Membrane Resistance

Prior to any flow box experiments, we conducted a stirred-tank bottle study to determine k_m of bromide for membrane resistance only (**Figure 4.1**). The bottle study was set up in a two-liter beaker filled with distilled deionized (DDI) water and covered with plastic wrap to prevent evaporation. Four 25 mL bottles were filled with 100 mg/L bromide solution, covered with the membrane, and submerged in the beaker. The membrane was sealed to the bottles using O-rings. Stir bars were placed inside the bottles and inside the beaker, and the beaker was placed on a stir plate to keep the system thoroughly mixed. The four bottles were analyzed for bromide concentration one at a time after three hours, six hours, 12 hours, and 24 hours. The experiment

was then repeated, and the bottles were sampled after six hours, 12 hours, 24 hours, and 48 hours. We then used the initial and final bromide concentrations of each bottle and Equation 4.2 to determine k_m for bromide for membrane resistance only.

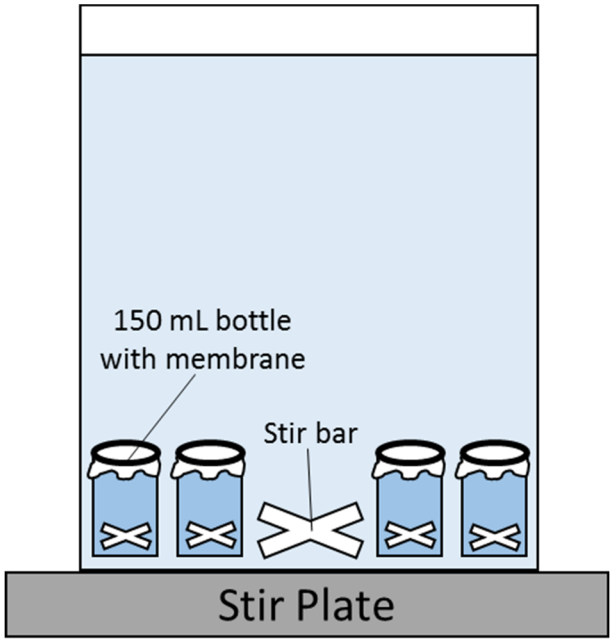

Figure 4.1. Conceptual schematic of stirred-tank bottle study to determine k_m of bromide for membrane resistance only. Bottles filled with bromide and beaker filled with DDI water.

4.1.1.2 Bench Scale Flow Box Experiments

The bench scale flow box system utilized a homogeneous coarse sand with a porosity of 0.37, and box dimensions that are outlined in **Figure 4.2 and 4.3**. The influent and effluent ends of the box were filled with pea gravel to promote consistent mixing of the water supply. Deionized water was pumped into and out of the box through evenly spaced flow ports to encourage straight and uniform flow lines across the fully saturated sand. The flow paths across the box were monitored visually through the use of dye tracer tests.

We added 100 mg/L of chloride to the influent water and allowed time for the flow box to equilibrate with the chloride solution. Chloride was used as an external conservative tracer in the same way as bromide, with the only difference being that chloride was transferred into the cells and bromide was transferred out of the cells. Thorough equilibration of the box was verified by collecting water samples from the side and effluent ports and comparing the sample concentrations of chloride to influent concentrations. The velocity of across the flow box was controlled through the use of inlet and outlet peristaltic pumps.

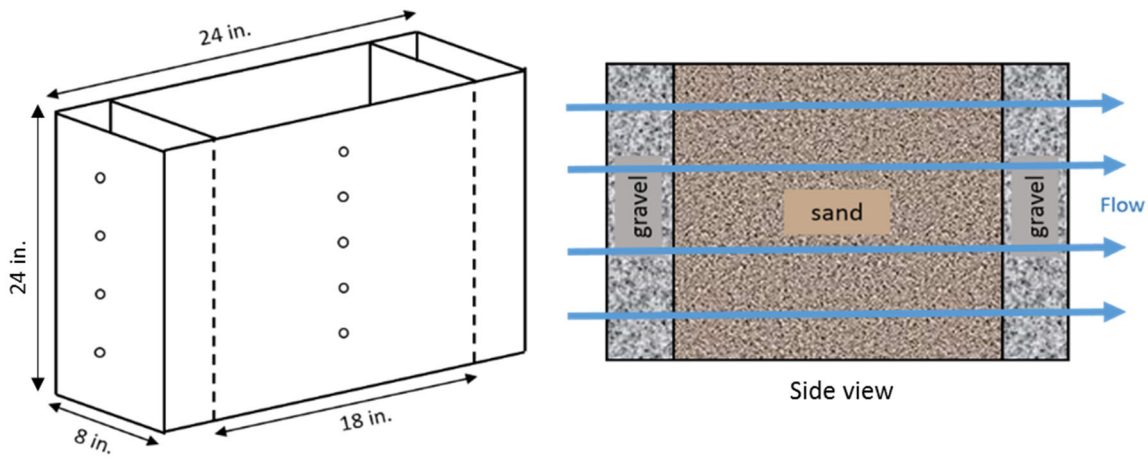

Figure 4.2. Dimensions, 3D view, and side view of laboratory flow box system.

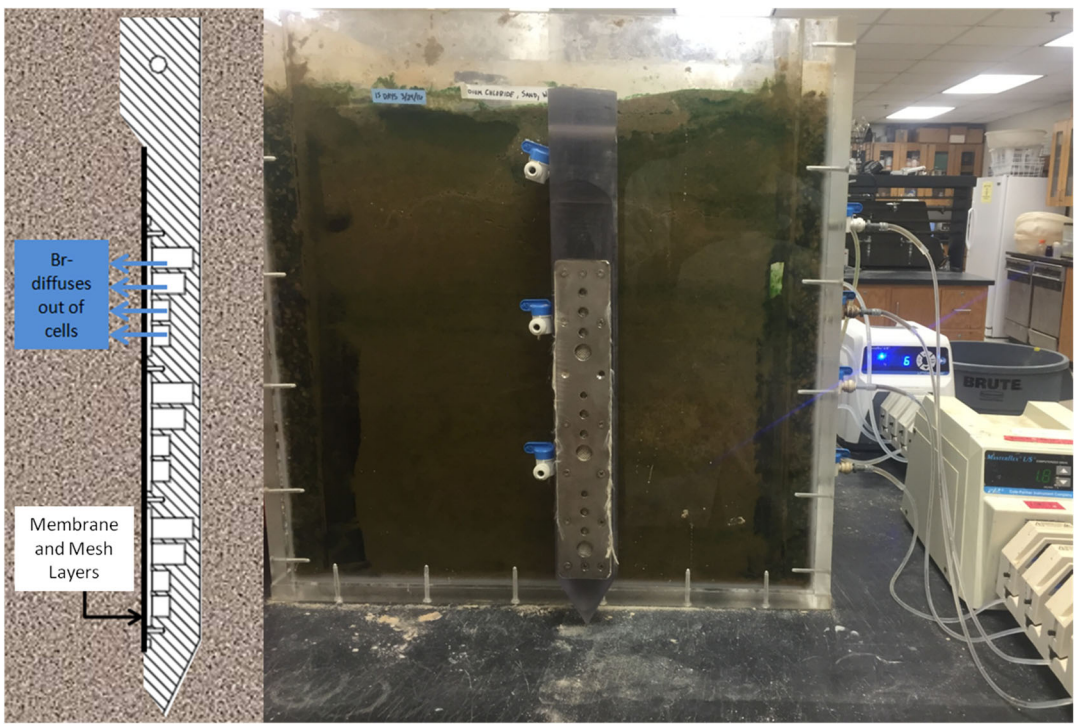

Figure 4.3. Velocity HRPP cross-section in sediment and laboratory flow box setup.

The samplers were made of polycarbonate, and the PES membrane was attached to the sampler with a stainless steel cover plate and stainless steel screws. Prior to insertion into the flow box, the sampler was assembled under water in a 100 mg/L bromide solution. The cell volumes, opening areas, and corresponding F factors that were utilized for the sampler in this study are outlined in Table 4.1. F factors (F=V/A) of the cells were specifically chosen so that the cells would reach a range of C/C_0 values between 0.2 and one in a deployment time of three weeks. The time the cells require to equilibrate with the pore water is dependent upon F, so F could be

adjusted to allow for a shorter or longer deployment time if desired. One set of sample cells included four different F factors, and the samplers were equipped with three sets of cells (**Figure 4.4**). The three data sets per sampler allowed for three measurements of k_m per experiment, which were used to evaluate the precision of the method.

Table 4.1 Area/Volume ratios utilized in laboratory flow box experiments.

Cell #	Opening Area (cm^2)	Volume (cm^3)	F (V/A) (cm)
1	0.3	6.3	21
2	0.5	5	10
3	0.5	2.8	5.5
4	2	2.8	1.5

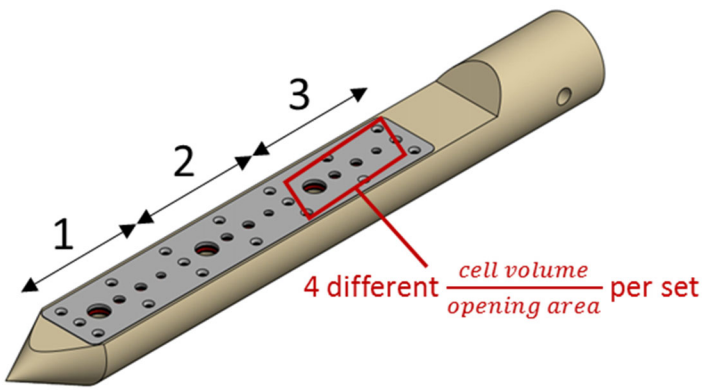

Figure 4.4. Lab scale passive sampler design: three sets of four cells with varying cell volume to opening area ratios (V/A).

One experimental sequence consisted of the following steps: 1) inserting an assembled sampler filled with 100 mg/L bromide solution into the flow box, which was saturated with 100 mg/L chloride solution; 2) removing the sampler after a time period of one to three weeks; 3) using ion chromatography to analyze the sample cells for bromide and chloride concentrations; 4) using the bromide concentration and Equation 4.2, and the chloride concentration and Equation 4.1, to determine k_m. An example of the data fitting for Br^- is presented in **Figure 4.5**.

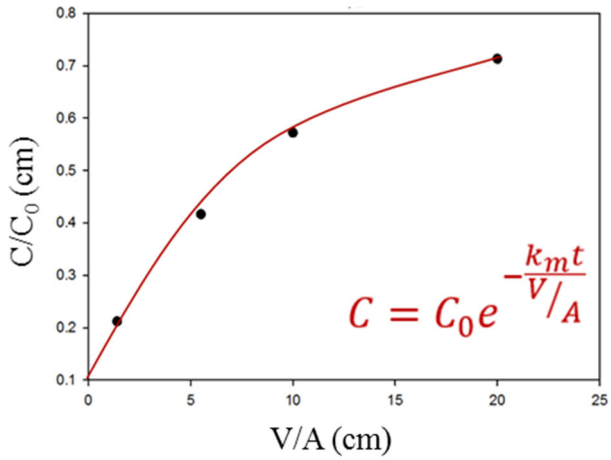

Figure 4.5. Example curve fit to determine k_m from four cell volume to opening area ratios (V/A).

A series of experiments was performed in which velocity of pore water was systematically varied (0, 1, 5, 10, 15, 60, and 100 cm/day). The samplers were ultimately intended to have a single deployment time of three weeks, but experiments were additionally run for durations of 6, 9, 12, 15, and 18 days to evaluate the possibility of k_m being dependent on deployment time. Other experiments evaluated the impact of sampler orientation. For the initial velocity experiments, the sampler was placed so that flow was perpendicular to the face of the peeper. A series of velocity experiments at 1, 10, and 100 cm/day were conducted with the sampler rotated 90 and then 180 from the original orientation (**Figure 4.6**).

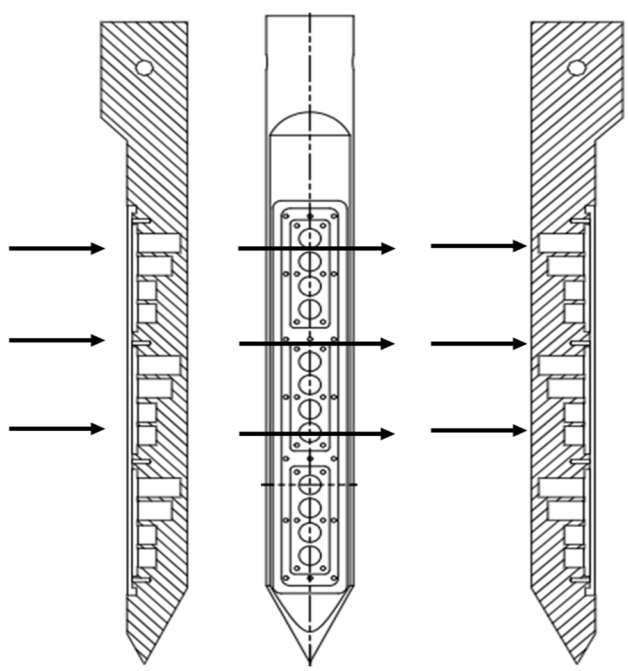

Figure 4.6. Sampler was tested at three orientations to flow: perpendicular to flow (left), parallel to flow (center), and 180° away from flow (right).

4.1.1.1.1 Intermediate Scale Experiments

The second experimental system was a two-layer structure of high permeability sand and low permeability clay in a larger flow box (**Figure 4.7**) that used full size HRPP samplers developed in Task 3; these same samplers were deployed at Alameda, CA during the field trial. The purpose of the larger, stratified system was to evaluate effects of soil permeability on the velocity-k_m correlation. The bottom half of the box was filled with a mixture of sand and kaolin clay with a hydraulic conductivity of 10^{-4} cm/s, and the top half of the box was filled with sand with a hydraulic conductivity of 10^{-2} cm/s. As with the small flow box experiments, the flow box was allowed time to equilibrate with 100 mg/L chloride solution that was pumped through the box using peristaltic pumps. The full-scale samplers are four feet (1.2 meters) long and have five sets of velocity cells evenly distributed over that length (**Figure 4.8**). The sampler was inserted into the box at a depth that allowed two sets of cells to rest in the sand and two sets of cells to rest in the clay, with the fifth set located at the sand-clay interface.

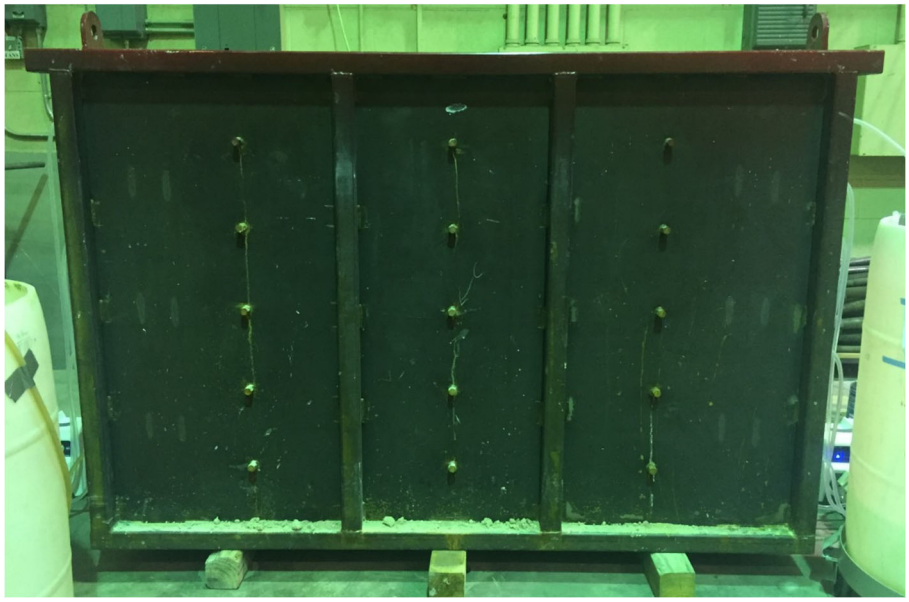

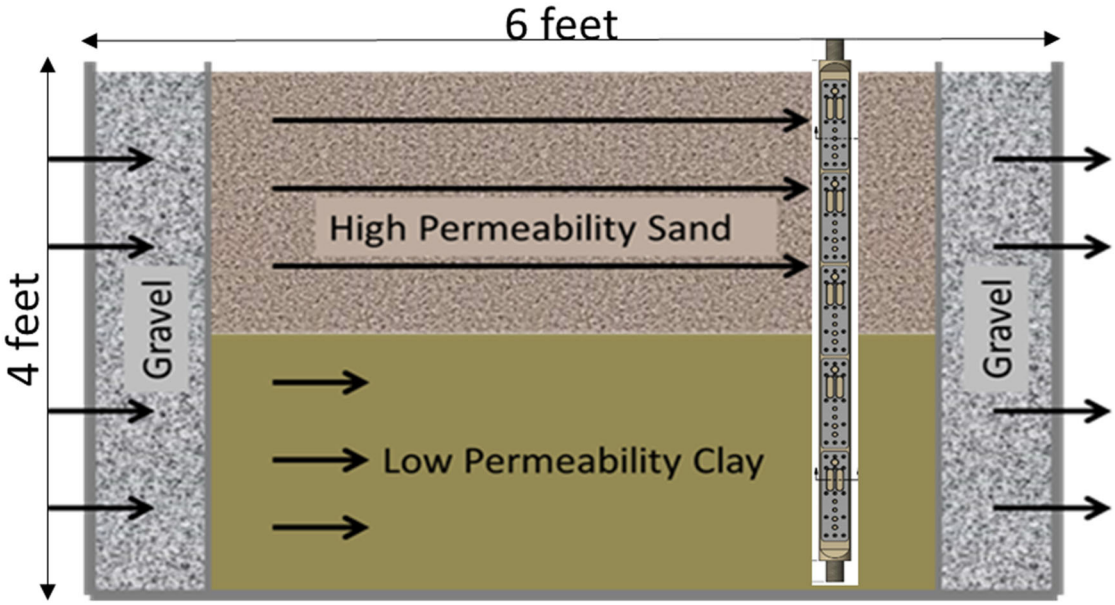

Figure 4.7. Large flow box system with clay on bottom half and sand on top half.

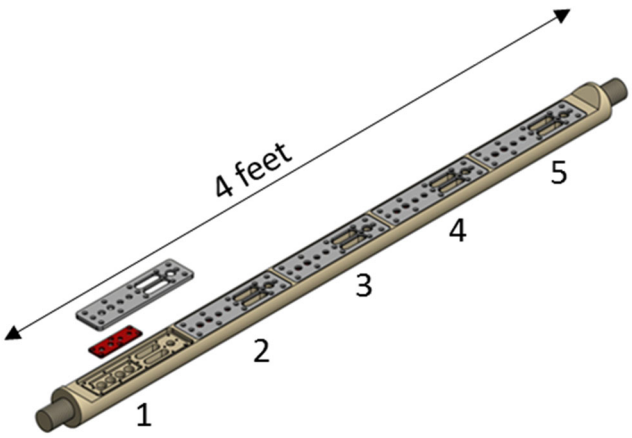

Figure 4.8. Four-foot sampler design with five sets of velocity cells

In the large flow box, velocity experiments were performed for velocities in the sand of 10 and 60 cm/day. Flow rates and velocities were calculated based on the assumption that a negligible amount of flow occurred through the clay, which was verified with tracer tests prior to the insertion of samplers. Samplers were inserted and allowed three weeks to equilibrate before extraction and sampling.

4.1.2 Verification of Using HRPP for Measurement of Contaminant Concentration and Flux

Analogous to Br^- migration from the HRPP cell, migration of dissolved contaminants (e.g., TCE) from groundwater into the HRPP cell occurs and is controlled via external mass transfer. Experiments to determine the relation of the equilibration rate of the contaminant (TCE) or other dissolved species of interest (e.g., Br^-) between the HRPP and the bulk groundwater were conducted in the flow chamber experiments as described in section 4.1.1. Water containing Cl^- and TCE was pumped through the flow box until constant concentrations were achieved based on effluent pore water concentrations. Samplers that included four V/A ratios (1, 1.5, 2, and 2.5 cm) were driven into the flow box and removed after 1, 3, and 6 days. Sample cells contained water with a Br^- tracer. After sampler removal, water in the sample cells was removed using a syringe and tested for concentrations of Cl^-, Br^-, and TCE. The change in concentration over time was modeled using Equations 4.1 or 4.2 for Br- and Cl^- and TCE, respectively.

4.2 Development and Validation of HRPP Micro-Biotraps To Evaluate CSIA of Adsorbed CVOCs and Microbial Community Structure and Activity.

Inclusion of bio-traps for microbial community analysis and CSIA of solvents trapped on the Bio-sep beads were evaluated in two experiments. The first experiments deployed an early prototype of the HRPP in wells at Fort Dix (NJ) and Kelley Air Force Base (TX) and compared the microbial community analysis and CSIA results between a standard Bio-trap deployed in the

well and HRPP micro-biotraps deployed in the wells. The second set of experiments used a lab scale HRPP and bench top flow cell.

4.2.1 Prototype Testing in Wells

The HRPP micro-biotrap units were incubated in the wells for 4-6 weeks, and then removed and shipped to the APTIM laboratory in Lawrenceville, NJ. The media were removed from the HRPP cells into sterile tubes, and these tubes and the standard Bio-traps were shipped to Microbial Insights (Knoxville, TN) for microbial analysis using qPCR (QuantArray-Chlor; http://www.microbe.com/quantarray-chlor/). This molecular technique provides densities of key dehalogenating bacteria and genes, methanogens, sulfate-reducers, select aerobic cometabolic genes, and total Eubacteria. Subsamples of the Bio-sep beads, GAC, and Ag-GAC deployed in Bio-traps and model HRPP micro-biotraps at Fort Dix and Kelley Air Force Base were also submitted for analysis of $\delta^{13}C$ in adsorbed TCE. Photographs of the model HRPP samplers are provided in **Figure 4.9**.

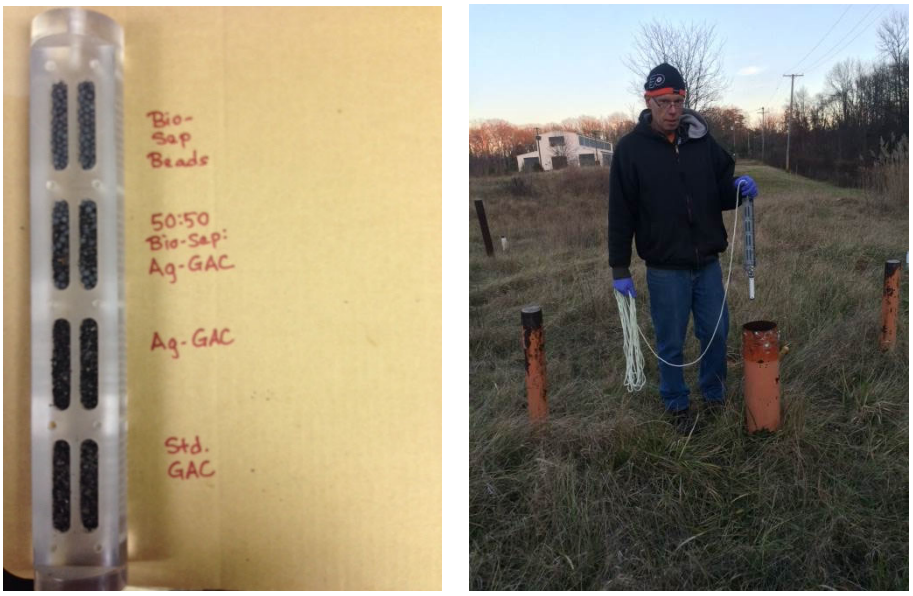

Figure 4.9. Photograph of HRPP unit packed with different media (left photograph) and HRPP and Bipotrap being lowered into monitoring well at Fort Dix, NJ (right photograph).

4.2.2 Lab Testing in Flow Cells

Testing was conducted in a flow cell, similar to that used in Section 3.1 with two layers of sediment differing in hydraulic conductivity by a factor of greater than 100 (**Figure 4.10**). The lower permeability layer had a hydraulic conductivity estimated to be approximately 7 x 10^{-4} cm/s, and the higher permeability layer was a well-sorted sand with a hydraulic conductivity that likely exceeded 0.1 cm/s based on its effective grain size. Influent water was continuously cycled immediately up-gradient from the layered sediments to ensure homogeneous concentrations. To distribute amendments in the lower permeability layer, water levels were lowered to force flow

through it, and water containing TCE (1 mg/L), emulsified oil, and a dechlorinating culture were sequentially added before raising water levels to saturate both layers of sediment again.

After loading of the lower permeability layer, influent water was continuously amended to include approximately 1 mg/L of TCE. TCE, *cis*-DCE, VC, and DO levels in the two layers were sampled using appropriately placed side ports. After an incubation period, lab scale HRPPs (see **Figure 4.11**) with micro-biotraps were emplaced for 25 days across the two layers to demonstrate their ability to distinguish differences in microbial populations. Bio-sep beads were removed from the HRPP micro-biotraps and sent to Microbial Insights for QuantArray-Chlor analyses. Subsamples of Bio-sep beads and pore water from the deployed samplers in each zone of the flow box were also submitted for CSIA.

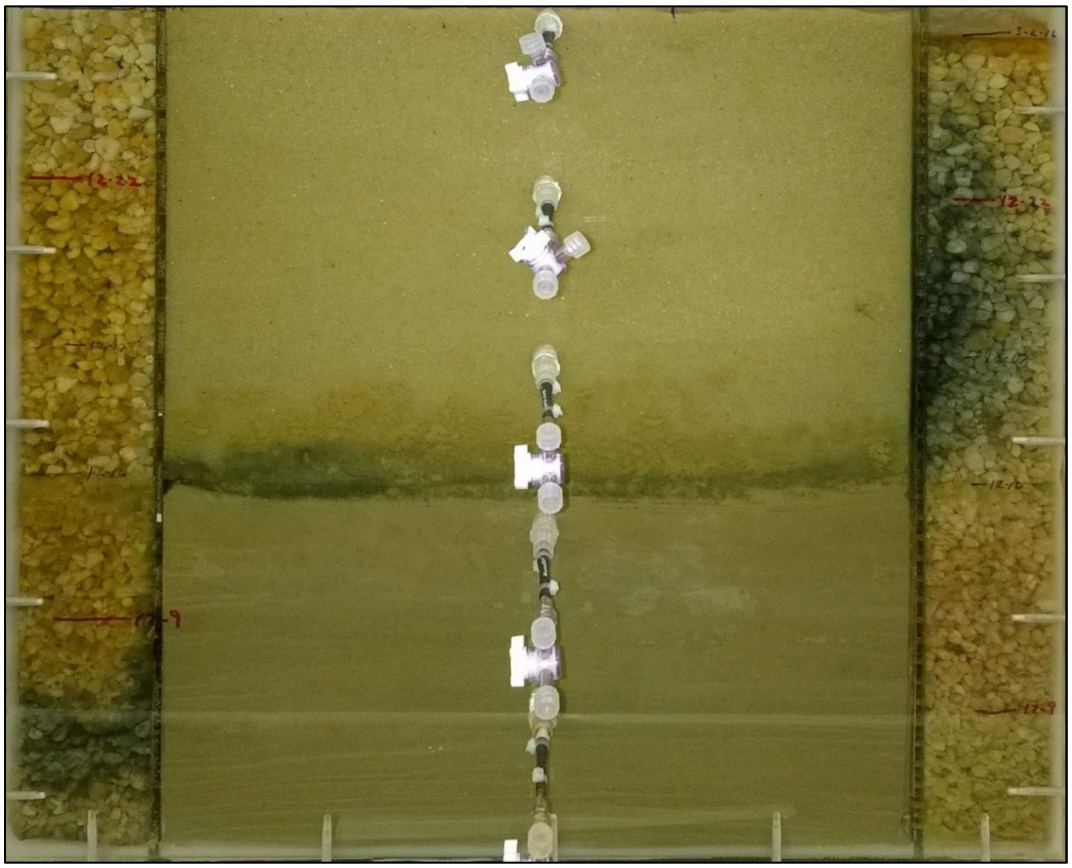

Figure 4.10. Sectional view of flow with two layers of differing hydraulic conductivities. Dark precipitates are visible at the oxic/anoxic interface.

Figure 4.11. Small scale HRPPs after removal from layered flow cell.

4.3 Development of an HRPP Capable of Direct Drive Insertion in Shallow Aquifers.

Three versions of the HRPP (A, B, and C) were developed over the course of the project. After design and production of each sampler, a field test was conducted to evaluate the HRPP performance and usability. The results of each field test were used to optimize the performance and usability of the next generation. The HRPP design was based on: (1) incorporating the volume requirements for equilibrated water and BioSep beads; (2) optimizing the V/A ratios and spacing of the cells used to measure velocity; and (3) providing enough structural integrity to prevent physical deformation of the structure during insertion. Each HRPP version was capable of measuring concentrations of dissolved species in pore water, groundwater velocity, microbial community abundance and composition, and stable isotopic composition of CVOCs**.**

4.3.1 HRPP General Design

The modular sampler was designed to consist of 1.2 m long stainless steel segments. The segments were coupled together to allow evaluation of any desired depth interval. The segment(s) were designed to be inserted into shallow aquifers via direct push using a Geoprobe. The HRPP design consists of three cell types with varying purposes that are repeated over the length of the HRPP. The three different cell types function to: (1) assess microbial community structure and CSIA of CVOCs; (2) quantify contaminant concentrations and geochemistry; and (3) measure groundwater velocity. There are five sets of each cell type over each HRPP segment (1.2 meters), resulting in one complete sample interval (including equilibrium, micro-bio-trap, and velocity) approximately every 20 cm. Cells that are designed to equilibrate with pore water are covered by a membrane of appropriate pore size (e.g. 0.45 µm), a fine (10 µm) woven nylon mesh to prevent intrusion of fine sediment, and a coarse (100 µm) stainless steel mesh to prevent membrane puncture from gravel/sediment. Cells containing Biosep beads are covered by only the 100 µm stainless steel mesh. The membrane and meshes are attached to the body of the sampler using a cover plate and screws.

4.3.2 HRPP-A

The first prototype (HRPP-A) was 5 cm in diameter and 1.2 m in length, with a tapered point on one end and threads on the other to allow attachment to a Geoprobe drive rod. The sampler consisted of five sets of cells over the length of the sampler. Each set of cells consisted of six velocity cells that varied in V/A ratios (F=V/A= 2.4, 2.8, 3.3, 5.7, 10, and 21.5 cm), two side by side cells for equilibrium with pore water (1.25 cm wide, 5 cm long, 1.25cm deep), and a cell for BioSep beads (2.5 cm diameter) with a 1 cm pass-through hole to allow pore water to pass through the beads (**Figure 4.12**). The equilibrium cells (~10 ml each) were designed for VOC monitoring and geochemical parameter monitoring (e.g. NO_3^-, NO_2^-, SO_4^{-2}, Cl^-, HS^-, and Fe (II, III, or Total)). The micro-biotrap was designed to monitor the microbial community and allow for CSIA of CVOCs. HRPP-A was field tested at Fort Dix near Trenton, New Jersey, in September 2015.

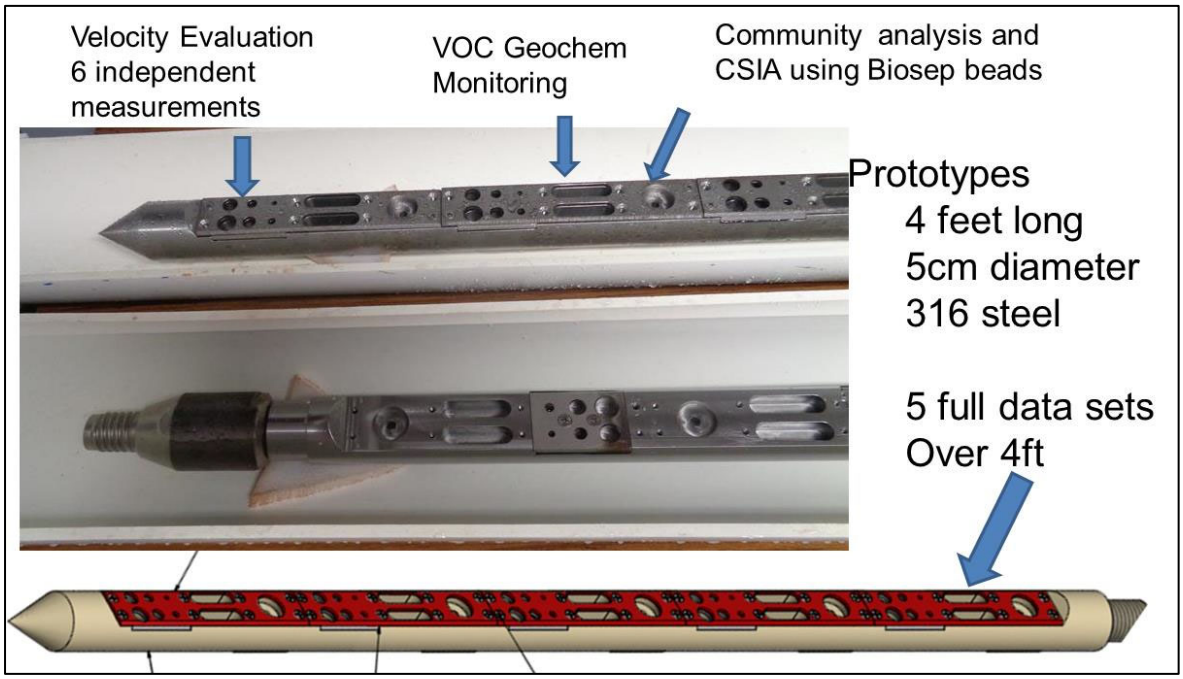

Figure 4.12. HRPP prototype 1.

4.3.3 HRPP-B

The second generation HRPP incorporated lessons learned from the deployment at Fort Dix. The length of the HRPP was kept at 1.2 m, with five sample intervals over the length. Threaded couplers were added at either end of the HRPP, allowing multiple sections to be coupled together to achieve a broader vertical range of data. The diameter of the HRPP was increased from 5 to 6.25 cm to allow more space between cells and allow cover plates to be inset. The three cell functionalities, equilibrium, micro-biotrap, and velocity were implemented in HRPP-B, but the number of velocity cells was reduced from six to four with volume to area ratios outlined in

Table 4.2. The dimensions of the micro-bio-trap were altered to make it narrower (1.3 cm) and deeper (1.3 cm) than the first-generation design. The cover plates were modified to be inset into the body of the HRPP (**Figure 4.13**) to provide greater resistance to soil intrusion around the edges of the plates. HRPP-B was field tested in 2016 at the former Alameda Naval Air Station in Alameda, California.

Table 4.2 Area/Volume ratios of velocity cells for second iteration HRPP design (Alameda, CA field trial).

Velocity Cell #	Opening Area (cm^2)	Volume (cm^3)	F (V/A) (cm)
1	0.3	6.3	21
2	0.5	5	10
3	0.5	2.8	5.5
4	2	2.8	1.5

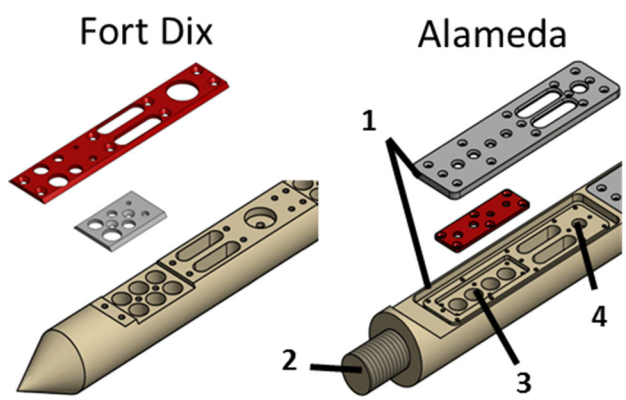

Figure 4.13. HRPP design modifications: 1) inset cover plates; 2) capable of coupling multiple four-foot sections; 3) fewer velocity cells; 4) smaller microbial/CSIA cells.

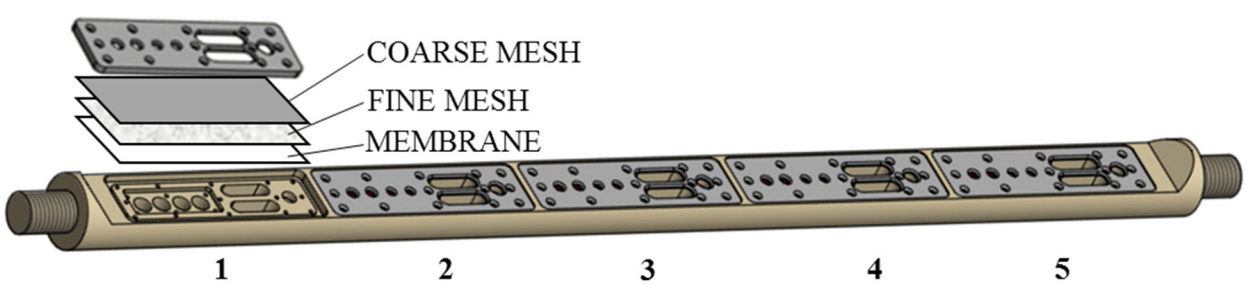

Figure 4.14. General design of the HRPP-B including five cells sets over four-foot length, coarse stainless steel mesh, fine nylon mesh, and 0.45 µm membrane attached with cover plate and screws.

4.3.4 HRPP-C

The final HRPP version (HRPP-C) was modified based on the results of the field test at Alameda Naval Air Station. The basic sampler design and dimensions stayed the same as HRPP-B, but reduced the number of screws used to retain the cover plates and redesigned the cover plates to increase the surface area in contact with the membrane and sampler. HRPP-C was field tested at the BARC site near Beltsville, Maryland in 2019.

4.4 Field Demonstrations

The HRPP was tested in three sequential field trials. The first field trial took place at Fort Dix near Trenton, New Jersey, in September 2015. Two HRPP-A samplers were installed and HRPP data were compared to nearby monitoring well data and standard Bio-traps. Design modifications were made to the HRPP before HRPP-B was tested a year later (September 2016) at the former Alameda Naval Air Station in Alameda, California. HRPP-A and HRPP-B samplers were deployed at Alameda, and HRPP data were once again compared to nearby monitoring well data, standard Biotraps, data from a Membrane Interface Probe (MIP) and Hydraulic Profiling Tool (HPT), and soil core data. On completion of the Alameda deployment, additional design changes were made and the new version (HRPP-C) was deployed at the USDA BARC site in Maryland.

4.4.1 Fort Dix Field Deployment

4.4.1.1 Site Description and Sampler Location

The HRPP was tested at Fort Dix in Trenton, New Jersey, in September 2015. The depth to groundwater table varied from 0.6 to 3.0 m BGS depending on location within the site, because the ground surface elevation (GSE) varied across the site. The site was characterized by two primary silty/fine sand aquifer formations, Kirkwood and Vincetown, physically divided by a 0.15 to 0.3 m thick fine sand and gravel interface (**Figure 4.15**). The upper Kirkwood formation was approximately 6 m thick and was characterized by low or non-detect TCE concentrations and *cis*-DCE concentrations of 20-200 µg/L (**Figure 4.16**). The lower Vincetown formation, hydraulically connected to the Kirkwood formation by the thin gravel interface, was approximately 10.5 m thick and was characterized by higher concentrations of both TCE (70-220 µg/L) and *cis*-DCE (300-800 µg/L). The TCE and *cis*-DCE concentration estimates were collected in August 2015 from a series of monitoring wells with varying screen intervals, three of which were centrally located in the plume (MAG 4, MAG 66, and MAG 112) (**Figure 4.16**) and were used as reference wells to evaluate performance of the HRPPs for the Fort Dix site. The well screen for MAG 4 was a 3 m screen that intersected both the Kirkwood and Vincetown formations as well as the gravel interface. MAG 66 was also a 3 m screen, but it lies predominantly in the lower Vincetown formation and barely intersects the gravel interface. MAG 112 is a 1.8 m screen that is completely below the interface in the Vincetown formation.

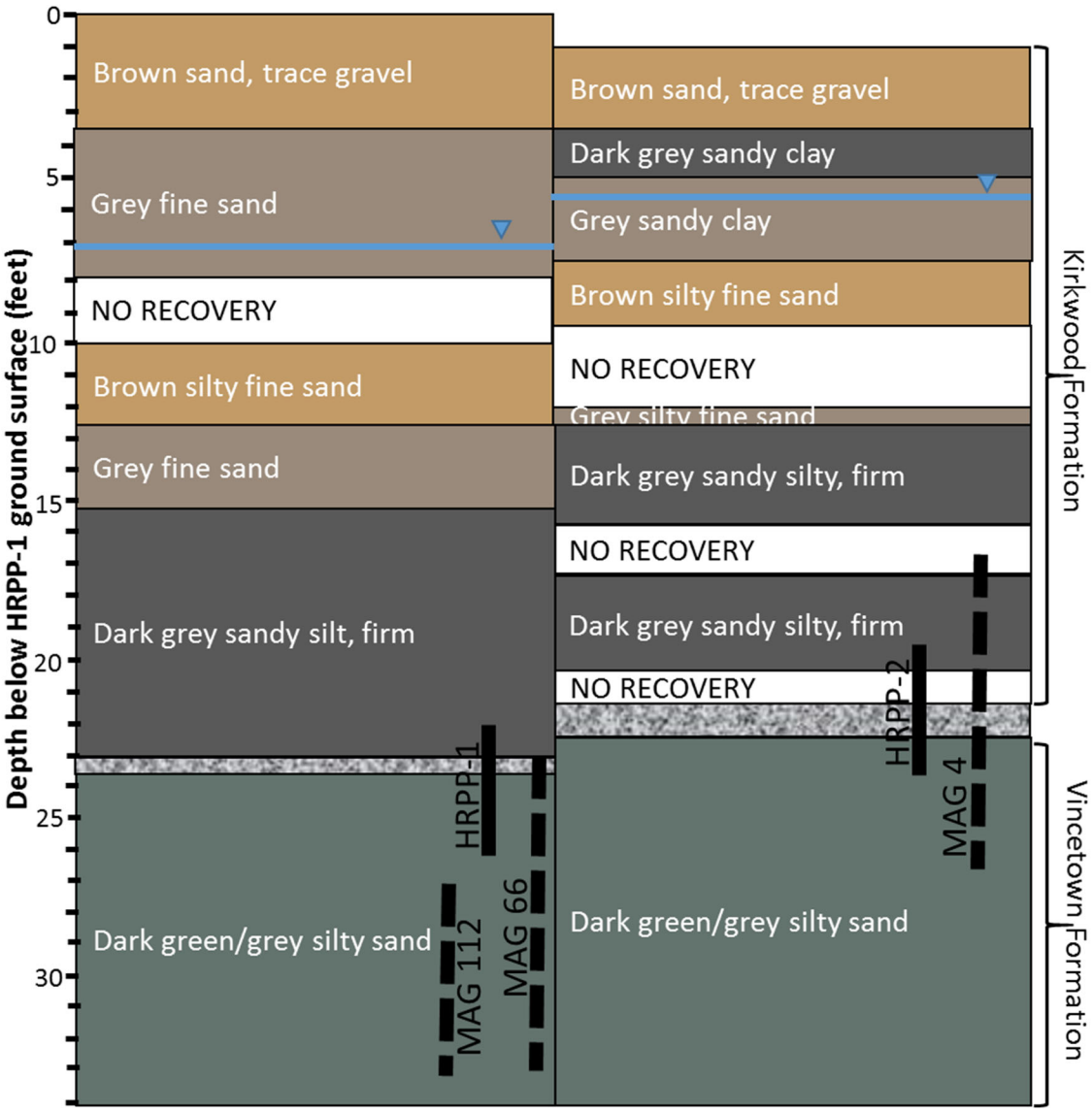

Figure 4.15. Installment depths (feet BGS) of well screens and HRPPs at Fort Dix site. Note: Ground surface elevation (GSE) varies between the two HRPP locations. GSE at HRPP-1 is used as reference for this figure.

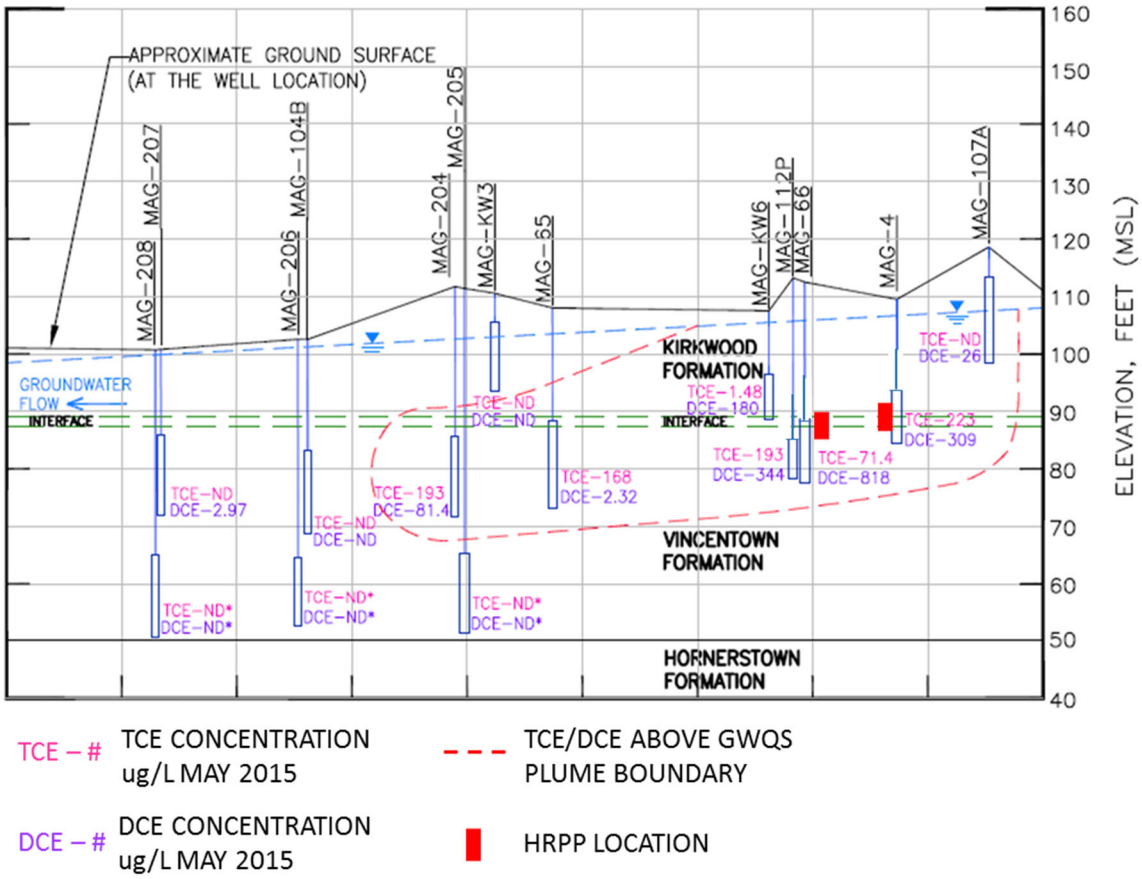

Figure 4.16. Cross-section of Fort Dix well and HRPP depths/locations showing plume concentrations of TCE and *cis*-DCE.

4.4.1.2 HRPP Installation, Retrieval and Sampling

Two HRPP-A samplers were installed in September 2015 for a deployment time of three weeks. HRPPs were prepared on-site in PVC troughs that were filled with DDI water spiked with bromide (~100 mg/L). The HRPPs were submerged in the bromide solution while membranes, meshes, and cover plates were attached. Each HRPP took approximately 30 minutes to assemble. Once assembled, the HRPPs were taken directly from the PVC trough and coupled to a Geoprobe rig for insertion.

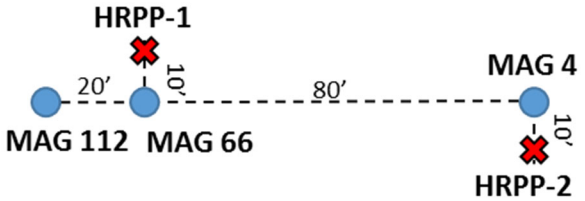

Figure 4.17. Aerial view of HRPP and well spacing at Fort Dix site.

HRPPs were installed using a Geoprobe up to 7.9 meters BGS within three meters of monitoring wells (**Figure 4.17 and 4.18**) in order to collect concentration, geochemistry, CSIA, and microbial community data sets for comparison at similar spatial and depth locations. After coring to a depth of 8.2 m BGS, HRPP-1 was installed into the core location at a depth of 6.7 to 7.9 m BGS. HRPP-1 was installed near MAG 66 and MAG 112, where the mean sea level elevation of the ground surface is approximately 34.4 m. After coring to a depth of 8.5 m BGS, HRPP-2 was installed into the borehole at a depth of 5.5 to 6.7 m BGS. HRPP-2 was installed near MAG 4, where the mean sea level elevation of the ground surface is approximately 33.5 m. Depths BGS of wells and HRPPs were calculated based on the respective location elevations. MAG 4 was screened from 4.6-7.6 m BGS, MAG 66 was screened from 7.6-10.7 m BGS, and MAG 112 was screened from 8.8 to 10.7 m BGS.

Bio-traps were deployed in MAG 4, MAG 66, and MAG 112 at the time of HRPP installment (September 2015) and were retrieved three weeks later at the time of HRPP retrieval to collect a comparative microbial community data set. Well water samples were collected from MAG 4, MAG 66, and MAG 112 one month prior to HRPP installment (August 2015) and analyzed for CVOCs (TCE, *cis*-DCE, and vinyl chloride), common anions (sulfate, phosphate, and chloride), CSIA of CVOCs, and microbial communities.

The HRPPs were extracted with a Geoprobe, and the faces were rinsed with DI water then blotted with KimWipes. Glass gas-tight syringes were used to extract the full volume of the equilibrium cells (10 mL). We used the 10 mL to fill 7 mL HCl preserved VOA vials (actual volume ~8.8 mL) for CVOC analysis, and the remaining 1-2 mL was stored in sterile plastic conical tubes for geochemistry analysis. Geochemistry samples were shipped on ice to Texas Tech University for anion analysis, and CVOC samples were shipped on ice to Aptim Analytical and Treatability Laboratory. Biosep beads were removed with a spatula, gently washed with sterile solution to remove sediment, and placed into sterile 50 mL plastic conical tubes, then shipped on ice to Microbial Insights (Knoxville, TN) for CSIA of CVOCs in conjunction with QuantArray analysis of organisms and functional genes. Velocity cells were sampled using a syringe. A list of analytical methods, location of analysis and sample vial and preservative is shown in Table 4.3.

Table 4.3 Analytical Parameters and Laboratories.

Analyte	Method	Vial and Preservative	Location
cVOCs	EPA 8260 (GC-MS)	7-mL VOA; HCL, 4ºC	APTIM
Methane, ethane, ethene		2-ml VOA; 4°C	APTIM
Anions (SO_4^-, NO_3^-, NO_2^-, Cl^-, Br^-)	EPA 300	15-mL SC tube; 4ºC	Texas Tech
Microbial community	Quantarray qPCR	Sterile 20 mL VOA; 4ºC	Microbial Insights
CSIA (TCE, cis-DCE, VC)	C-stable isotope analysis	Sterile 20 mL VOA 4ºC	Microbial Insights

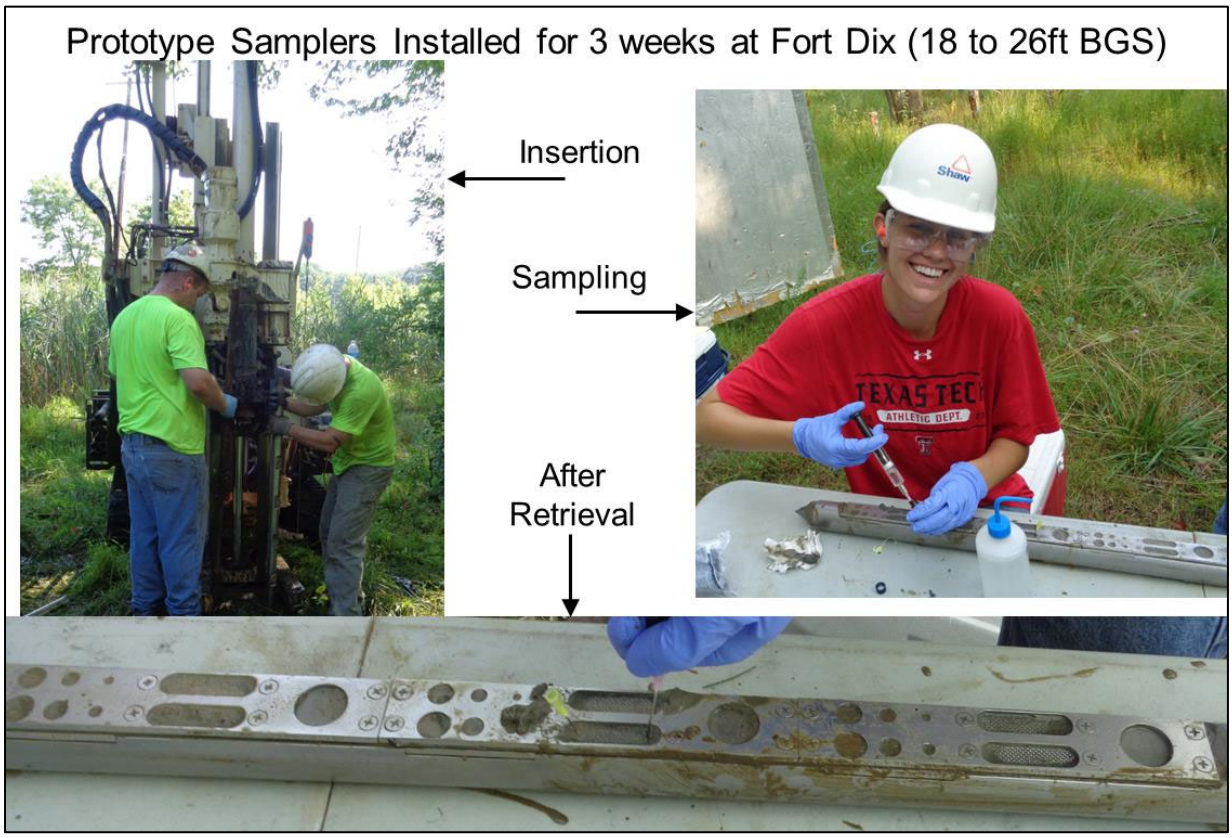

Figure 4.18. Photographs of: 1) prototype samplers (HRPP-P1) being installed at Fort Dix in September of 2015 (upper left); 2) HRPP-P1 being sampled (upper right); and 3) sampler after insertion (bottom center).

4.4.2 Alameda Naval Air Station Field Deployment

4.4.2.1 Site Description and Sampler Location

The second HRPP design (HRPP-B) was tested at the former Naval Air Station in Alameda, California. The site was characterized by a shallow groundwater table approximately 1.5 m BGS and heterogeneous stratigraphy (**Figure 4.19**). The area of interest is a DNAPL source zone of TCE that is approximately 9.3 m^2. There are several multilevel and standard monitoring wells in the DNAPL source zone (**Figure 4.20**) from which CVOC concentration measurements, geochemistry, microbial data, and CSIA were taken in August of 2016, one month prior to deployment of the HRPPs. The wells were found to have TCE concentrations up to 3.5×10^4 µg/L, and *cis*-DCE and vinyl chloride concentrations up to 1.3×10^5 µg/L and 2.3×10^4 µg/L, respectively. There is significant variability in CVOC concentrations with depth based on multilevel wells.

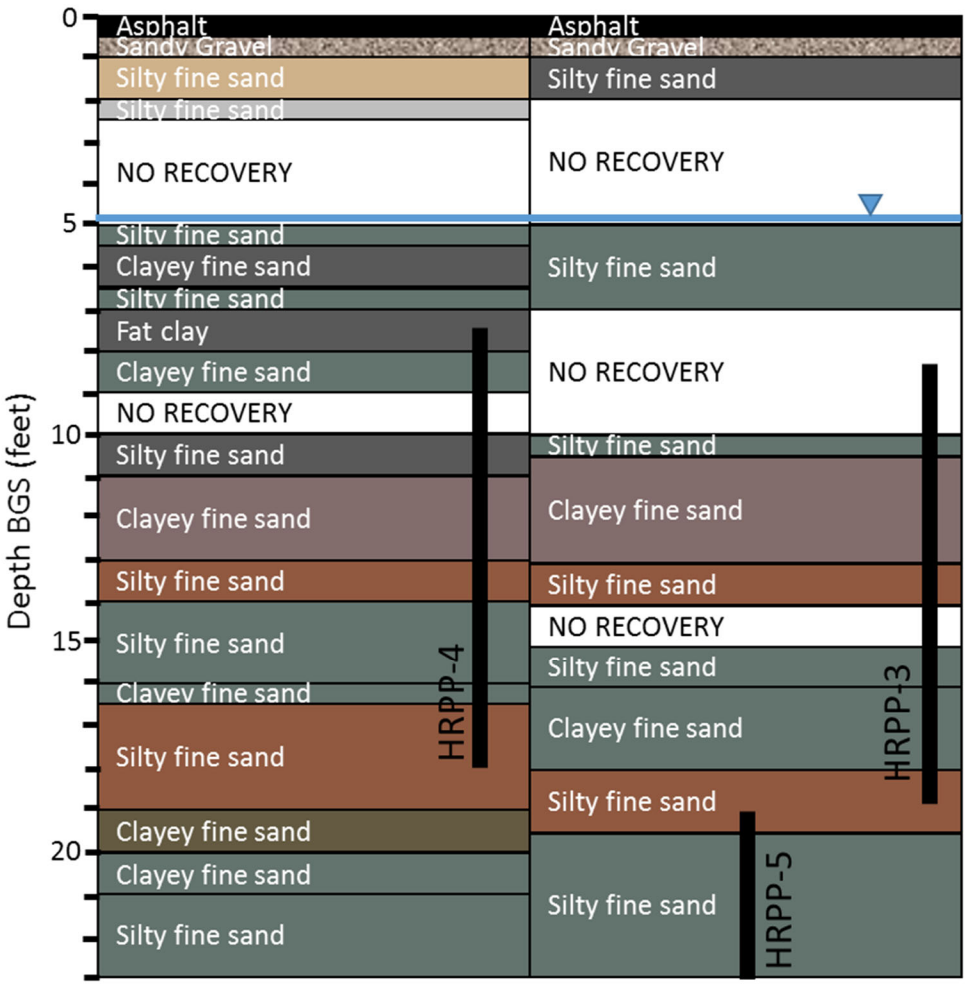

Figure 4.19. Alameda site stratigraphy and HRPP insertion depths.

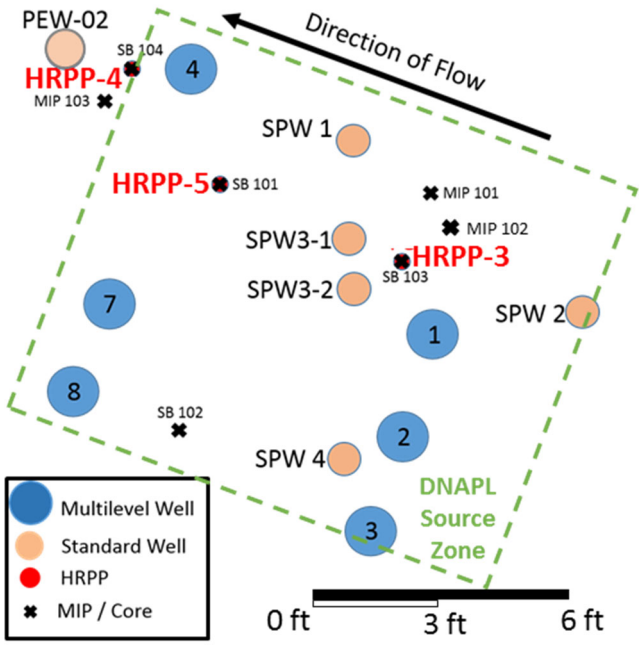

Figure 4.20. Alameda DNAPL source zone and location of wells, MIP/HPT, soil cores, and HRPPs.

4.4.2.2 HRPP Installation, Retrieval and Sampling

Six HRPP-B samplers were constructed to field test at Alameda. The velocity, equilibrium, and microbial cells of the Alameda HRPPs function the same as those for the Fort Dix prototype. In addition to the six second-generation HRPPs, one first-generation HRPP was deployed at Alameda. At the time of HRPP insertion, an MIP/HPT tool was used to evaluate the relative hydraulic conductivity and distribution of VOCs at two locations adjacent to HRPP insertion.

Similar to the Fort Dix deployment, the Alameda HRPPs were prepared on-site in PVC troughs that were filled with DDI water spiked with bromide (100 mg/L). The HRPPs were submerged in the bromide solution while membranes, meshes, and cover plates were attached. Each HRPP took approximately 30 minutes to assemble. The HRPP-B samplers (HRPP-3 and HRPP-4) were coupled together in two sets of three coupled samplers, resulting in two 3.7 m sample lengths. One HRPP-A (HRPP-5) was also installed.

All three HRPPs (3, 4, and 5) were installed inside the DNAPL source zone near standard and multilevel monitoring wells (**Figure 4.20**). HRPP-5 was installed in September 2016 at a midpoint between the anticipated future HRPP-3 and HRPP-4 locations. A soil core was taken up to 6 m BGS, and HRPP-5 was direct-push inserted into the boring hole to a depth of 5.8 to 7 meters BGS. In October 2016, when HRPP-5 was retrieved and sampled, HRPP-3 and HRPP-4 were deployed. A soil core for HRPP-3 (SB 103) was taken down to 6.9 m BGS, and HRPP-3 was installed into the boring at a depth of 2.1 to 5.8 meters BGS. The HRPP-3 insertion location was next to two standard wells, SPW 3-1 and SPW 3-2, and one multilevel well, SMLS 1 (**Figure 4.21**). SPW 3-1 and SPW 3-2 are 0.8 meter well screens at depths of 5.7 and 6.5 m BGS and 6.5 and 7.6 m BGS, respectively. SMLS 1 was comprised of seven 0.15 m screen intervals

from 4.5-7.6 m BGS. HRPP-4 was installed into a boring (SB 104, 0-6.9 m BGS) at a depth of 1.8 to 5.4 m BGS. The HRPP-4 insertion location was next to one standard well, PEW 02, and one multilevel well, SMLS 4 (**Figure 4.21**). PEW 02 was a 3 m well screen at a depth of 4.5-7.5 m BGS. SMLS 4 was screened at identical intervals to SMLS 1.

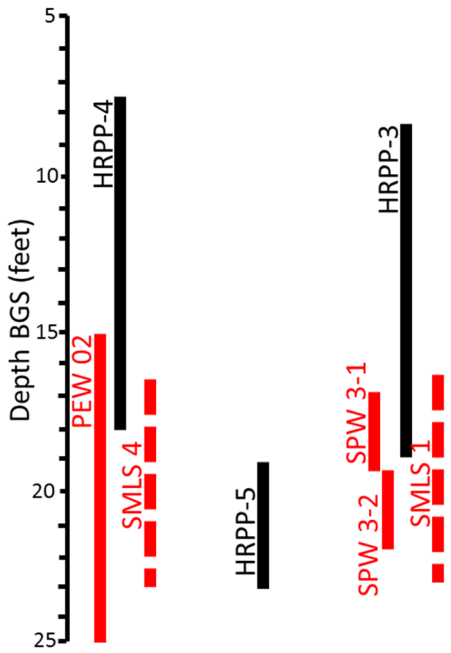

Figure 4.21. Alameda cross-section of well and HRPP grouping by location. Note: Horizontal dimensions are visual approximation, not to exact scale.

The HRPPs were extracted with a Geoprobe, and the faces were rinsed with DI water then blotted with KimWipes. Glass gas-tight syringes were used to extract the liquid solution from the equilibrium cells (10 mL). We used the 10 mL to fill 7 mL HCl preserved VOA vials (actual volume ~8.8 mL) for CVOC analysis, and the remaining 1-2 mL were stored in sterile plastic conical tubes for geochemistry analysis. Geochemistry samples were shipped on ice to Texas Tech University for anion analysis, and CVOC samples were shipped on ice to Aptim Analytical and Treatability Laboratory. Bio-sep beads were removed with a spatula, rinsed with sterile solution to remove sediment, placed into sterile 50 mL plastic conical tubes, then shipped on ice to Microbial Insights (Knoxville, TN) for CSIA of CVOCs and microbial analyses. Velocity cells were sampled using a syringe.

At the Alameda site, multiple sets of comparative data were obtained in addition to the standard and multilevel monitoring wells, such as MIP/HPT profiles, soil cores, and passive flux meters. Well water samples were taken in August 2016, from which CVOC concentrations, anion concentrations, CSIA of CVOCs, and microbial community composition were measured. One soil core (SB 101) and three MIP/HPT profiles (MIP 101, 102, 103) were taken in September 2016 when HRPP-5 was installed. The MIP/HPT was inserted up to the deepest monitoring well depth (7.5 m) at three locations: one approximately 1.5 meters away from HRPP-5, and the other

two directly adjacent to the HRPP-3 and HRPP-4 locations. The MIP/HPT tool yielded qualitative depth profiles of contaminant concentrations as well as permeability indicators such as hydraulic pressure and electrical conductivity. Bio-traps were placed in wells SPW 3-1 and PEW 02 in October 2016, when HRPP-3 and HRPP-4 were inserted, to gather additional CSIA and microbial community data. Velocity estimates were obtained from a previous study of the site (August 2016) in which passive flux meters (Annable et al., 2005) were installed in the monitoring wells. The complete timeline of sampling activities is outlined in **Table 4.4**.

Table 4.4 Timeline of sampling activities in Alameda, California.

Date	Sampling Activity
8/11/2016	• Well water samples tested for CVOC concentrations, geochemistry, microbial communities, and CSIA
9/13/2016	• MIP/HPT 101, 102, and 103 • Soil core at HRPP-5 location (SB 101) • HRPP-5 installed
10/5/2016	• HRPP-5 retrieved and sampled • Bio-traps put in wells SPW 3-1 and PEW 02 • Soil cores at HRPP-3 and HRPP-4 locations (SB 103, 104) • HRPP-3 and HRPP-4 installed
10/25/2016	• HRPP-3 and HRPP-4 retrieved and sampled • Bio-traps in wells SPW 3-1 and PEW 02 retrieved and sampled

4.4.3 USDA BARC Site, Beltsville, MD (BDRLF) Deployment

4.4.3.1 Site Description and Sampler Location

The BDRLF Site located at the USDA Beltsville Agricultural Research Center (BARC) in Beltsville, MD is a 6,600-acre facility that includes agricultural fields, laboratories, and office buildings. Several areas at the BARC facility, including the BDRLF, were previously identified as having environmental contamination, and the site was added to the National Priorities List (NPL) under the Superfund Program in 1994 (BMT, 2017).

The BDLRF site is a two-acre landfill bordered by a road to the north (Beaverdam Road), a wooded area to the east and south, and a field to the west. The landfill was reportedly used from 1943 through the 1980s for disposal of nonhazardous materials, and was closed and capped thereafter (BMT, 2017). Environmental investigations subsequently identified a plume of groundwater with TCE of unknown source to the southeast of the landfill, that was ~ 650 ft wide

by 450 ft long, with a maximum concentration of ~ 600 µg/L (**Figure 4.22**). Site investigation data indicated only a very small amount of cis-1,2-dichloroethene (cis-DCE; < 10 µg/L) and no detection of ethene or vinyl chloride (VC) in the plume (Schanzle, 2018). These data suggested that reductive dechlorination was not occurring to a significant extent in the plume, and that enhanced treatment in the form of an in situ biobarrier to cut off the plume was warranted.

In July 2013, a 300 m long biowall consisting of sand, wood mulch, and municipal leaf compost was installed at the site as a cut-off barrier for the TCE plume (**Figure 4.22**; Schanzle, 2018). A trencher was used to install the barrier to a maximum depth of 6.9 m BGS. A series of upgradient and downgradient transect wells (TWs) were also installed to monitor the performance of the barrier and to conduct additional tests. These wells are shown in the inset to **Figure 4.23**. Data from 2018 indicate that the biobarrier has effectively enhanced reductive dechlorination of TCE, because downgradient wells show lower levels of TCE than upgradient (< 10 µg/L), with much higher concentrations of typical dechlorination products *cis*-DCE (130-260 µg/L), VC (15 – 56 µg/L) and ethene (4-6 µg/L) (Schanzle, 2018). However, these data also indicate that complete reductive dechlorination to ethene is not occurring within the biobarrier.

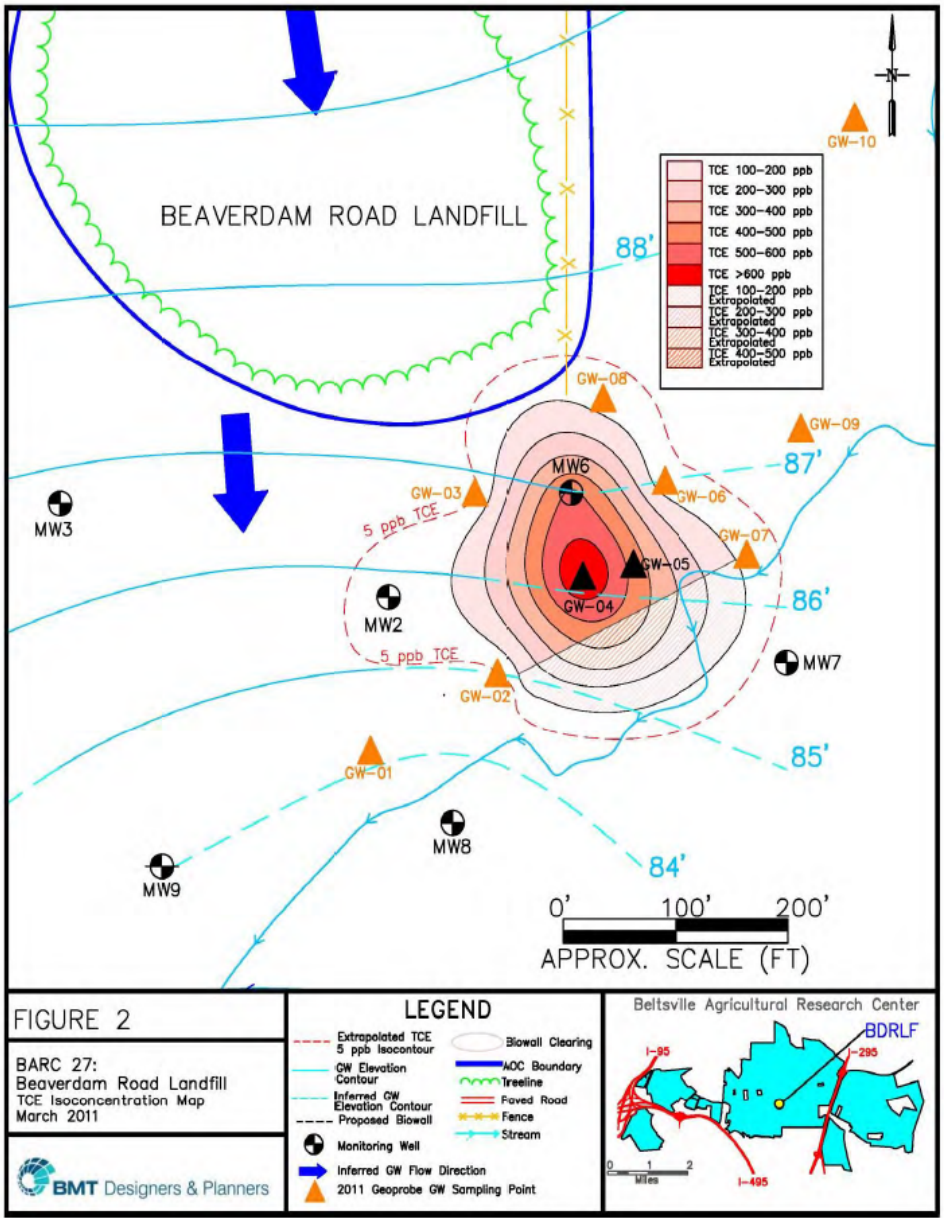

Figure 4.22. Beaverdam Road Landfill at the BARC site. Contours of the TCE plume are provided. Figure from BMT (2017). The shallow geology of the BDRLF site consists of 20 to 30 ft of alluvial Quartenary river terrace deposits that are underlain by the lower Cretaceous Arundel Clay Formation, which itself is estimated to be more than 30 m thick (BMT, 2017). The layered geology includes silty sands (SM), silts and fine sands, clayey silts (ML), and clays (CL) (Figure A).

BMT Designers & Planners	SOIL BORING LOG	Beaverdam Road Landfill BORING ID: SB09

Client:	USDA, ARS
Project Number:	3110-001
Location:	BARC BDRLF
Date Started - Completed:	2/23/2011
Top of Pad Elevation:	NM
Top of Well Elevation:	NM
Total Depth:	24'
Boring Diameter:	1.375"
Driller:	BMT
Drill Method:	Direct Push
Drill Rig:	54DT
Inspector:	L. Hall, D. Schanzle

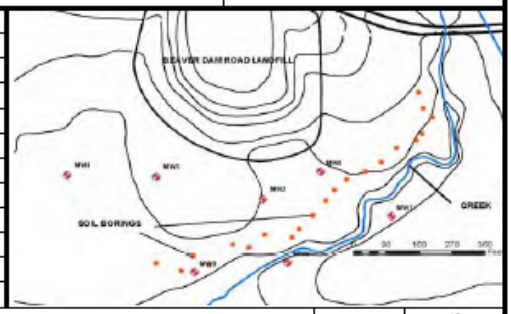

Depth ('bgs)	Recovery (%)	USCS	Description	Lithology	Comments
		ML	0-4" Dark brown silt with fine sand and organics		
4'	65	SM	4"-6' Gray fine to medium sand with silt. Very wet		
8'	75	SM	6-7' Gray very fine sand with silt and some clay. Wet		
		SM	7-9' Gray medium sand with silt and trace gravel. Wet		
12'	75	CL	9-10.5' Reddish-brown clay		
		ML	10.5-11.5' Gray compact silt with very fine sand. Moist		
16'	100	CL	11.5-17' Reddish-brown clay with inclusions of gray compact silt and sand		
20'	100	ML	17-19.75' Gray fine sand with silt. Very wet		
24'	100	CL	19.75-24' Reddish-brown clay (Arundel)		

End of Boring

Figure 4.23. Typical soil boring at the BDRLF site. Figure from BMT (2017).

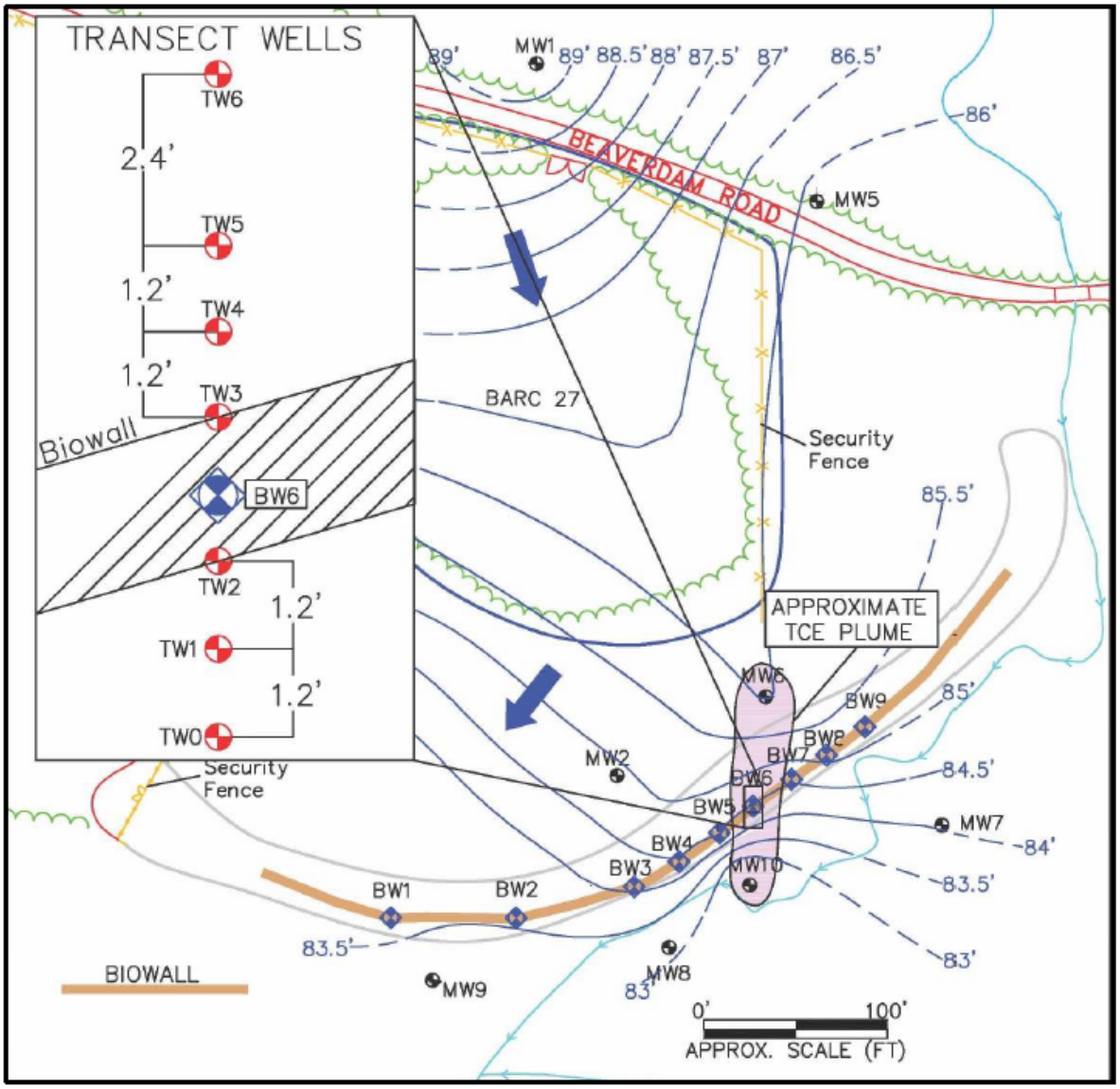

Figure 4.24. Location of the biowall at the BDRLF site. The inset shows transect wells installed to monitor biowall performance. Figure from Schanzle (2018).

4.4.3.2 HRPP Installation, Retrieval and Sampling

Three strings of HRPP-C samplers (3.6m) and two 1.2 m sections of HRPP-B samplers were deployed in April 2019. The HRPP-C strings were deployed upgradient of the biowall near well MW-6, in the biowall near BW-6 and downgradient of the biowall near MW-10 (**Figure 4.25**). One 1.2 m HRPP-B sampler was deployed between the biowall and MW-10, and the other in the stream bed downgradient of MW-10. HRPP MW6, BW6 and MW10 were all installed within 1 m of the corresponding well. HRPP MW6 was located upgradient of the biowall within the core of the TCE plume to provide data on the source area. It was deployed from a depth of 0.4 m down to 4.2 m BGS (**Figure 4.26**). HRPP BW6 was located in the biowall to evaluate processes occurring in the wall itself. It was deployed 1.6 to 5.4 m BGS. HRPP MW6 was deployed downgradient of the biowall to assess differences in all parameters caused by the passage of groundwater through the biowall. It was deployed 0.4 to 4.2 m BGS. HRPP-Inter was deployed roughly midway between the biowall and downgradient MW10 location, from 2.2 to 3.2 m BGS. The final HRPP (HRPP-Stream) was deployed at the edge of the stream to evaluate if groundwater discharge or CVOCs were entering the stream (and at what depth). It was deployed from 0.7 to 1.7 m BGS.

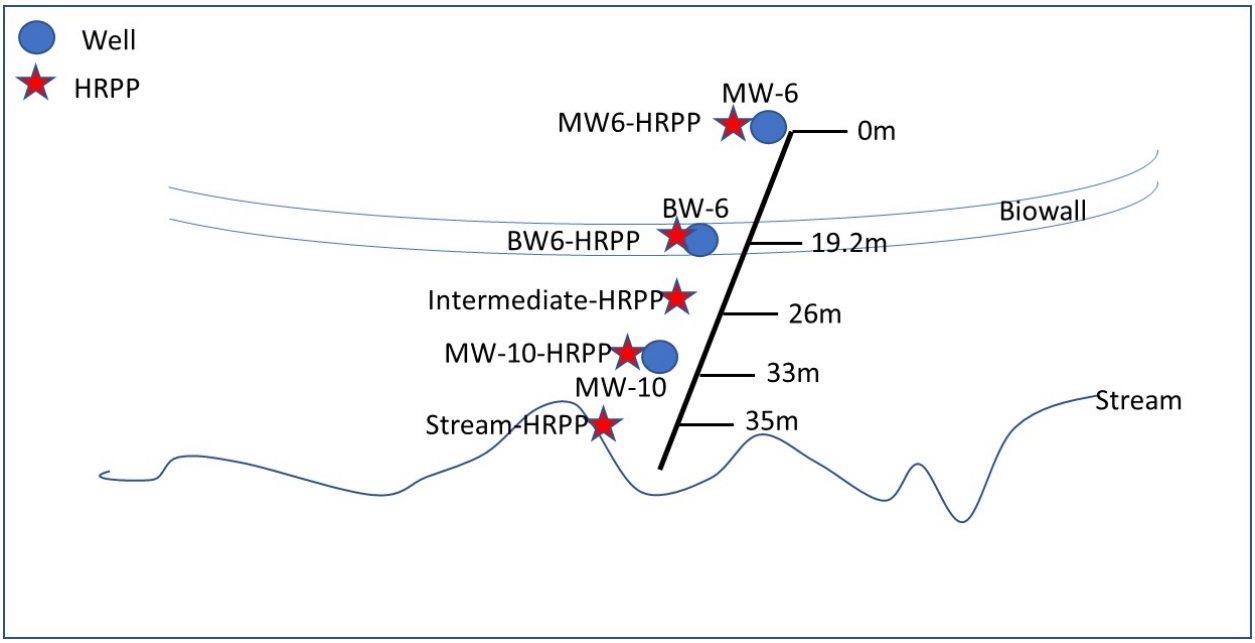

Figure 4.25. General locations for deployment of HRPPs at the BDRLF site. The circles in red demarcated A, B, C, and D represent likely locations for installing HRPPs. Figure modified from Schanzle (2018).

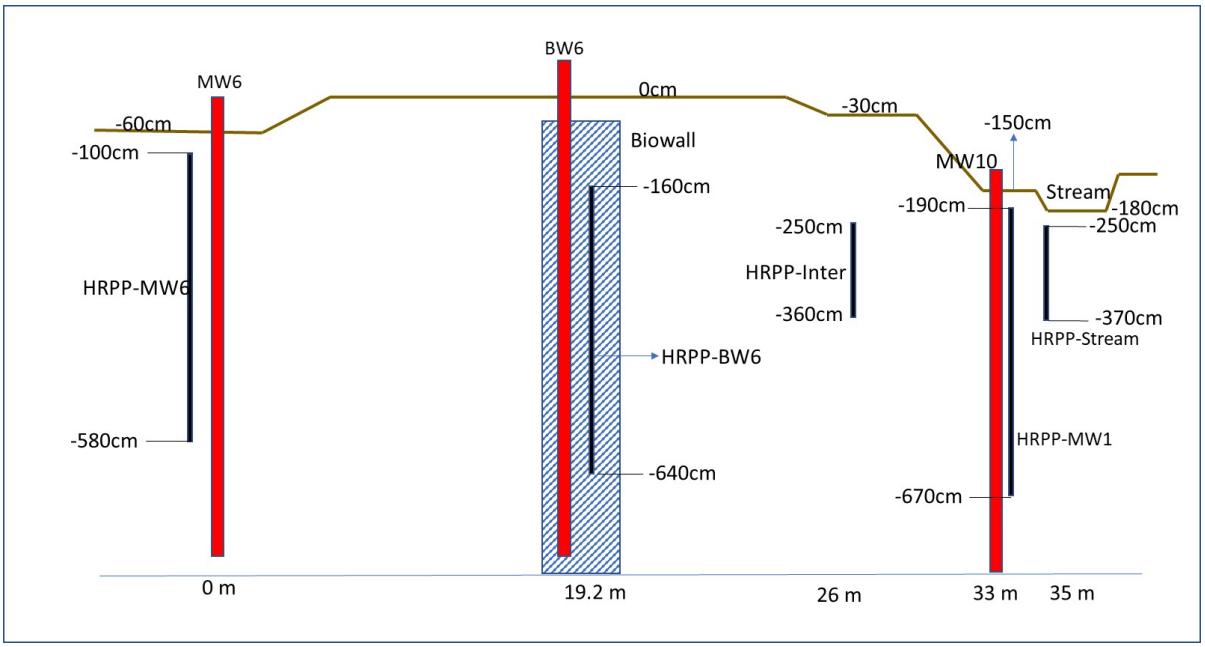

Figure 4.26. Cross section of site illustrating deployment depths.

4.4.3.3 HRPP Installation, Retrieval and Sampling

The HRPP units were prepared for insertion in the field as described previously. The HRPPs were installed by direct push method using a Geoprobe. At the time of HRPP installation, each well located near an HRPP (MW6, BW6, MW10) was sampled using traditional low flow sampling to evaluate the concentrations of cVOCs, geochemical parameters (NO_3^-, NO_2^-, Fe_T, SO_4^{-2}), and dissolved gases (ethane, ethene, methane). Well water was also collected from MW6, BW6 and MW10 for microbial analysis and CSIA. Standard Biotraps were installed in wells MW6 and BW6. The HRPPs were removed by GeoProbe after 4 weeks. Each HRPP sampler was immediately sampled as descried previously.

5 RESULTS AND DISCUSSION

5.1 Development and Validation of the Use of HRPP to Determine In-Situ Transport Parameters at High Resolution

In the following sections, the observations from the lab scale homogeneous flow box experiments are summarized, focusing on the correlation between velocity and k_m. Experimental results from the large, stratified flow box were compared with the small homogeneous experiments. As a final point, we utilized an analytical model to evaluate the integrity of the experimental results. More detail can be found in Haley et al., (2019).

5.1.1 Velocity Effect on k_m in Homogeneous System

Concentrations of Cl^- and Br^- in sample cells increased and decreased, respectively, with an increase in equilibrium time for a range of pore velocities (**Figure 5.1**). The rate at which the samplers approached equilibrium was directly related to the pore velocity and inversely related to the V/SA. The Cl^- and Br^- data were modeled using Equations 4.1 and 4.2 to calculate k_m values for velocities ranging from 0-100 cm/day. The velocity magnitude had a significant impact on k_m (**Figure 5.2**). Experimentally determined k_m values varied from 0.40-2.5 cm/day over a velocity range of 0-100 cm/day. No-flow k_m values were similar to values at one cm/day velocity, but k_m clearly increased with order of magnitude increases in velocity. Variation for k_m measured at a single velocity was generally 10-20 percent of the value. There was also no observed effect on calculated k_m values as a result of orientation of the sampler (perpendicular, parallel, and 180 degrees to direction of flow) for various flow velocities (**Figure 5.2**). Based on results from variable equilibrium times (1-2 weeks), deployment time does not have an effect on the calculated k_m (**Figure 5.3**). As described in the previous section, our cells were designed with volume to area opening ratios (F=V/A) to achieve a range of 20-90 percent equilibrium after a three-week deployment. It is ideal to reach a range of 20-90 percent equilibrium in the cells in order to generate optimum curves for fitting k_m; however, we generated comparable k_m values from lower, narrower equilibrium ranges resulting from shorter deployment times.

The correlation between velocity and k_m is a result of the tradeoff between diffusion-dominated and advection-dominated transport over the range of experimental velocities. When mass transport is controlled by diffusion, the rate-limiting step for the mass transfer of bromide is diffusion through the porous media (Webster et al., 1998). When mass transport is controlled by advection, the rate-limiting step for the mass transfer of bromide is transfer through the membrane (Harper et al., 1997); which approaches the rate of 18 cm/day measured in the stirred-tank bottle study. Because diffusion through the membrane is much faster than diffusion through the porous media, it is logical that k_m is faster at higher velocities, under which conditions advection is the dominant transport process.

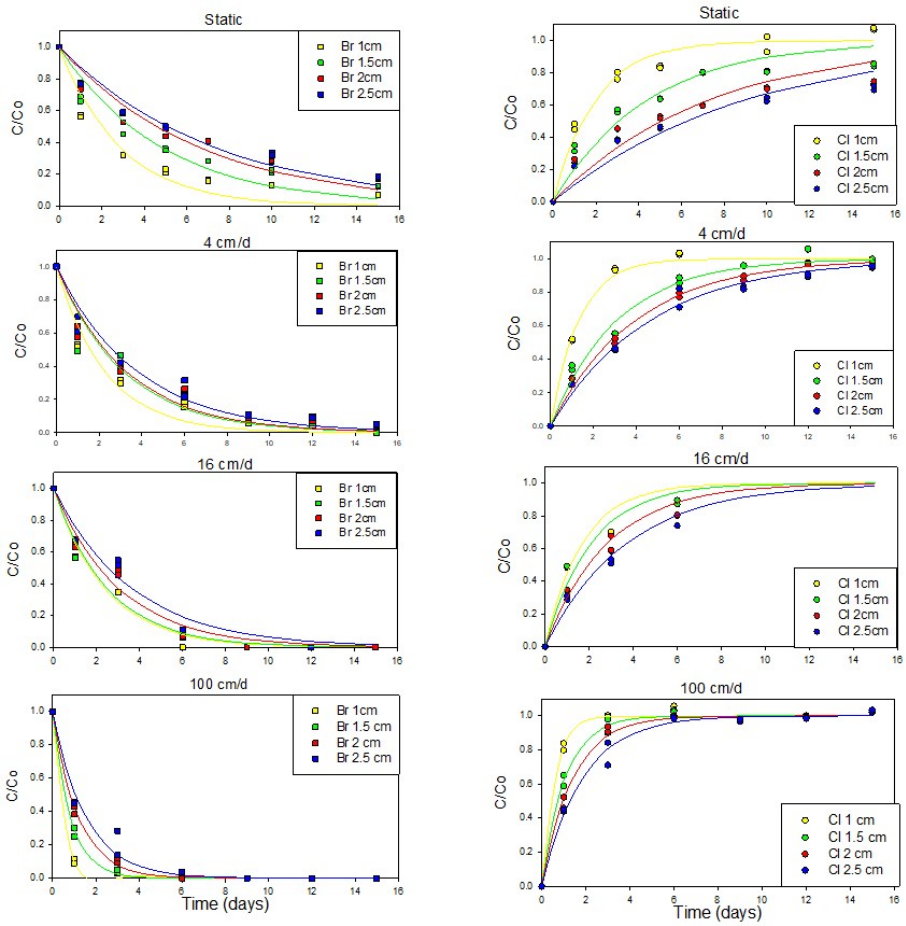

Figure 5.1. Chloride (Cl^-) and Br^- concentration in the HRPP equilibration cells as a function of time for pore velocities of 0, 4, 16, and 100 cm/d.

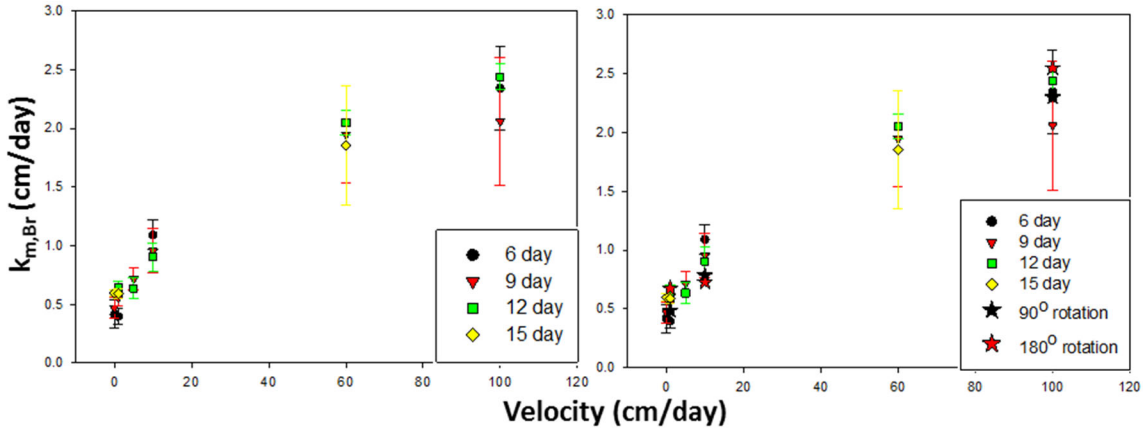

Figure 5.2 Mass transfer coefficients for bromide in the small flow box. (a) k_m values for sampler orientation perpendicular to flow; (b) comparative k_m values for orientation parallel to flow and 180° away from flow. Error bars indicate standard deviations of triplicate measurements.

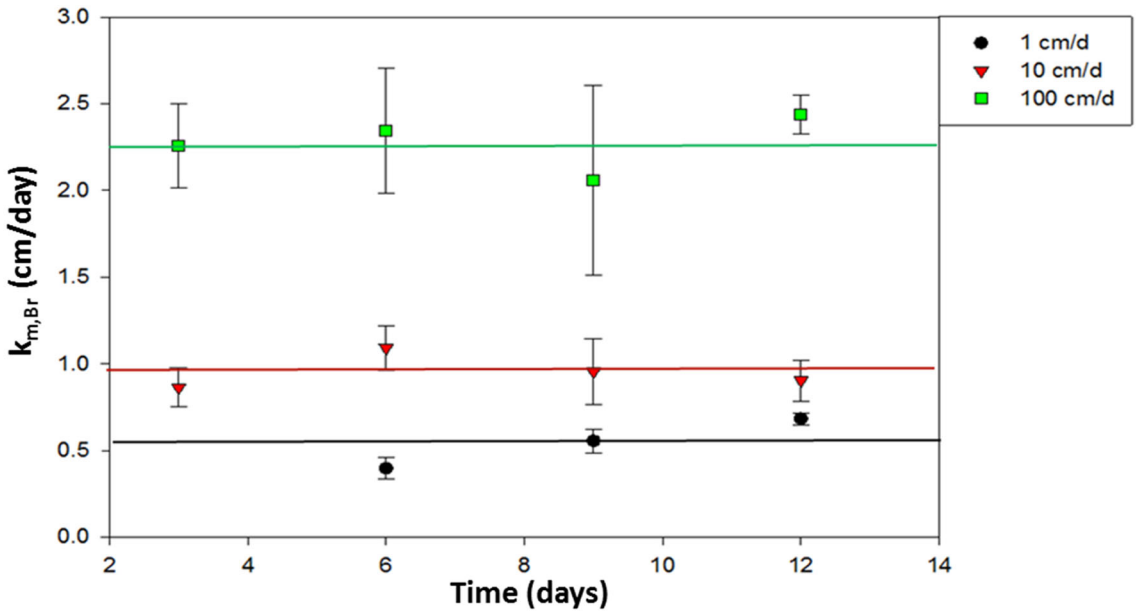

Figure 5.3. Mass transfer coefficients for bromide in the small flow box are independent of time.

5.1.2 Contaminant Concentration and Flux

Similar to the results for the conserved tracer (Br^-) equilibrating with the bulk pore water, the mass transfer co-efficient for Cl^- in the bulk solution equilibrating with the sampler cell is independent of cell depth and dependent on velocity (**Figure 5.4**). This is highlighted by the observed 1:1 ratio of Cl^- and Br^- in the experiments, supporting the ability to use Br^- as an equilibrium reporting compound. We also evaluated the rate of TCE equilibrium and compared the mass transfer coefficient for TCE to Cl^- and Br^-. Based on the similarity between Br- and TCE mass transfer coefficients, our data supports the ability to use Br^- as an equilibrium reference compound to establish the extent of equilibration reached in each HRPP cell.

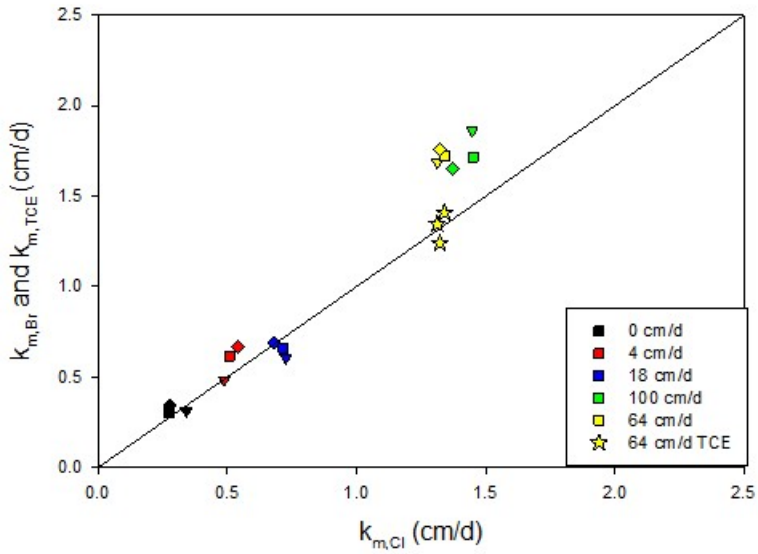

Figure 5.4. Relation between the mass transfer coefficient of Br^- as an equilibrium reporter and Cl^- as a model species equilibrating with the HRPP. The mass transfer coefficient for TCE at a pore velocity of 64 cm/d is represented by the star symbols. The solid line is a 1:1 line for comparison.

5.1.3 Verification of the HRPP Ability to Measure Velocity for Heterogenous Meso-scale Systems

The ability of a full size fully functional HRPP to measure groundwater velocity was evaluated in a mesoscale flow box,using the HRPP-B samplers deployed at the Alameda demonstration site. For controlled velocities of 10 and 60 cm/day through the high permeability sand, the measured k_m values after 21 days of sampler equilibration were 1 ± 0.1 cm/day for v=10 cm/day through the sand, 1.9 ± 0.04 cm/day for v=60 cm/day through the sand, and 0.5 ± 0.08 and 0.5± 0.06 for the clay at both sand velocities, 10 and 60 cm/d, respectively (**Figure 5.5**). The assumption of negligible flow through the low permeability clay/sand mixture was verified with a tracer test. The k_m values in the sand matched measured k_m for the lab scale samplers in the small flow box, and the k_m values in the clay indicated no-flow conditions according to the correlation between velocity and k_m from the small flow box experiments.

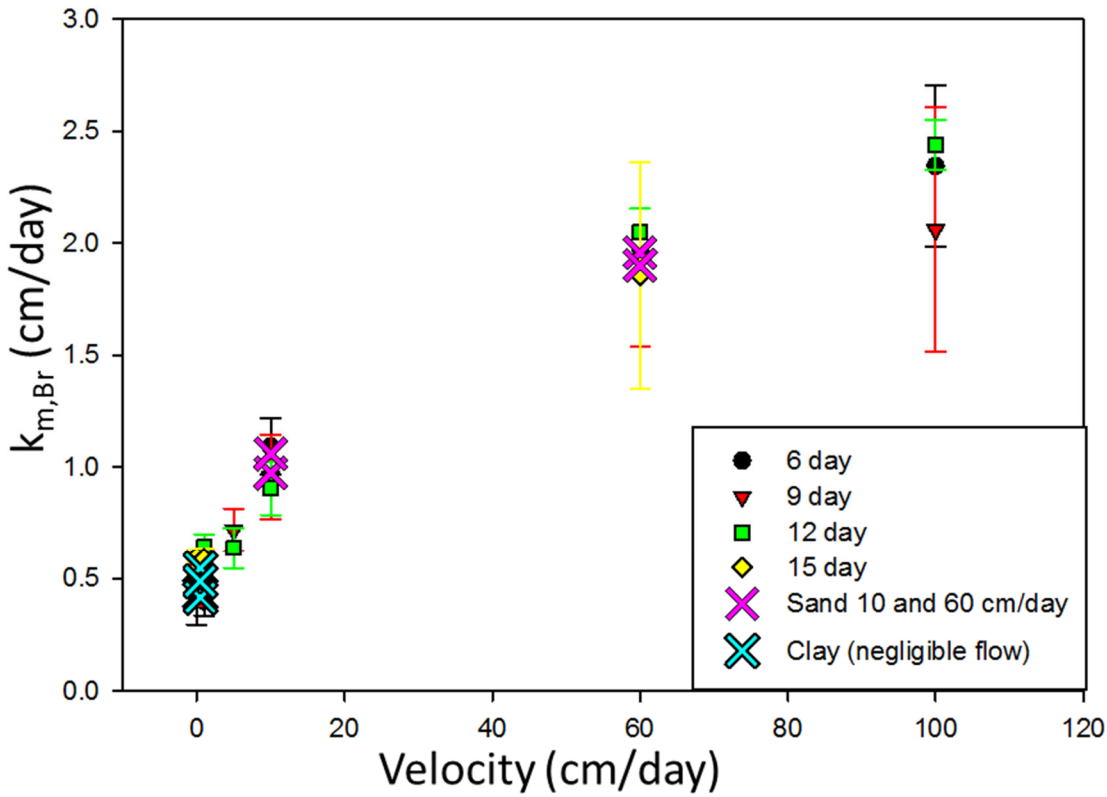

Figure 5.5. Measured k_m (bromide) in the big, two-layer flow box system for 10 and 60 cm/day velocity through the sand and negligible flow in the clay compared to lab-scale k_m vs. velocity results.

5.1.4 Comparison of Analytical Model and Experimental Results

We applied a two dimensional quasi-steady state analytical model for a flat sheet undergoing advective and diffusive fluxes in a porous bed (**Figure 5.6**) to our experimental data in order to evaluate the integrity of our results, as well as to further predict the effects of soil permeability and groundwater velocity on theoretical k_m values for our geometry.

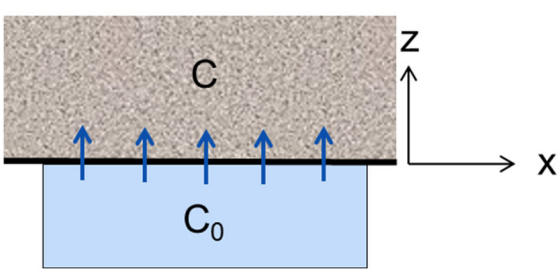

Figure 5.6. Conceptual schematic of 2D quasi-steady state analytical model for a flat sheet undergoing diffusion in the z direction and advection in the x direction.

The model adhered to the following equations and boundary conditions, for which a solution has been found by Choy and Reible (2000):

$$v_x \frac{dC}{dx} = D_{eff} \frac{d^2C}{d^2z} \qquad \text{Eq. 5.1}$$

where v_x is velocity in the x direction and D_{eff} is the effective soil diffusion coefficient in the z direction, calculated by Equations 5.2 through 5.7(Millington and Quirk, 1961):

$$\alpha \approx \frac{d_p}{10} \qquad \text{Eq. 5.2}$$

where α is a transverse dispersion coefficient, and d_p is particle diameter,

$$\frac{\emptyset}{\tau} \approx \emptyset^{\frac{4}{3}} \qquad \text{Eq. 5.3}$$

where ∅ is porosity and τ is tortuosity, and

$$D_{eff} = D_w \frac{\emptyset}{\tau} + \alpha v_x \qquad \text{Eq. 5.4}$$

where D_w is the diffusion coefficient in water. Equation 5.5 is made dimensionless by substituting $\theta = C_0 - C$ so that it becomes

$$v_x \frac{d\theta}{dx} = D_{eff} \frac{d^2\theta}{d^2z} \qquad \text{Eq. 5.5}$$

We applied the following boundary conditions:

$$\theta = C_0 \;\; at \;\; z = 0 \rightarrow \infty, x = 0 \qquad \text{Eq. 5.6}$$

$$D_{eff} \frac{dC}{dz} = \frac{D_m}{\delta}\theta \;\; at \;\; z = 0 \rightarrow \infty, x > 0 \qquad \text{Eq. 5.7}$$

where D_m is the diffusivity of a conservative tracer across the membrane, and δ is the characteristic diffusion length of the system. The solution for the equation and boundary conditions (Choy and Reible, 2000) is

$$\Theta = C_0 \left\{ erf\left(\frac{z}{\sqrt{4D_{eff}{}^{x}/v_x}}\right) + exp\left(\frac{\frac{D_m}{\delta}z}{D_{eff}} + \frac{(\frac{D_m}{\delta})^2 x/v_x}{D_{eff}}\right) erfc\left(\frac{z}{\sqrt{4D_{eff}{}^{x}/v_x}} + \frac{D_m}{\delta}\sqrt{\frac{x/v_x}{D_{eff}}}\right)\right\} \qquad \text{Eq. 5.8}$$

so that k_m can be defined as

$$k_m = \frac{D_m}{\delta}\left\{exp\left(\frac{\left(\frac{D_m}{\delta}\right)^2 x/v_x}{D_{eff}}\right) erfc\left(\frac{D_m}{\delta}\sqrt{\frac{x/v_x}{D_{eff}}}\right)\right\} \qquad \text{Eq. 5.9}$$

We took x to be half of the length of the membrane. A D_m/δ value of 18 cm/day was determined for diffusion of bromide across only the membrane thickness (110 μm). The D_m/δ measured in the membrane-only bottle study did not account for the increased δ in the real system due to sediment tortuosity and layers of protective nylon and stainless-steel mesh added on top of the

membrane. Therefore, we adjusted D_m/δ until the shape and magnitude of the curve generated by the analytical model matched our experimental correlation between velocity and k_m (**Figure 5.7**). The D_m/δ value implemented in Equation 5.9 was three cm/day, adjusted from 18 cm/day in the membrane-only bottle study. Because D_m is an unchanging property of the membrane and diffused species, the adjusted D_m/δ of three cm/day implies that the characteristic diffusion length was increased from $\delta_{membrane}$=110 µm to δ_{actual}=660 µm to account for sediment tortuosity and the layers of nylon and stainless-steel mesh.

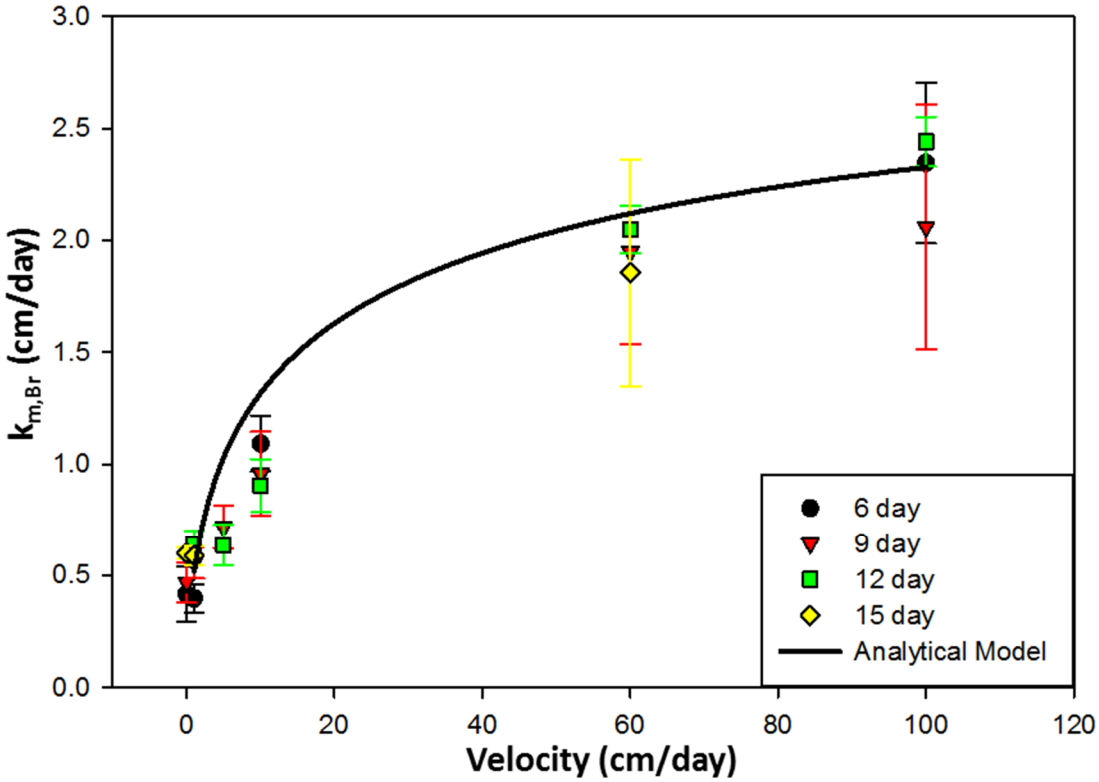

Figure 5.7. Experimental mass transfer coefficients for bromide plotted against 2D quasi-steady state analytical model (Equation5.9).

We performed sensitivity analysis on the model by varying the membrane impedence, D_m/δ, and porosity, ϕ, variables (**Figure 5.8**). The model predicted that large variance in porosity (0.15 to 0.75) can have an impact on k_m, particularly for velocities between 0 and 60 cm/day. The variance in the analytical model k_m due to porosity change could lead to an error in velocity prediction up to approximately a factor of two. Large variance in D_m/δ (0.1-10) had an impact on both the shape of the curve and the magnitude of k_m for all velocities between 0 and 100 cm/day. We do not believe the impact of D_m/δ will affect applicability of the HRPP because it is a parameter that is dependent upon the geometry of the sampler and can be experimentally measured. The impact of porosity is important to consider because particle diameter is a highly variable parameter that is often difficult to measure in real-world site applications.

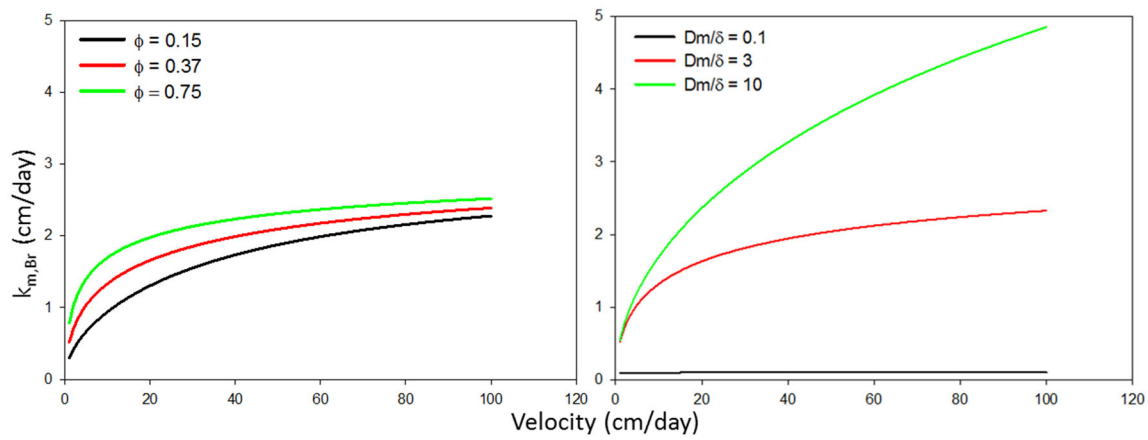

Figure 5.8. Sensitivity analysis of 2D quasi-steady state analytical model or (a) porosity, φ, of 0.15, 0.37, and 0.75, and (b) membrane impedance, D_m/δ of 0.1, 3, and 10.

5.1.5 Conclusion

This study demonstrated the ability of the HRPP to estimate groundwater velocity from a single deployment using the impact of groundwater velocity on the rate of mass transfer across the membrane of the HRPP. Previous studies examined the effects of solute transport on in-cell passive sampler equilibration dynamics (Webster et al., 1998) in addition to the effects of the rate of pore water resupply on passive sampler equilibration with saturated sediments (Harper et al., 1997). However, previous studies have not explicitly investigated the relationship between groundwater velocity and mass transfer regarding the practical implication of using a passive sampler to determine groundwater velocity. Our study, based on a 2D analytical model and equilibration of conservative tracer concentrations in saturated sediment flow boxes, quantitatively illustrates the relationship between velocity and the mass transfer rate for a passive diffusion sampler. The results show that the membrane mass transfer coefficient can not only differentiate between high permeability ($K_p=10^{-2}$ cm/s) sand and low permeability ($K_p=10^{-5}$ cm/s) clay, but also can detect differences in velocity. This method is capable of detecting groundwater velocity changes over orders of magnitude, and it is realistically able to detect velocity differences within a factor of two at ranges of 3-100 cm/day. However, this method is not precise enough to detect velocity differences on the order of a single cm/day, particularly as it pertains to the difference between no-flow conditions and a one cm/day velocity. The results of this study allow for passive diffusion samplers to be used as tools for fine scale delineation of groundwater velocity in aquifers. The HRPP sampler's ability to be inserted by direct push removes the limitations of measuring velocity using monitoring wells, such as mixing within the well, preferential flow through heterogenous layers, and interference with the flow path around well screens.

5.2 Development and Validation of HRPP Micro-biotraps to Evaluate CSIA of Adsorbed CVOCs and Microbial Community Structure and Activity.

Bio-traps made by Microbial Insights have been developed during the past decade as a means to characterize microbial communities in groundwater aquifers, and in some cases to provide

evidence of microbial degradation of a target contaminant (see Busch-Harris et al., 2008 and references therein). During this project, we evaluated the potential to utilize a micro-scale bio-trap placed within the HRPP to provide fine scale assessment of microbial communities and degradative organisms in an aquifer, as well as measure the stable isotopic composition of adsorbed CVOCs on the micro-biotraps.

5.2.1 Prototype Testing in Wells

The microbial community abundance was measured using standard Biotraps and prototype HRPP micro-biotraps from two wells at Fort Dix (**Table 5.1** and **Table 5.2)**, and one well from Kelly AFB (**Table 5.3)**. All data have been standardized on a cells/g media basis. Overall, the standard Biotraps (with Biosep beads) and HRPP cells with Biosep beads provided comparable results in the Fort Dix wells, and there was no appreciable difference for most organisms/genes between cells that allowed groundwater to flow through open compartments, and those that did not (closed compartments) in the HRPPs. For example, for Fort Dix well Mag 70, numbers of *Dehalococcoides mccartyi* were between 1.3 x 10^7/g beads and 2.6 x $10^{7/}$g beads among the three treatments (BioTrap, open HRPP cell, closed HRPP cell) (**Table 1**). Results were generally similar among the other bacterial species/genes quantified. It is interesting to note that high densities of both dechlorinating organism/genes and aerobic cometabolic genes were present in the wells.

In general, the cell densities on the GAC and Ag-GAC were somewhat lower than for the Biosep beads. However, the Ag-GAC, which should have anti-microbial properties from the impregnated Ag, usually had population densities similar to those of the GAC alone. Ag-GAC was evaluated to determine if it would prevent microbial growth and reduce the possibility for degradation of adsorbed VOCs, which would interfere with CSIA analysis (see below). It should also be noted that the MAG-112P well at Fort Dix had an elevated pH (~ 9) due to the addition of NaOH in the area to neutralize naturally acidic groundwater pH (**Table 2**). The microbial population densities and diversity were lower in this well than in the Fort Dix Mag 70 well, as reflected in both the Biotrap and HRPP data. Both test systems gave comparable results between the two Fort Dix wells with differing geochemistry.

For the Kelly AFB samples (**Table 5.3**), the densities in the Bio-traps and open HRPP cells were generally similar to those observed at Fort Dix. For a few of the dehalogenating organisms, somewhat lower densities were observed in the closed HRPP cells compared to the open cells or Bio-traps. This observation was apparent for *Dehalogenimonas* and *Desulfitobacterium,* in particular, as well as total sulfate-reducing bacteria, where the difference was more than an order of magnitude. However, results were reasonably comparable for most other strains/genes (including all of the aerobic cometabolic genes) and there was generally no difference in the types of organisms detected. Also different than the Fort Dix results, the Ag-GAC had a higher density of cells/genes in the KAFB samples than the Biosep beads in several instances.

Table 5.1 Quantarray data from the MAG-70 Well at Fort Dix.

QuantArray Chlor results from MAG-70		Standard Biotrap cells/g	BioSep Beads Open cells/g	BioSep Beads Closed cells/g	Ag-GAC Open cells/g	Ag-GAC Closed cells/g
Reductive Dechlorination						
Dehalococcoides spp.	DHC	**2.60E+07**	**1.08E+07**	**1.31E+07**	**6.56E+06**	**5.10E+06**
tceA Reductase	TCE	3.08E+03	3.08E+03	3.08E+03	**1.08E+03**	1.00E+03
BAV1 Vinyl Chloride Reductase	BVC	3.08E+03	3.08E+03	3.08E+03	1.00E+03	1.00E+03
Vinyl Chloride Reductase	VCR	**2.08E+05**	**1.17E+05**	**1.66E+05**	**7.94E+04**	**4.20E+04**
Dehalobacter spp.	DHBt	**1.81E+05**	**3.73E+05**	**2.08E+05**	1.00E+04	1.00E+04
Dehalobacter DCM	DCM	3.08E+04	3.08E+04	3.08E+04	1.00E+04	1.00E+04
Dehalogenimonas spp.	DHG	**1.44E+05**	**6.53E+05**	**1.44E+05**	**2.12E+05**	**4.82E+05**
Desulfitobacterium spp.	DSB	**7.88E+04**	**3.23E+04**	**3.30E+04**	***3.68E+03***	***3.16E+03***
Dehalobium chlorocoercia	DECO	3.08E+04	3.08E+04	3.08E+04	1.00E+04	1.00E+04
Desulfuromonas spp.	DSM	3.08E+04	3.08E+04	3.08E+04	1.00E+04	1.00E+04
Chloroform reductase	CFR	3.08E+04	3.08E+04	3.08E+04	1.00E+04	1.00E+04
Aerobic Cometabolic						
Soluble Methane Monooxygenase	SMMO	**2.03E+06**	**2.41E+06**	**9.91E+06**	**1.82E+06**	**2.41E+05**
Particulate Methane Monooxygenase	PMMO	**7.92E+05**	**2.88E+06**	**7.84E+06**	**4.44E+05**	**8.89E+04**
Toluene Dioxygenase	TOD	**1.77E+06**	**2.75E+06**	**3.93E+06**	**3.15E+05**	**2.34E+05**
Phenol Hydroxylase	PHE	**8.33E+07**	**7.68E+07**	**7.45E+07**	**8.51E+06**	**4.02E+06**
Trichlorobenzene Dioxygenase	TCBO	3.08E+04	3.08E+04	3.08E+04	1.00E+04	1.00E+04
Toluene Monooxygenase 2	RDEG	**1.42E+07**	**8.21E+06**	**1.10E+07**	**2.56E+06**	**1.83E+06**
Toluene Monooxygenase	RMO	**1.35E+07**	**2.06E+07**	**2.23E+07**	**7.97E+06**	**5.30E+06**
Ethene Monooxygenase	EtnC	3.08E+04	3.08E+04	3.08E+04	1.00E+04	1.00E+04
Epoxyalkane transferase	EtnE	3.08E+04	3.08E+04	3.08E+04	1.00E+04	1.00E+04
Other						
Total Eubacteria	EBAC	**2.46E+09**	**1.87E+09**	**3.41E+09**	**3.94E+08**	**4.02E+08**
Sulfate Reducing Bacteria	APS	**4.31E+08**	**1.88E+08**	**1.85E+08**	**1.43E+08**	**6.70E+07**
Methanogens	MGN	**6.56E+04**	**5.18E+04**	**3.51E+05**	**9.37E+04**	**1.50E+04**

Values shaded in gray were below detection. Values in italics are estimated values

Table 5.2 Quantarray data from the MAG-112P Well at Fort Dix.

QuantArray Chlor results from MAG-112P		Standard Biotrap cells/g	BioSep Beads Open cells/g	BioSep Beads Closed cells/g	Ag-GAC Open cells/g	Ag-GAC Closed cells/g
Reductive Dechlorination						
Dehalococcoides spp.	DHC	3.08E+03	3.08E+03	3.08E+03	1.00E+03	1.00E+03
tceA Reductase	TCE	3.08E+03	3.08E+03	3.08E+03	1.00E+03	1.00E+03
BAV1 Vinyl Chloride Reductase	BVC	3.08E+03	3.08E+03	3.08E+03	1.00E+03	1.00E+03
Vinyl Chloride Reductase	VCR	**3.08E+03**	**3.08E+03**	**3.08E+03**	**1.00E+03**	**1.00E+03**
Dehalobacter spp.	DHBt	**3.39E+05**	**3.30E+05**	**2.82E+05**	1.00E+04	1.00E+04
Dehalobacter DCM	DCM	3.08E+04	3.08E+04	3.08E+04	1.00E+04	1.00E+04
Dehalogenimonas spp.	DHG	**5.36E+06**	**4.33E+07**	**7.80E+06**	**1.14E+06**	**4.91E+05**
Desulfitobacterium spp.	DSB	**3.85E+05**	**6.07E+05**	**1.87E+05**	**6.13E+04**	**2.51E+04**
Dehalobium chlorocoercia	DECO	3.08E+04	3.08E+04	3.08E+04	1.00E+04	1.00E+04
Desulfuromonas spp.	DSM	3.08E+04	3.08E+04	3.08E+04	1.00E+04	1.00E+04
Chloroform reductase	CFR	3.08E+04	3.08E+04	3.08E+04	1.00E+04	1.00E+04
Aerobic Cometabolic						
Soluble Methane Monooxygenase	SMMO	**2.92E+05**	**2.98E+05**	**7.98E+05**	**2.45E+05**	**8.05E+04**
Particulate Methane Monooxygenase	PMMO	**2.72E+05**	**7.48E+04**	**5.74E+03**	***3.10E+03***	***4.71E+03***
Toluene Dioxygenase	TOD	**3.68E+04**	**4.72E+04**	**2.03E+05**	**5.75E+04**	***1.11E+03***
Phenol Hydroxylase	PHE	**9.29E+05**	**2.78E+06**	**3.10E+06**	**5.27E+06**	**2.78E+06**
Trichlorobenzene Dioxygenase	TCBO	3.08E+04	3.08E+04	3.08E+04	1.00E+04	1.00E+04
Toluene Monooxygenase 2	RDEG	3.08E+04	3.08E+04	**2.00E+05**	**1.09E+05**	***8.25E+03***
Toluene Monooxygenase	RMO	3.08E+04	3.08E+04	3.08E+04	**7.18E+04**	***3.79E+02***
Ethene Monooxygenase	EtnC	3.08E+04	3.08E+04	3.08E+04	1.00E+04	1.00E+04
Epoxyalkane transferase	EtnE	3.08E+04	3.08E+04	3.08E+04	1.00E+04	1.00E+04
Other						
Total Eubacteria	EBAC	**1.16E+09**	**3.58E+09**	**1.87E+09**	**5.30E+08**	**3.84E+08**
Sulfate Reducing Bacteria	APS	3.08E+04	3.08E+04	3.08E+04	***2.52E+03***	1.00E+04
Methanogens	MGN	***9.43E+03***	**3.67E+04**	**4.58E+04**	**1.54E+04**	**1.60E+04**

Table 5.3 Quantarray data from the WP022MW357 Well at Kelly AFB.

QuantArray Chlor results from Well WP022MW357		Biotrap cells/g	BioSep Beads Open cells/g	BioSep Beads Closed cells/g	Ag-GAC Open cells/g	Ag-GAC Closed cells/g	GAC Open cells/g
Reductive Dechlorination							
Dehalococcoides spp.	DHC	**8.58E+03**	**4.11E+04**	**8.93E+03**	1.00E+03	**6.03E+03**	1.00E+03
tceA Reductase	TCE	3.08E+03	**3.63E+03**	3.08E+03	1.00E+03	**1.75E+03**	1.00E+03
BAV1 Vinyl Chloride Reductase	BVC	3.08E+03	**9.10E+03**	3.08E+03	1.00E+03	1.00E+03	1.00E+03
Vinyl Chloride Reductase	VCR	3.08E+03	3.08E+03	3.08E+03	1.00E+03	1.00E+03	1.00E+03
Dehalobacter spp.	DHBt	**2.66E+06**	**1.22E+06**	**1.64E+05**	1.00E+04	1.00E+04	1.00E+04
Dehalobacter DCM	DCM	3.08E+04	3.08E+04	3.08E+04	1.00E+04	1.00E+04	1.00E+04
Dehalogenimonas spp.	DHG	**1.14E+06**	**1.45E+06**	**3.20E+04**	**1.96E+04**	**3.78E+05**	**2.21E+04**
Desulfitobacterium spp.	DSB	**1.08E+06**	**1.39E+06**	**3.37E+04**	1.00E+04	**1.10E+05**	1.00E+04
Dehalobium chlorocoercia	DECO	3.08E+04	3.08E+04	3.08E+04	1.00E+04	1.00E+04	1.00E+04
Desulfuromonas spp.	DSM	**4.20E+05**	**4.20E+05**	**4.20E+05**	1.00E+04	**6.68E+05**	1.00E+04
Chloroform reductase	CFR	3.08E+04	3.08E+04	3.08E+04	1.00E+04	1.00E+04	1.00E+04
1,1-DCA Reductase	DCA	3.08E+04	3.08E+04	3.08E+04	1.00E+04	1.00E+04	1.00E+04
1,2-DCA Reductase	DCAR	3.08E+04	3.08E+04	3.08E+04	1.00E+04	1.00E+04	1.00E+04
Aerobic Cometabolic							
Soluble Methane Monooxygenase	SMMO	**2.14E+06**	**1.77E+06**	**4.84E+06**	**9.49E+04**	**1.17E+06**	1.00E+04
Particulate Methane Monooxygenase	PMMO	**8.58E+05**	**5.20E+05**	**2.16E+06**	**8.05E+06**	**1.15E+06**	**2.80E+04**
Toluene Dioxygenase	TOD	**2.87E+06**	**2.11E+06**	**3.83E+06**	**8.42E+04**	**2.95E+06**	1.00E+04
Phenol Hydroxylase	PHE	**6.02E+06**	**2.50E+06**	3.08E+04	**1.77E+05**	**1.38E+06**	**1.72E+05**
Trichlorobenzene Dioxygenase	TCBO	**5.73E+04**	3.08E+04	3.08E+04	1.00E+04	1.00E+04	1.00E+04
Toluene Monooxygenase 2	RDEG	**8.46E+05**	**1.18E+06**	3.08E+04	1.00E+04	**1.29E+06**	**6.63E+02**
Toluene Monooxygenase	RMO	**6.93E+05**	3.08E+04	3.08E+04	**1.21E+06**	**3.92E+05**	1.00E+04
Ethene Monooxygenase	EtnC	3.08E+04	3.08E+04	3.08E+04	1.00E+04	1.00E+04	1.00E+04
Epoxyalkane transferase	EtnE	3.08E+04	3.08E+04	3.08E+04	1.00E+04	1.00E+04	1.00E+04
Dichloromethane dehalogenase	DCMA	3.08E+04	3.08E+04	3.08E+04	1.00E+04	1.00E+04	1.00E+04
Other							
Total Eubacteria	EBAC	**2.11E+09**	**2.14E+09**	**7.61E+08**	**3.29E+07**	**2.18E+08**	**1.17E+07**
Sulfate Reducing Bacteria	APS	**3.74E+08**	**9.85E+08**	**2.25E+07**	**1.19E+04**	**6.29E+07**	**2.31E+06**
Methanogens	MGN	**6.88E+04**	**6.64E+05**	**2.76E+05**	***2.53E+03***	**2.39E+04**	1.00E+04

Values shaded in gray were below detection. Values in italics are estimated values

Of the three sites evaluated, only one well (Mag 70) returned reliable values on the stable isotopic composition of TCE; this result is likely due to the relatively low concentrations of TCE at the other sites due to the significant transformation of TCE to *cis*-DCE from biostimulation efforts (only TCE analysis was requested). The measured $\delta^{13}C$ of TCE in well Mag-70 captured using a standard Biotrap placed in the well was similar to TCE captured using the prototype HRPP micro-biotrap containing Biosep beads (**Table 5.4**). However, $\delta^{13}C$ of TCE captured on Ag-GAC from the HRPP was substantially lighter. This could be due to a general reduction in TCE biodegradation on the Ag-GAC compared to the Biosep beads, or possibly some other process that leads to less fractionation of TCE adsorbed to this matrix (e.g., extraction effects). Groundwater samples were not collected for CSIA in this case. Regardless, the results demonstrate that the deployment of Biosep beads in the HRPP returned comparable data to standard Biotraps.

Table 5.4 δ^{13}C-TCE for Bio-sep beads and Ag coated GAC deployed at Ft. Dix and Kelley AFB in existing wells compared to standard Bio-traps deployed in the same wells.

Location	δ^{13}C-TCE				
	HRPP				Standard Bio-trap
	Ag-GAC 1	Ag-GAC-2	Bio-sep	Bio-sep 2	Bio-sep
Ft Dix Mag-70	-26.2	-28.0	-22.0	-23.0	-24.0
Ft. Dix Mag112	-5.3(J)	Non Detect	0.7(J)	-1.1(J)	2.0(J)
Kelley AFB	Non Detect	Non Detect	Non Detect	Non Detect	Non Detect

Taken as a whole, the data suggested that the HRPP and standard Biotrap system provide comparable results for microbial community structure and stable isotope composition in most instances. The silver-GAC was not effective at preventing growth or accumulation of bacteria. The data suggested that the HRPP cells with Biosep beads in a compartment that allows through-flow would be the best method to incorporate in full scale HRPP testing.

5.2.2 Lab Testing in Flow Cells

In order to further reevaluate the use of micro-biotraps, flow cell testing was conducted using a two-layer media. The system was equilibrated with TCE, inoculated with a reductive dechlorinating culture (SDC-9), and biostimulated with edible oil. After an incubation period, the two layers exhibited different DO and TCE/DCE/VC concentrations (See **Figures 5.9, 5.10 and 5.11**), as well as a visible layer at the presumed oxic/anoxic interface. Reductive dehalogenation within the flow cell appeared effective at transforming TCE to *cis*-DCE within the lower permeability layer, but reduction to more reduced compounds such as VC appeared limited. The greater concentrations of *cis*-DCE in the low permeability layer than was supplied as TCE may be associated with the solvent cement used to assemble the flow cell, which may have contained TCE. The slow flow in the low permeability layer may have allowed for sufficient time for TCE, and degradation products, from the cement to diffuse to the sampling port. After the incubation period, small-scale HRPPs with BioSep beads were emplaced for 25 days across the two layers to demonstrate their ability to distinguish differences in microbial populations. BioSep beads were removed from the peepers and sent to Microbial Insights for Quant Array-Chlor analyses.

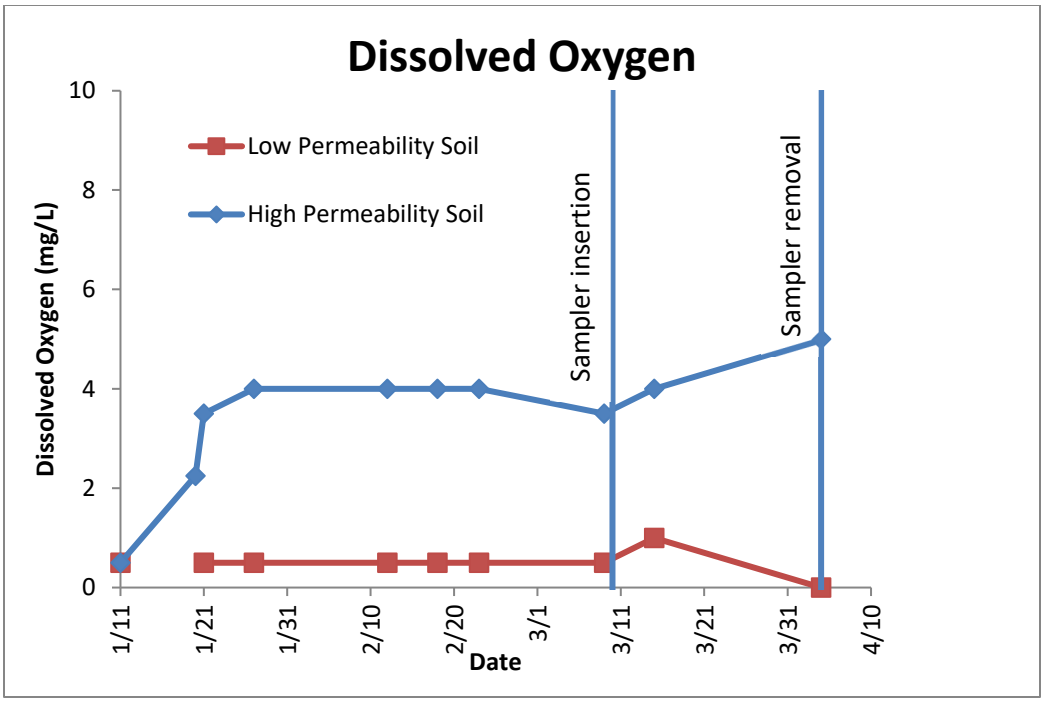

Figure 5.9 Dissolved Oxygen (DO) in two soil layers of differing hydraulic conductivities. The lower permeability layer had been exposed to TCE, a dechlorinating culture, and emulsified oil.

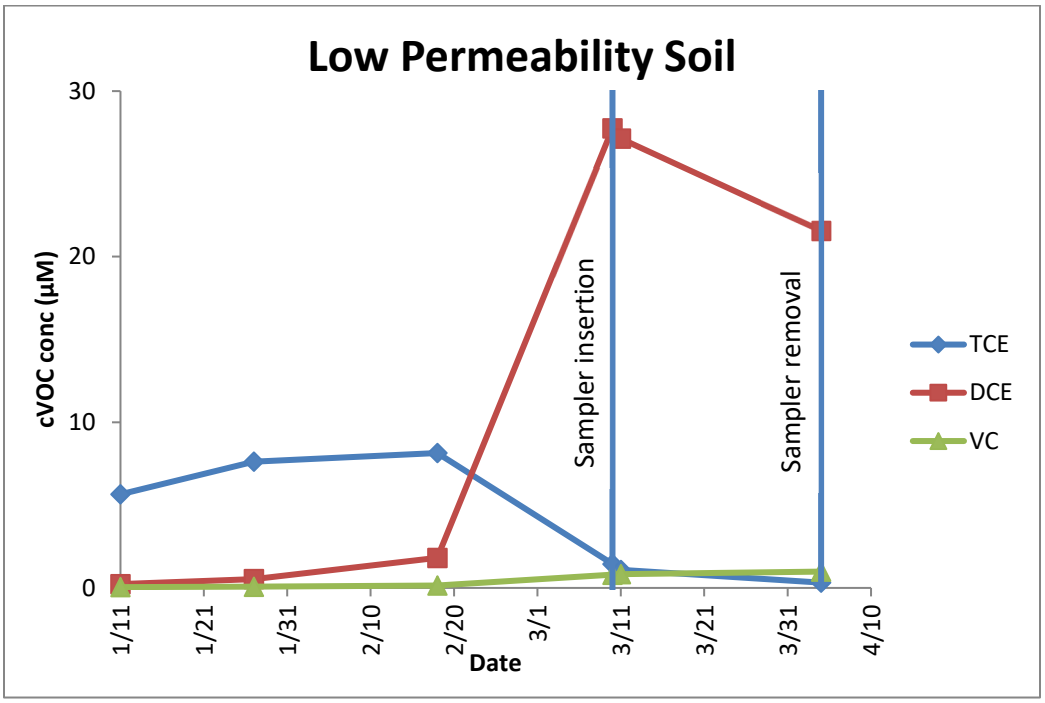

Figure 5.10. TCE, DCE, and VC in a lower permeability layer that had been exposed to TCE, a dechlorinating culture, and emulsified oil.

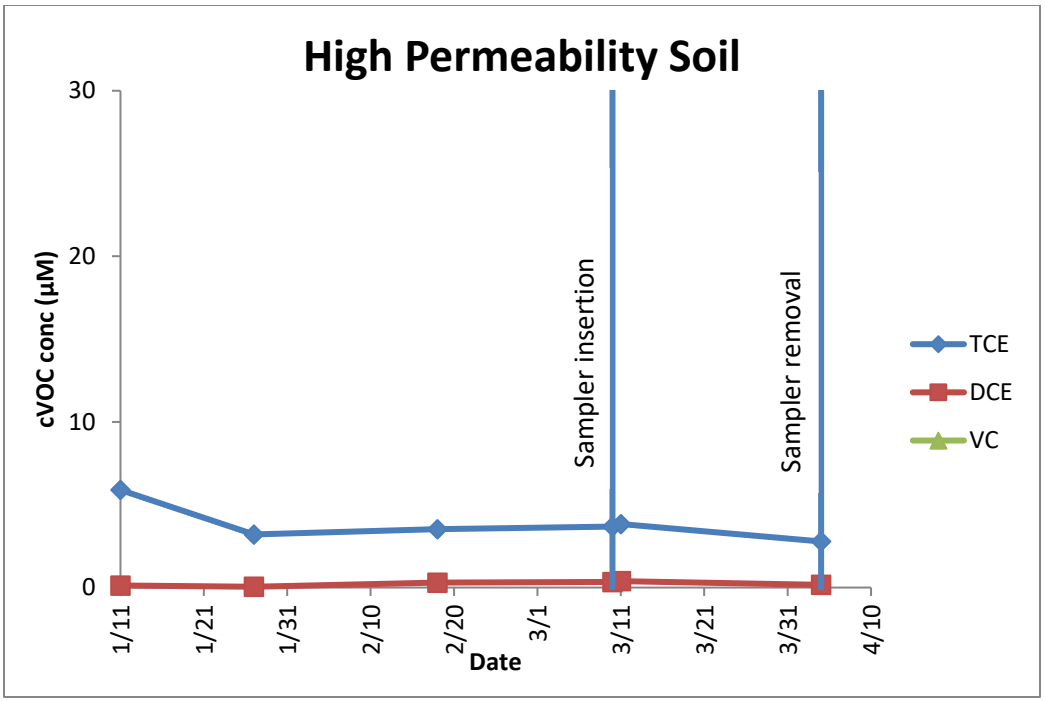

Figure 5.11. TCE, DCE, and VC in a lower permeability layer.

Figure 5.12 shows genes counts associated with dehalogenating microbial populations and sulfate reduce bacteria collected using the lab scale HRPP micro-biotraps. Elevated populations of *Dehalobacter* spp. (DHBt) and *Desulfitobacterium* spp. (DSB) were observed in the anoxic lower permeability layer, whereas much smaller populations of *Dehalococcoides* spp. (DHC) were collected in both layers. These results are consistent with the TCE reduction in the lower permeability layer, but stalling at *cis*-DCE, as DHBt and DSB are not known to reduce DCE to VC, but DHC may. **Figure 5.12** also shows elevated populations of sulfate reducing bacteria in areas with greater anoxia in the flow cell. **Figure 5.13** shows genes counts more closely associated with oxidized environments, as was observed in the higher conductivity layer of the flow cell. Consistent with observations of more dissolved oxygen in the high conductivity layer, epoxyalkane transferase (EtnE), phenol hydroxylase (PHE), toluene monooxygenase 2 (RDEG), and soluble methane monooxygenase (sMMO) all appeared greater than in the lower conductivity layers.

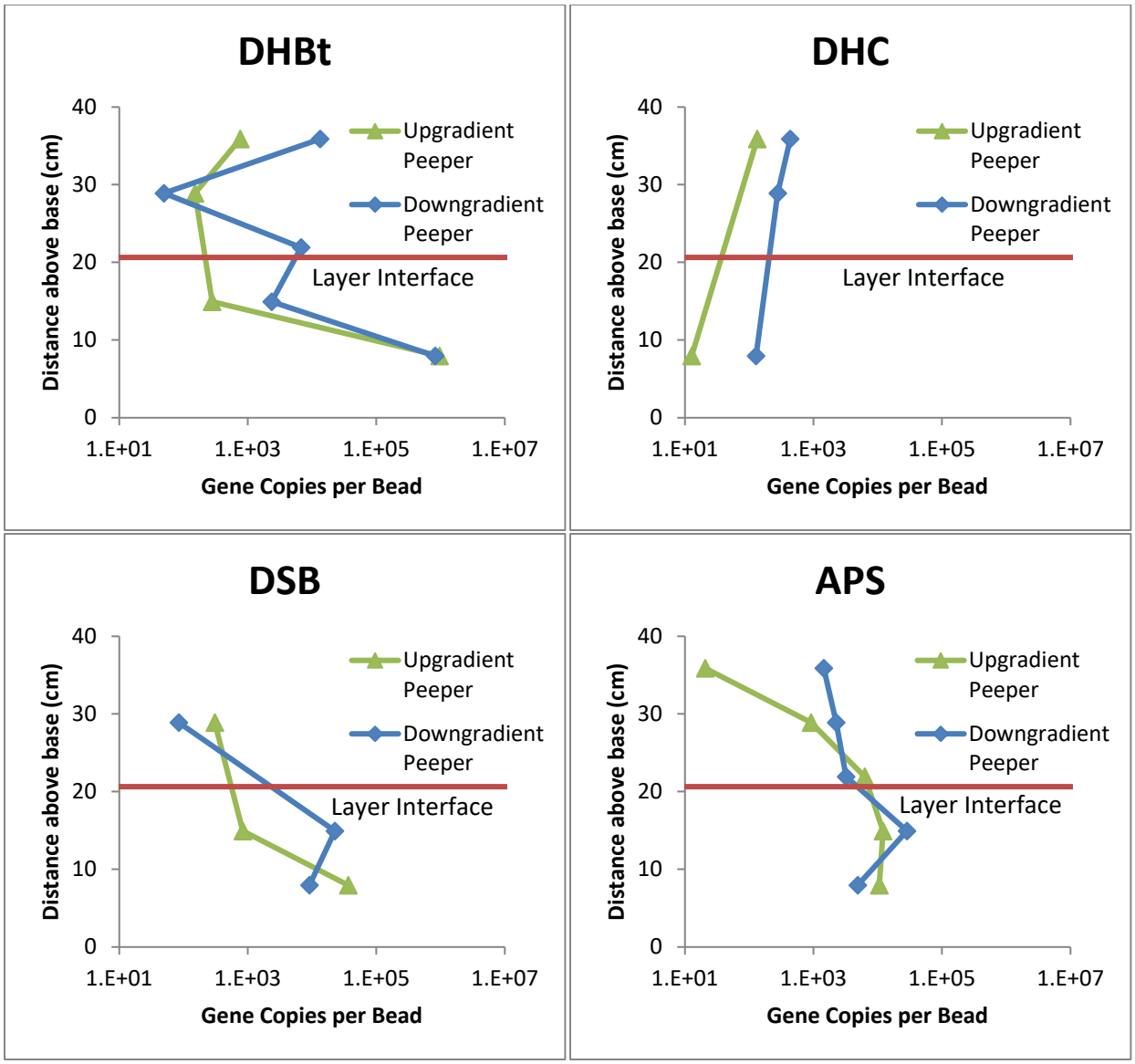

Figure 5.12. Gene copies of Dehalobacter spp. (DHBt), Dehalococcoides spp. (DHC), Desulfitobacterium spp. (DSB), and Sulfate Reducing Bacteria (APS) as measured by QuantArray-Chlor. Only intervals with detections are indicated.

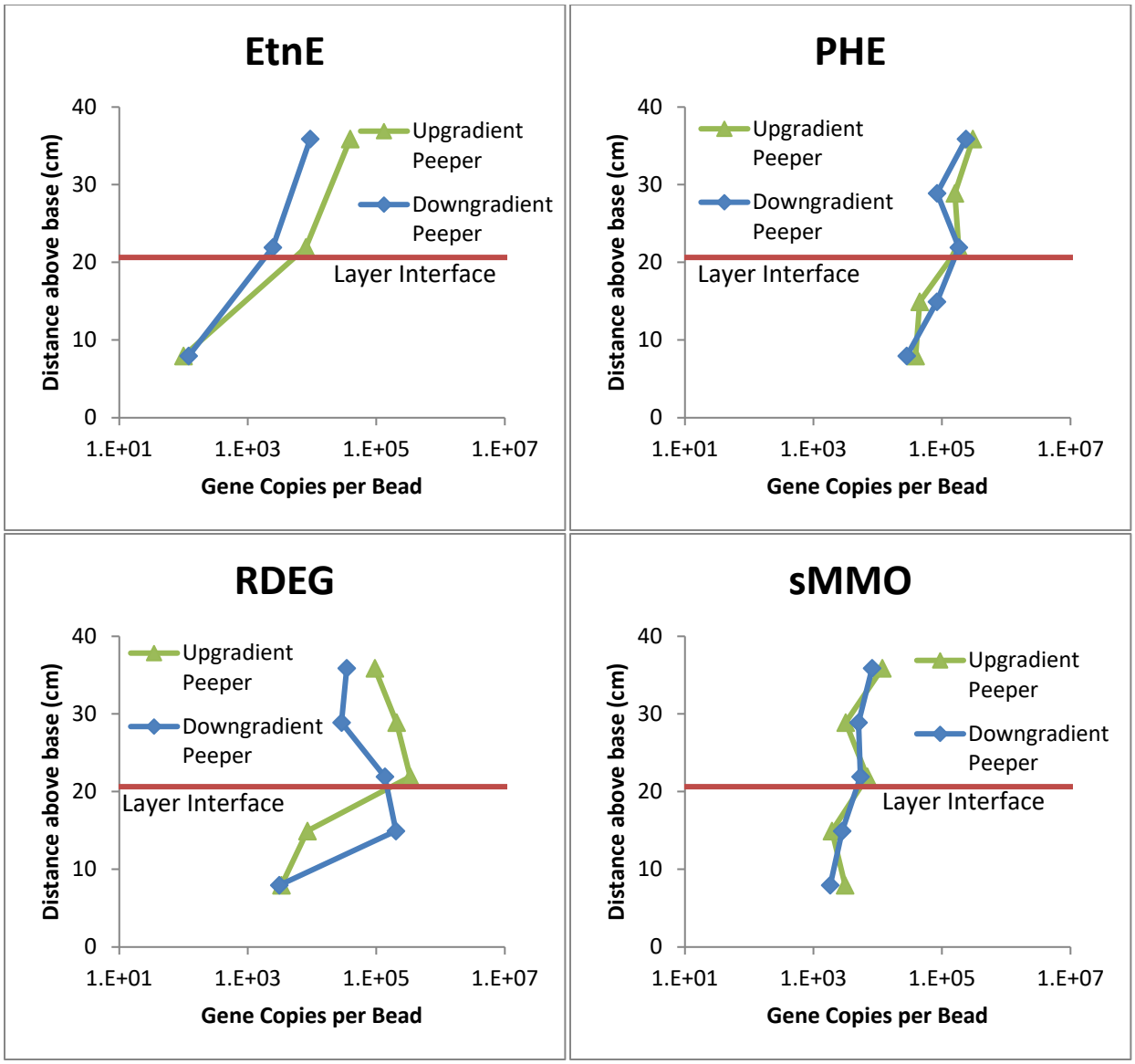

Figure 5.13. Gene copies of epoxyalkane transferase (EtnE), phenol hydroxylase (PHE), toluene monooxygenase 2 (RDEG), soluble methane monooxygenase (sMMO) as measured by QuantArray-Chlor. Only intervals with detections are indicated.

Samples of BioSep beads and co-located water collected during the small-scale experiments were sent for carbon isotope analysis of the chlorinated compounds TCE, DCE, and VC. **Figure 5.14** shows the carbon isotope composition ($\delta^{13}C$ values) of TCE, extracted from the BioSep beads and co-located water with depth, as well as the $\delta^{13}C$ value of the influent TCE of -31 ‰. The aqueous samples of TCE have very similar isotope composition to the starting material, despite greater than 90 % transformation in the lower permeability layer. This may indicate that preferential flow occurred and that the sampled water does not represent pore water from the low hydraulic conductivity zone. The $\delta^{13}C$ values of TCE on the BioSep beads are within 4 ‰ of the measured aqueous values. The reported $\delta^{13}C$ values of extracted TCE are more positive than the $\delta^{13}C$ values of TCE in co-located water, suggesting that the micro-biotraps are less subject to preferential flow. **Figure 5.15** shows $\delta^{13}C$ values of TCE, DCE, and VC extracted from Bio-Sep

beads and water from locations in the low permeability/anaerobic sediments where decreases in TCE were observed. However, with the exception of the $\delta^{13}C$ values of TCE described above, there was consistency among both the HRPP derived values and those from the aqueous phase. This suggests that little isotope fractionation occurs during uptake on BioSep beads.

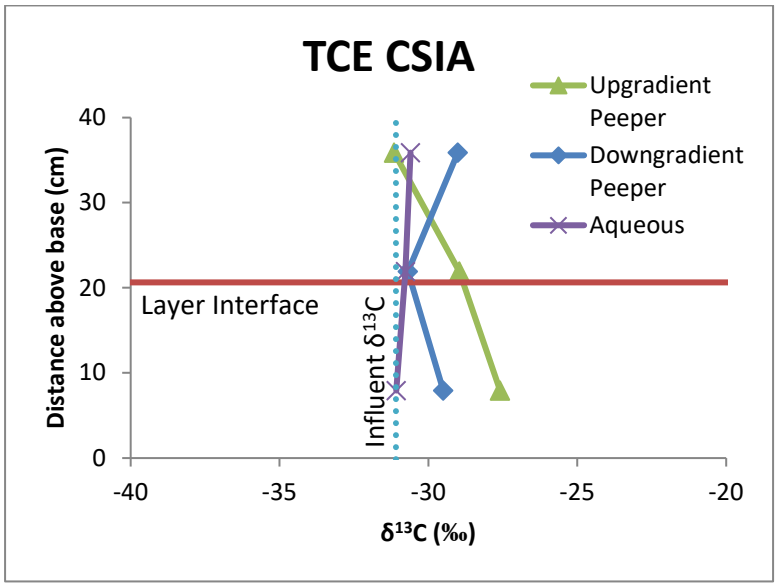

Figure 5.14. Carbon isotope composition (as δ13C) of TCE in the HRPPs ("Peepers") and co-located water ("Aqueous").

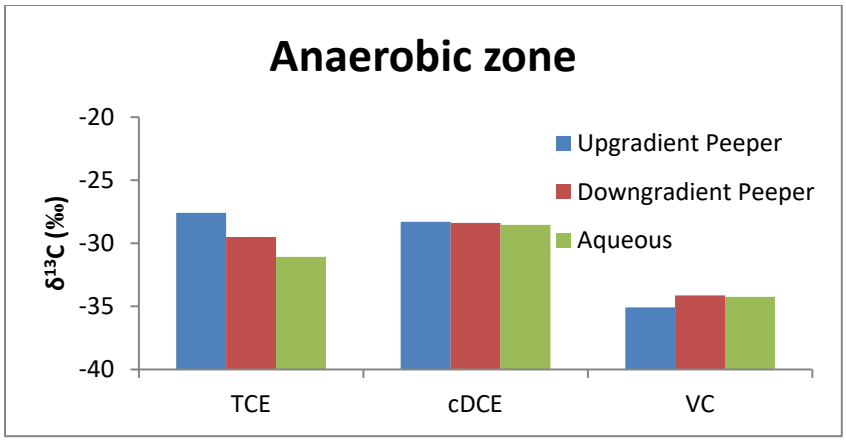

Figure 5.15. Carbon isotope composition (as δ13C) of TCE, cDCE, and VC in the anaerobic sediment layer as collected by HRPP ("Peepers") and co-located water ("Aqueous").

5.3 Development and Field Validation of a HRPP Capable of Insertion in Shallow Aquifers.

Three generations of HRPP samplers (HRPP-A, B, and C) were sequentially field tested to validate the HRPP performance against traditional site assessment techniques, with the results of each field test used to update the design. The results of each field test are described below.

5.3.1 Fort Dix Field Trial

The first field trial took place at Fort Dix near Trenton, New Jersey, in September 2015. Two HRPP-A samplers were installed and HRPP data were compared to nearby monitoring well data and standard Biotraps.

5.3.1.1 Geochemistry Results

MAG 66, which partially intersects the Kirkwood-Vincetown interface, had a chloride concentration of 37 mg/L. MAG 112, which is less than 20 feet (6.1 meters) from MAG 66 and does not intersect the Kirkwood-Vincetown interface, had a chloride concentration of 38 mg/L. MAG 4, which is approximately 80 feet (24.4 meters) away from MAG 66 and MAG 112, had the highest chloride concentration of 67 mg/L (**Figure 5.16**). Based on well data alone, there appears to be a locational difference in chloride concentration between the MAG 4 site and MAG 66/MAG 112 site. This is possibly due to ongoing remediation efforts including an active injection of solutions to stimulate degradation. No injections incurred during the deployment. MAG 66 and MAG 112 had sulfate concentrations of 0.5 and 6.8 mg/L, respectively (**Figure 9.16**). The difference in sulfate concentrations between MAG 66 and MAG 112 could be a result of MAG 66 partially intersecting the interface, while MAG 112 is entirely in the lower Vincetown formation. MAG 4, which intersects the Kirkwood and Vincetown formations as well as the interface, had a sulfate concentration of 2 mg/L.

The amount of bromide remaining in the equilibrium cells of the HRPPs after retrieval ranged from 3-17 mg/L (out of an initial 100 mg/L), which indicates that 83-97 percent equilibration was reached with the pore water for those cells. HRPP-1 and HRPP-2 both acquired chloride and sulfate as geochemical indicators.

HRPP-1 chloride concentrations were relatively constant with the lowest concentration (6 mg/L) occurring above the Kirkwood-Vincetown interface and slightly higher concentrations (15-18 mg/L) occurring below the interface (**Figure 5.16**). HRPP-2 chloride concentrations increase with depth from 30 to 50 mg/L above the interface then return to 30 mg/L below the interface. Maximum chloride concentrations for both HRPP-1 and HRPP-2 occured in sample intervals at the Kirkwood-Vincetown interface. Duplicate samples of chloride at each depth for both HRPP-1 and HRPP-2 had small standard deviations.

HRPP-1 detected sulfate in only two sample depth intervals, both with concentrations of 1.5 mg/L. HRPP-2 detected sulfate in three sample intervals with concentrations of 1.5-2 mg/L. As was the case with HRPP chloride concentrations, all HRPP duplicate samples for sulfate had small standard deviations (< 0.2).

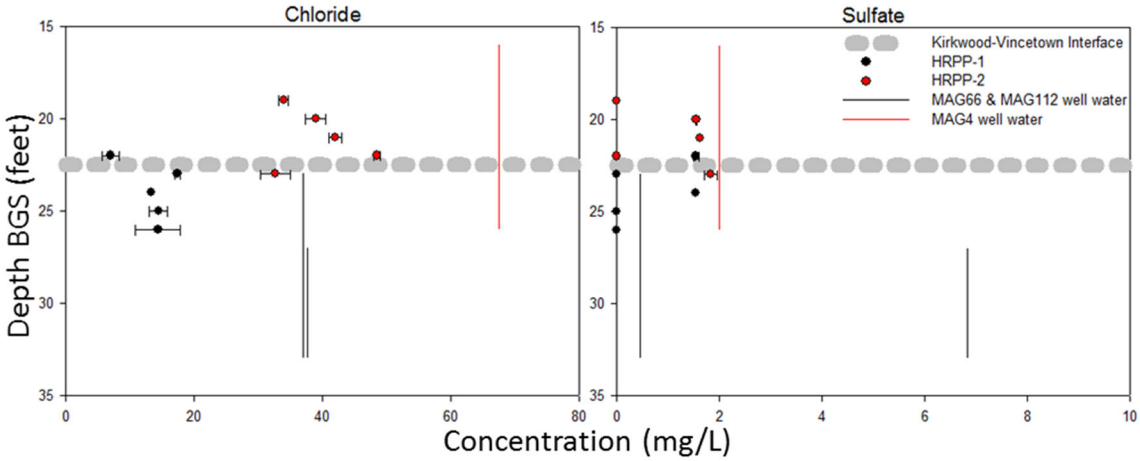

Figure 5.16. Fort Dix geochemical indicators (chloride, sulfate) detected by HRPP-1 and HRPP-2 compared to well water from MAG 4, MAG 66, and MAG 112.

Chloride concentrations were consistently higher in HRPP-2 and MAG 4 than in HRPP-1, MAG 66, and MAG 112, so both well water and HRPP data indicate a locational difference in chloride. For both locations, well water chloride concentrations were higher than HRPP chloride concentrations. It is possible that the higher chloride concentrations in the well water with respect to HRPPs were due to the well screen intersection of the Kirkwood-Vincetown interface, where the highest chloride concentrations were detected for both HRPPs. Sulfate concentrations in both well water and HRPP samples were consistently low. The HRPP sulfate concentrations correlate best with the MAG 4 sulfate concentrations (~2 mg/L). Compared to both MAG 4 and the HRPP sulfate concentrations, MAG 66 was a relatively low outlier and MAG 112 was a relatively high outlier.

HRPPs at both locations acquired chloride and sulfate concentrations similar to those in the respective wells. Overall, the HRPPs demonstrated the ability to quantify geochemical indicators that were detected in monitoring well water. Duplicate depth samples for both HRPPs indicate good reproducibility for the HRPP method for measuring geochemical indicators.

5.3.1.2 CVOCs Concentrations

In contrast to chloride, CVOC concentrations were expected to vary with location due to increasing distance from the source as well as the impact of active remediation at the site. At MAG 112, concentrations were lower than MAG 66 concentrations for both *cis*-DCE (533 µg/L vs. 1040 µg/L) and vinyl chloride (22 µg/L vs. 115 µg/L). MAG 66 and MAG 112 were in close spatial proximity, so the higher concentrations of *cis*-DCE and vinyl chloride seen in MAG 66 may be due to large local spatial variations or a longer well screen pulling from areas that MAG 112 does not intersect (e.g. Kirkwood-Vincetown interface). At MAG 4, *cis*-DCE (315 µg/L) and vinyl chloride (non-detect) were both lower than the MAG 66 and MAG 112 location.

At the MAG 66 and MAG 112 location, concentrations of *cis*-DCE captured using HRPP-1 decreased from above the interface (800 µg/L) to below the interface (400 µg/L), then increased again and fluctuated between 600-800 µg/L (**Figure 5.17**). HRPP-1 vinyl chloride concentrations

were consistent and ranged from 8-13 µg/L. At the MAG 4 HRPP insertion location, concentrations of *cis*-DCE captured using HRPP-2 were all approximately 200 µg/L above the interface, then decreased below the interface to 111 µg/L. HRPP-2 vinyl chloride concentrations were non-detect above the interface and were 11 µg/L at the interface. Duplicate samples at the same depths for both HRPP-1 and HRPP-2 had small standard deviations at most depths for both *cis*-DCE and vinyl chloride, although a few HRPP-1 sample depths had larger variations. (**Figure 5.17**).

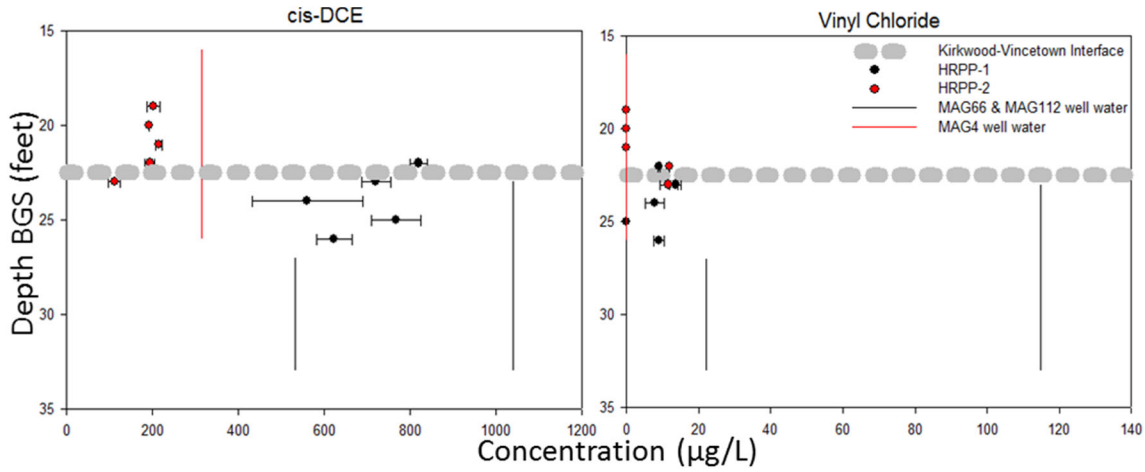

Figure 5.17. Fort Dix CVOCs (cis-DCE, vinyl chloride) detected by HRPP-1 and HRPP-2 compared to well water from MAG 4, MAG 66, and MAG 112.

The trend of HRPP-1 *cis*-DCE concentrations, generally decreasing below the Kirkwood-Vincetown interface, supports the difference in *cis*-DCE concentrations seen in MAG 112 and MAG 66. Well MAG 112, which is only screened below the interface, had significantly lower *cis*-DCE concentrations than MAG 66, which partly intersects the interface. The same trend was seen in the well concentrations of vinyl chloride, but not in HRPP-1 vinyl chloride. HRPP-1 vinyl chloride concentrations are constant at and below the interface, and they remain lower than both MAG 112 and MAG 66. HRPP-2 cis-DCE concentrations are approximately 100 µg/L lower than MAG 4 cis-DCE, and HRPP-2 data reflects a decrease in cis-DCE below the interface that cannot be detected in MAG 4 due to lack of resolution. Like MAG 4, HRPP-2 is mostly non-detect for vinyl chloride, with the exception of two low concentration samples at the Kirkwood-Vincetown interface. As was the case with *cis*-DCE, the slight change in vinyl chloride concentration cannot be detected in MAG 4 due to the 10-foot (3 meters) screen.

Overall, CVOC concentrations produced by the HRPP samplers are in general agreement with the well data. Differences are likely due to spatial concentration differences even over small distances, and more importantly due to preferential flow in wells that biases well data to the most permeable depths. The very close agreement between independent cells at the same depth supports the reproducibility of the HRPP data.

5.3.1.3 Microbial Community Results

Well water samples were taken from MAG 4 and MAG 66 in August 2015, and bio-traps were deployed in MAG 4, MAG 66, and MAG 112 in September 2015 to gather microbial community data for comparison to HRPP micro-biotraps. A direct quantitative comparison cannot be made between Biosep bead samples (well bio-trap, HRPP micro-biotrap) and well water samples because the former is measured in units of cells per bead and the latter is measured in units of cells per milliliter. Therefore, the most direct quantitative comparison can be made between the bio-traps in the wells and the HRPP micro-bio-traps. Well water samples are viewed as an additional qualitative reference.

Total Eubacteria, Sulfate-Reducing bacteria, Methanogens- At the MAG 66 and MAG 112 site, HRPP-1 concentrations of total eubacteria captured using the HRPP-1 microbio-traps were closer to the concentrations measured using well Biotraps than those in well water (**Figure 5.18**). Cell quantities in HRPP-1 micro-bio-traps, MAG 66 well water, and the MAG 112 well bio-trap were similar for concentrations of sulfate-reducing bacteria, which brings into question why the MAG 66 Bio-trap did not detect sulfate-reducing bacteria. HRPP-1 concentrations of methanogens were up to an order of magnitude higher than MAG 66 well water and the MAG 112 Bio-trap. Like sulfate-reducing bacteria, methanogens were not detected in the MAG 66 bio-trap.

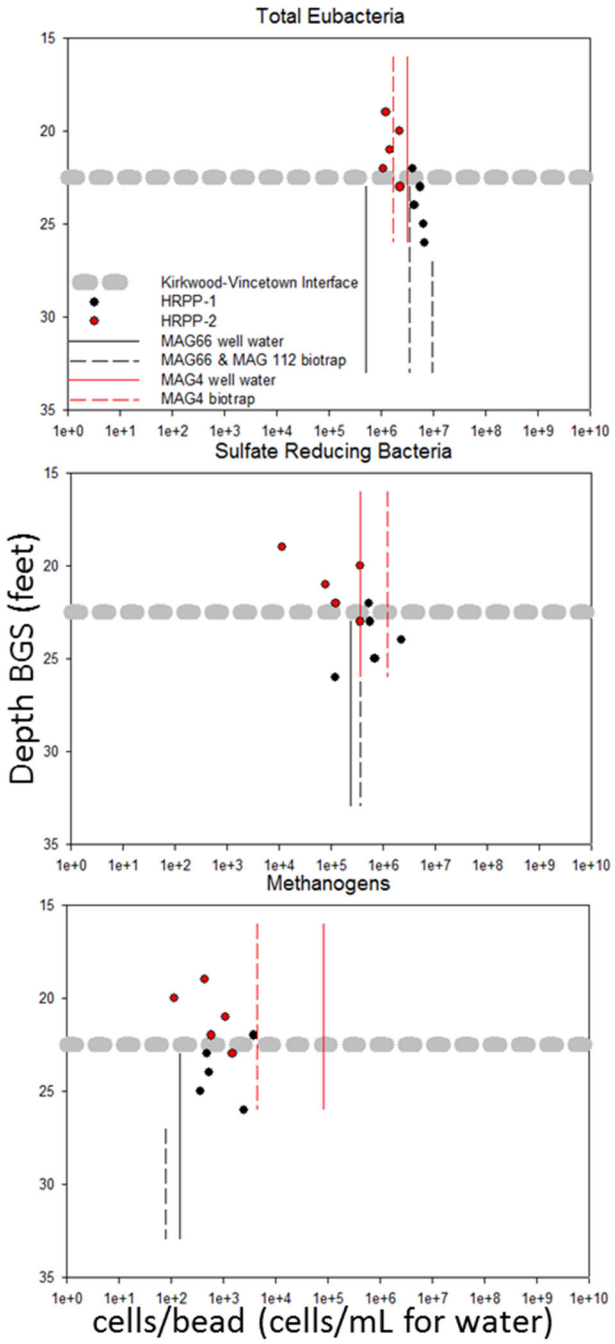

Figure 5.18. Fort Dix HRPP-1 and HRPP-2 total eubacteria, sulfate-reducing bacteria, and methanogens compared to well water and bio-traps from MAG 4, MAG 66, and MAG 112.

At the MAG 4 site, concentrations of total eubacteria captured using the HRPP-2 micro-biotraps were almost identical to well bio-trap concentrations, which were only slightly lower than well water concentrations. Sulfate-reducing bacteria concentrations captured in the HRPP-2 micro-biotraps varied with depth. Some HRPP-2 measurements were similar to the MAG 4 bio-trap,

and other HRPP-2 measurements were up to one order of magnitude lower than those measured using the MAG 4 bio-trap. Methanogen concentrations captured using the HRPP-2 micro-biotraps were lower than those measured in MAG 4 water and using the MAG 4 bio-trap, but generally were within an order of magnitude of the bio-trap. At both locations, variation between HRPP-1 and HRPP-2 in total eubacteria, sulfate-reducing bacteria, and methanogens was much smaller than variation between the wells. The HRPP micro-biotraps captured variability of sulfate-reducing bacteria and methanogens with depth that the broadly screened wells did not detect.

Reductive Dechlorination- Four species of bacteria capable of reductive dechlorination and two reductive dechlorination genes were detected in both MAG 66 and MAG 4 well water (**Figure 5.19**). The Biotrap in MAG 66 detected all species and genes that were detected in the well water. The Biotrap in MAG 4 did not detect any of the reductive genes nor *Dehalococoides* consistent with the lower abundances in MAG 4 well water than MAG 66 or 4 for these species/genes. For the species/genes, there was no consistent trend on which measurement technique, well water or Biotrap produced greater or lower abundances. The MAG 112 Biotrap only measured *Dehalobacter, Dehalogenimonas, and Desulfitobacterium,* and in all three cases was higher than the MAG 66 Bio-trap despite being in approximately the same spatial location, possibly due to its deeper depth.

Concentrations of reductive dechlorinators captured using HRPP-1 were generally consistent with MAG 66 well water, MAG 66 bio-trap, and the MAG 112 bio-trap even for genes that were only detected in a single interval of the HRPP. In cases where MAG 66 Biotrap differed from MAG 66 well water, the HRPP-1 concentrations were typically closer to the Biotrap concentrations. Concentrations of reductive dechlorinators captured using HRPP-2 were closer to concentrations captured with the MAG 4 Biotrap than those in MAG 4 well water for all but *Dehalogenimonas*, for which HRPP-2 concentrations were scattered between well water and Biotrap concentrations. The MAG 4 Biotrap and HRPP-2 were both non-detect for tceA and vinyl chloride reductase. The MAG 4 bio-trap was also non-detect for *Dehalococcoides* and concentrations of *Dehalococcoides* captured using HRPP-2 are over an order of magnitude lower than concentrations MAG 4 well water. The reductive dechlorination results from MAG 4 and HRPP-2 suggest that *Dehalococcoides* may have been more readily available suspended in water rather than attached to Biosep beads.

Generally, HRPP-1 and HRPP-2 were not only consistent with each other, but also with data from well water and Biotraps. The HRPPs showed a tendency to correlate more closely with Biotraps than well water in cases where the two well measurement methods differed by an order of magnitude.

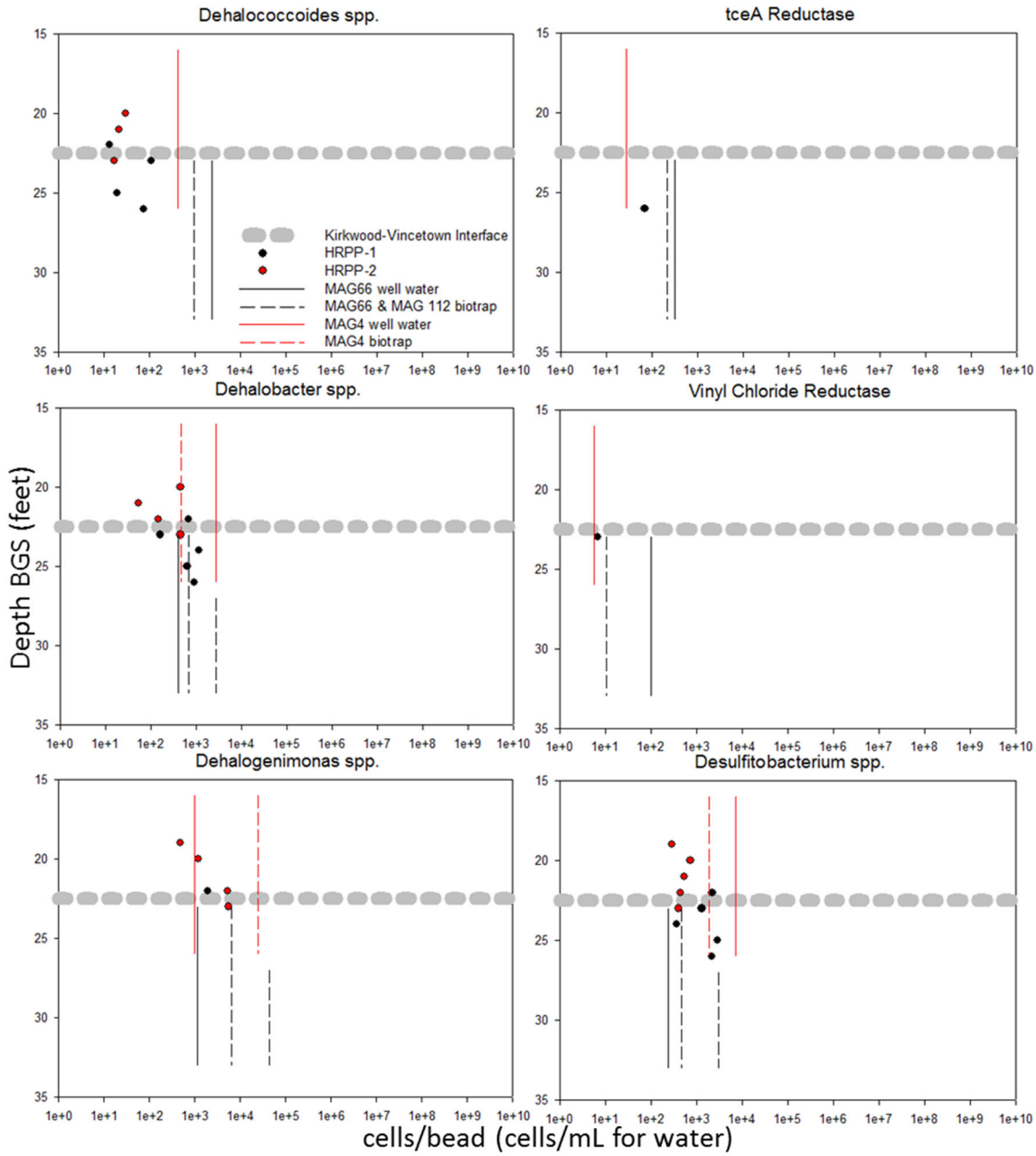

Figure 5.19. Fort Dix HRPP-1 and HRPP-2 reductive dechlorination microbial data compared to well water and bio-traps from MAG 4, MAG 66, and MAG 112.

Aerobic Co-metabolism- Well water data indicate significantly different aerobic cometabolic profiles between MAG 66 and MAG 4. MAG 66 and MAG 4 well water differed by over an order of magnitude for five of the six aerobic cometabolic genes that were detected (**Figure 5.20**). In some cases, concentrations in MAG 66 are higher than MAG 4, and in some cases the opposite is true. MAG 66 was non-detect for toluene dioxygenase, and MAG 4 was non-detect for toluene monooxygenase 2. The MAG 66 Bio-trap was non-detect for all aerobic cometabolic genes aside from phenol hydroxylase, even though MAG 66 well water had detectable concentrations for all genes. The MAG 4 Bio-trap was over three orders of magnitude higher

than the MAG 4 well water for particulate methane monooxygenase, but was over an order of magnitude lower than MAG 4 well water for soluble methane monooxygenase and toluene dioxygenase. The only aerobic cometabolic enzyme that had moderately consistent concentrations for all wells (water and Bio-traps) was phenol hydroxylase.

Soluble methane monooxygenase concentrations captured using the HRPP-1 microbio-trap generally increased with depth below the Kirkwood-Vincetown interface, but particulate methane monooxygenase concentrations decreased by approximately two orders of magnitude across the interface. The other three aerobic cometabolic genes were detected with HRPP-1 at consistent concentrations that did not vary significantly with depth. Both soluble methane monooxygenase and phenol hydroxylase concentrations captured using HRPP-2 micro-biotraps appear to have a moderate concentration peak at approximately 22 feet (6.7 meters) BGS. Particulate methane monooxygenase concentrations captured using HRPP-2 increase by approximately three orders of magnitude from above to below the interface; this trend is opposite the trend seen in concentrations captured using HRPP-1.

Aerobic cometabolic bacteria concentrations captured using HRPP-1 microbio-traps generally match up best with MAG 112 or MAG 66 (when detectable) bio-trap concentrations. The increase in HRPP-1 soluble methane monooxygenase below the interface was mimicked in the difference between MAG 66 well water and the MAG 112 bio-trap, and the decrease in HRPP-1 particulate methane monooxygenase below the interface was also reflected in MAG 66 and MAG 112. Aerobic cometabolic bacteria concentrations captured using HRPP-2 micro-biotraps generally fell between concentrations in MAG 4 well water and the MAG 4 bio-trap. Most notably, particulate methane monooxygenase concentrations captured using HRPP-2 match concentrations in MAG 4 well water above the interface then increase by three orders of magnitude and match concentrations in the MAG 4 bio-trap below the interface. Toluene monooxygenase 2 was detected with HRPP-2 but was not found in MAG 4 well water nor in the MAG 4 Biotrap.

Overall microbial concentrations produced by the HRPPs were in agreement with the well data. In some cases, well water and Biotraps for the same well were not in agreement with one another, but the HRPPs generally matched one or the other in such cases. Differences in HRPP and well data were possibly attributed to more uniform and aqueous environments inside well casings or preferential flow in wells, which over-represents the most permeable depths.

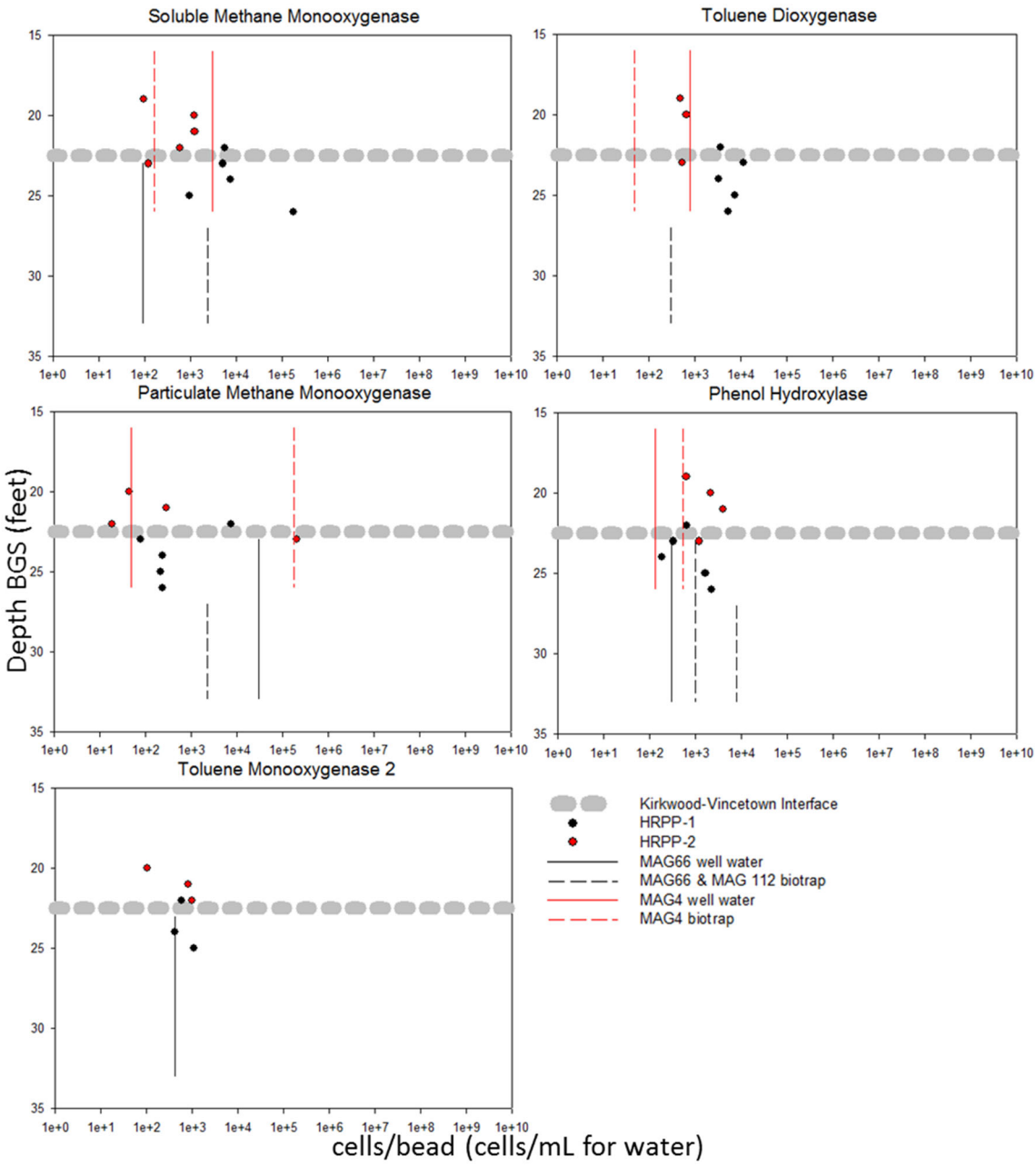

Figure 5.20. Fort Dix HRPP-1 and HRPP-2 aerobic cometabolic microbial data compared to well water and bio-traps from MAG 4, MAG 66, and MAG 112.

5.3.1.4 CSIA of CVOCs

The MAG 4 well water $\delta^{13}C$ values for TCE and *cis*-DCE (-27 and -26 ‰) were significantly lighter than TCE and *cis*-DCE in MAG 66 (both -16‰) (**Figure 5.21**). However, the MAG 4 and MAG 66 bio-trap $\delta^{13}C$ values for cis-DCE (-9 and -11‰) were much more positive than well water in either well. Neither well Biotrap returned CSIA data for TCE. CSIA data for *cis*-DCE but not TCE was obtained for HRPP-1 and HRPP-2 micro-biotraps. The single value of *cis*-DCE

$\delta^{13}C$ captured with HRPP-1 above the interface was -23 ‰, and the single value captured below the interface was -21 ‰. The single value of *cis*-DCE $\delta^{13}C$ captured with HRPP-2 above the interface was -21 ‰, and the single value below the interface was -20 ‰.

Both HRPP micro-biotraps produced $\delta^{13}C$ values of *cis*-DCE that were more similar to well water values than the in-well Bio-Trap. The HRPP-1 microbio-trap detected lighter $\delta^{13}C$ *cis*-DCE values than MAG 66 well water, MAG 66 Biotrap, and the MAG 112 Biotrap, but similar values to the HRPP-2 micro-biotrap. The HRPP-2 micro-biotrap $\delta^{13}C$ *cis*-DCE values fell between the MAG 4 well water and MAG 4 Biotrap values, but were closer to the lighter well water value. The similarity in CSIA results for CVOCs in HRPP-1 and HRPP-2 indicate good reproducibility with the HRPP method of sampling.

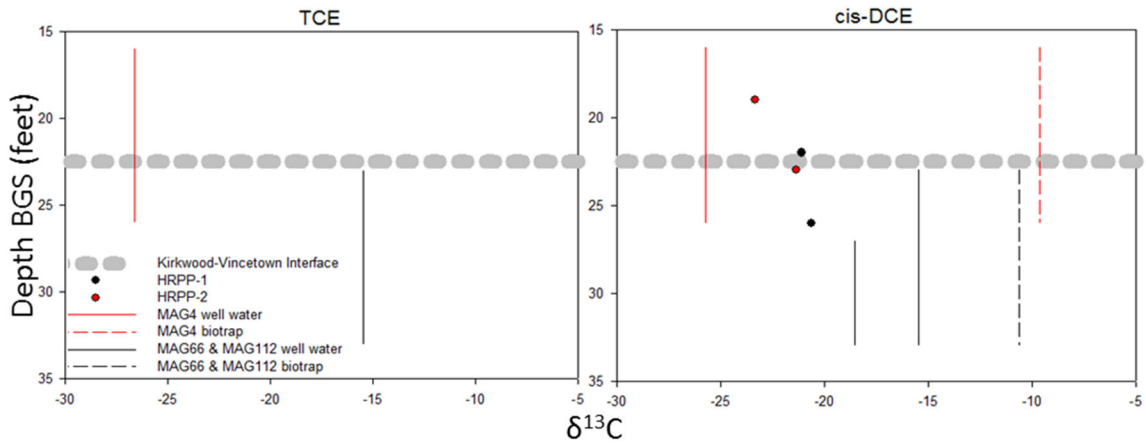

Figure 5.21. Fort Dix HRPP-1 and HRPP-2 CSIA for cis-DCE and vinyl chloride compared to well water and Biotraps from MAG 4, MAG 66, and MAG 112.

5.3.1.5 Velocity Results

Based on mass transfer of bromide out of the velocity cells, HRPP-1 and HRPP-2 measured velocities ranging from 1 to 10 cm/day (**Figure 5.22**). Measured velocities within the Kirkwood and Vincetown formations above and below the highly permeable interface between the formations were similar (~5 cm/d). For both HRPP-1 and HRPP-2, the maximum velocity (10 cm/d) occurred near the upper fringe of the interface and the lowest (1 cm/d) occurred at the lower fringe of the interface. The estimated average annual velocity across the site is 7.5 cm/day based on hydraulic gradient, which is within the range of velocities estimated by HRPP-1. The similarities of measured velocities with depth for both HRPP at two different locations as well as the similarity to the average site formation support the ability of the HRPP to estimate velocity.

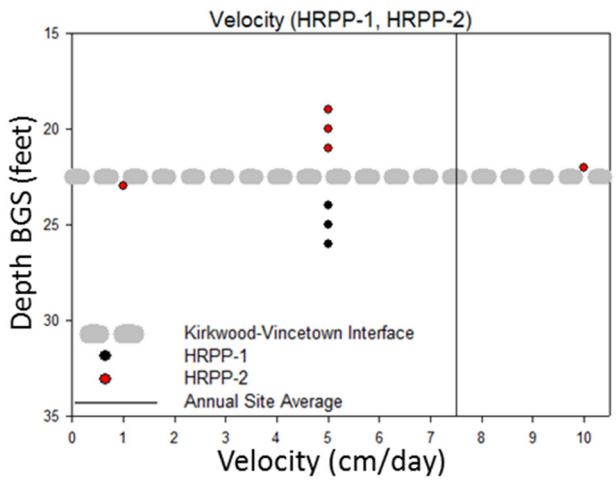

Figure 5.22. HRPP-1 and HRPP-2 estimated velocities based on mass transfer of bromide. Note: HRPP-2 data points lay on top of HRPP-1 data points at depths 22 and 23 feet BGS.

5.3.1.6 Summary

The Fort Dix field trial validated the ability to direct drive HRPP-A up to 7.9 meters BGS and to produce data on groundwater velocity, contaminant concentrations, geochemistry, microbial community structure, and CSIA of CVOC that is comparable to what is typically collected from monitoring wells(s). HRPP duplicate depth samples exhibit good reproducibility of HRPP data. The HRPPs captured concentration variability (of CVOCs, geochemical indicators, and microbial communities) that is not represented in broadly screened wells. The Fort Dix field trial allowed the physical design of the prototype HRPP to be tested and make modifications to improve the durability and utility of the sampler. Experience from the first field trial led to the fabrication of a second HRPP model (HRPP-B).

5.3.2 Former Naval Air Station, Alameda Field Trial

Two sets of three coupled HRPP-B samplers (3.7 m) and one HRPP-A sampler were installed in a source zone. Data from HRPPs were compared to HPT/MIP data, core extractions, standard monitoring wells (including Biotrap deployment and passive flux meters), and multiple depth interval well screens (multi-level wells) taken at the time of insertion.

5.3.2.1 Geochemistry Results

Peaks in Cl^- concentrations were detected in both SMLS 1 and SMLS 4 at approximately 5.5 meters BGS (**Figure 5.23**). Chloride concentrations then decreased to a depth of 6.1 meters BGS for both SMLS 1 and SMLS 4, and a second peak occurred in SMLS 1 and SMLS 4 at a depth of 6.7 m BGS. Cl^- concentrations measured in HRPP-3 and HRPP-4 both peaked at a depth of approximately 3.7 meters BGS and remained elevated to a depth of ~6 m. Below this depth, HRPP Cl^- concentrations increased. Concentrations of Cl^- in HRPP-3, 4 and 5 were generally similar to concentrations in multilevel well SMLS 4. However, concentrations in multi-level well SMLS-3 were much lower than HRPP concentrations or the other multi-level well (SMLS-4).

Standard monitoring wells, SPW 3-1, SPW 3-2, and PEW 02, all have lower Cl^- concentrations than even the minimum concentrations observed from the multilevel wells or HRPPs over similar depths. Chloride concentration depth profiles were very similar between HRPPs.

However, Cl^- concentrations in well water were much more variable depending on well screen interval and location even though they are only a few meters apart. Even for the multilevel wells, Cl^- concentrations differed dramatically for the same depth. The differences in standard, multilevel wells, and HRPP concentration distributions are likely due to concentrations from wells representing only the most permeable layers, a condition that is exaggerated by large well screens.

SMLS 1 and SMLS 4 both generally increase in sulfate concentrations with depth from 125-240 mg/L and 50-190 mg/L, respectively. PEW 02 sulfate falls within the range of the multilevel wells, but SPW 3-1 and SPW 3-2 are lower than the lowest concentrations for SMLS 3 but similar to those from SMLS4 and those from HRPP samples at similar depths. Sulfate concentration profiles from HRPP samplers qualitatively mimic Cl^- profiles at depths above ~4 m. However, as Cl^- profiles remain relatively constant until ~6m BGS, SO_4^{-2} concentrations rapidly decrease and remain at a minimum to a depth of ~6 m. The divergence of Cl^- and SO_4^{-2} profiles in both HRPP and multi-level wells is a clear indication of SO_4^{-2} reduction at depths. HRPP measured concentrations generally match concentrations measured in SMLS 4 and standard wells. For both Cl^- and SO_4^{-2}, concentrations from multi-level well SMLS 3 do not appear to match either standard wells or concentrations from HRPP at similar depths.

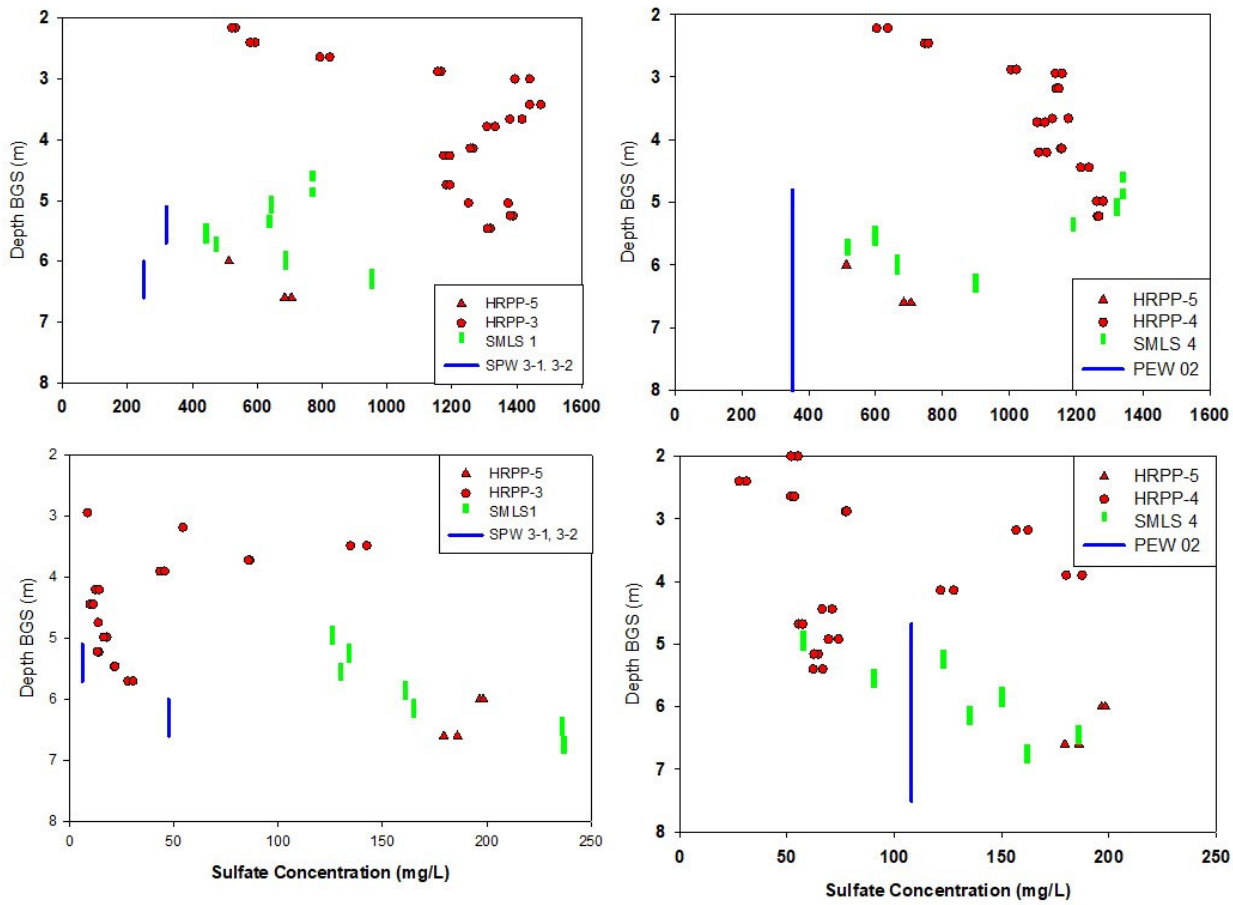

Figure 5.23. Alameda geochemical indicators (chloride, sulfate, phosphate) detected by HRPP-3,4,5 compared to nearby monitoring wells.

5.3.2.2 CVOC Concentrations

CVOC concentration profiles were remarkably similar for those produced by multi-level wells, HRPP samplers, and soil cores (**Figure 5.24**). All three methods produced concentration profiles that exhibit sharp peaks in *cis*-DCE and VC at 5.8m BGS, with concentrations decreasing by orders of magnitude within <2 m. HRPP profiles also reflect an additional zone of elevated CVOC concentrations at ~ 4m BGS (near the peak Cl^- and SO_4^{-2} concentration), which is reflected in soil cores but not well water as there are no wells that are screened over that depth interval. This shallower peak also coincides with a zone of low permeability sediment identified in field inspections of cores. Standard monitoring wells (SPW3-1, 3-2, and PEW 02) generally have concentrations that are near the average concentration over which they are screened. At the HRPP 3 location, the MIP-PID detected two VOC peaks (3.7 and 4.6 m BGS), and the MIP-ECD detected one CVOC peak at 3.7 meters BGS. The upper peak identified by the ECD and PID correspond to the upper peak from the HRPP and core profiles. However, neither the ECD or PID identified the main CVOC peak at 6 m, which was reflected in well, HRPP and core data. At the HRPP location, the MIP detected one VOC peak (PID) at 4 m BGS and two VOC (PID) and CVOC (ECD) peaks at 5.5 and 6.1 m BGS. The concentration profiles based on PID response generally reflect the peaks in concentrations from wells and HRPP, although the magnitude of the lower peak based on PID is much reduced. The concentration profile of the ECD did not reflect the upper peak identified by core or HRPP data.

Overall, the CVOC concentrations captured with the HRPPs reproduce the same concentration profiles created by multilevel wells and soil core samples. CVOC concentrations captured with HRPPs also generally match standard monitoring well concentrations, but the HRPPs have higher resolution capabilities and therefore create more complete concentration profiles than standard wells. There was generally poor agreement between qualitative MIP profiles and any other data set.

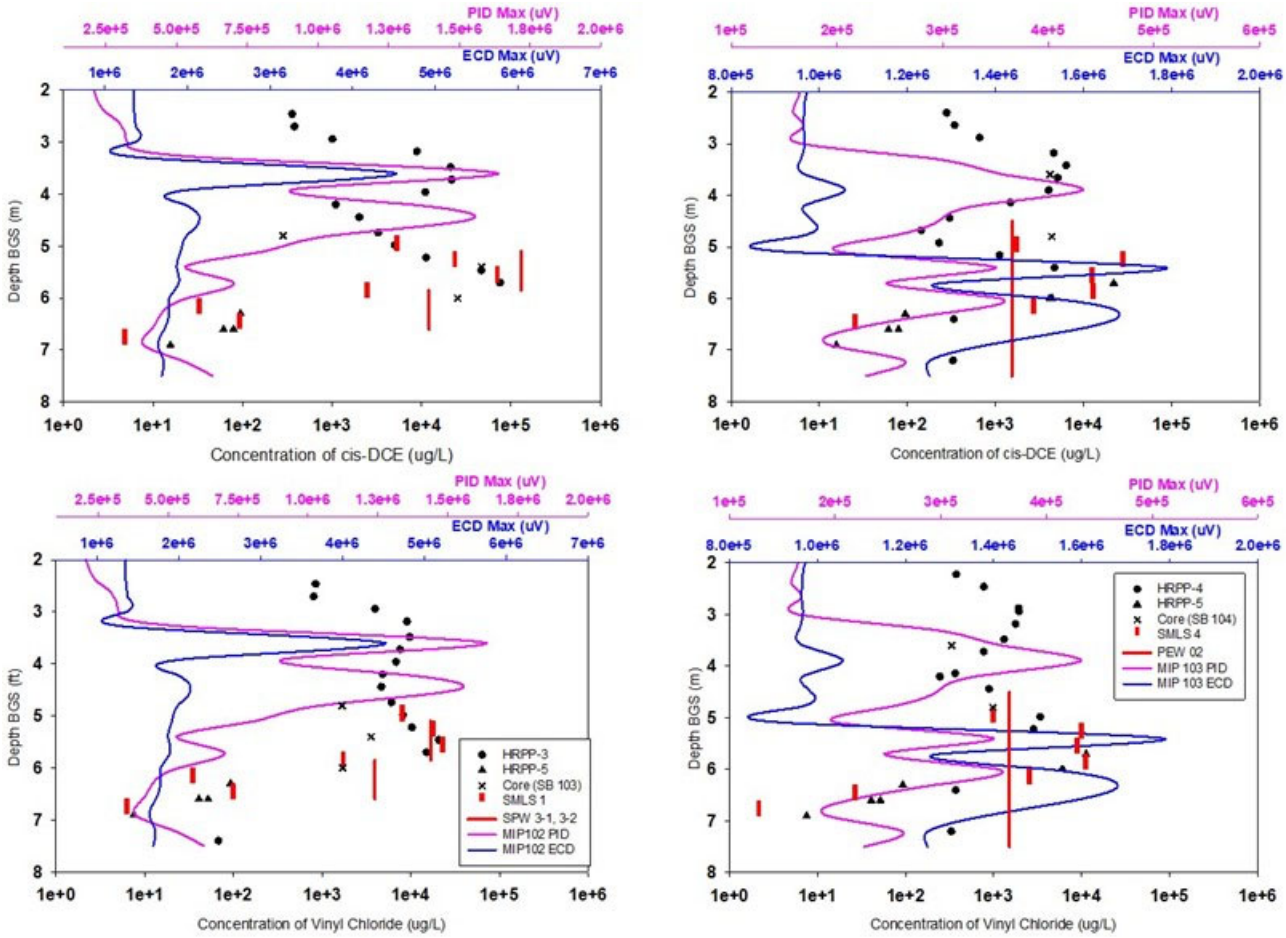

Figure 5.24. Alameda CVOC concentrations (cis-DCE, vinyl chloride) detected by HRPP-3,4,5 compared to monitoring well concentrations, MIP-PID, MIP-ECD, and soil cores.

5.3.2.3 Microbial Community

Well water samples were taken from standard wells (SPW 3-1, SPW 3-2, and PEW 02) and multilevel wells (SMLS 1 and SMLS 4) in August 2016, and Biotraps were deployed in standard wells SPW 3-1 and PEW 02 in September 2016 to gather microbial community data for comparison to the HRPP micro-biotraps. A direct quantitative comparison cannot be made between Biosep bead samples (well Biotrap, HRPP microbio-trap) and well water samples because the former is measured in units of cells per bead and the latter is measured in units of cells per milliliter. Therefore, the most direct quantitative comparison can be made between the Biotraps in the wells and the HRPP micro-biotraps. Well water samples were viewed as an additional qualitative reference.

Total Eubacteria, Methanogens, Sulfate-Reducing- Biotraps, well water, and HRPP micro-biotraps all produced similar distributions of Total Eubacteria at both sample locations (**Figure 5.25**). The abundances of sulfate reducers were also similar for data produced by well water and in well Biotraps. Peak abundances produced by the HRPP micro-biotraps were similar to well water and in well Biotraps at similar depths but there were large changes in the abundance of sulfate reducers with depth based on HRPP results. The abundance of methanogens was

generally similar between all measurement methods. Although no methanogens were detected in PEW 02 well water even though installed Biotrap reflected abundances near those of multi-level well water.

Reductive Dechlorination- In general, reductive dechlorinating bacteria concentrations measured in SPW 3-1, SPW 3-2, and SMLS 1 well water were all similar (**Figure 5.26**). Peak concentrations generally occurred around 6 m BGS corresponding to peak CVOC concentrations. For multi-level well SMLS 4, abundances of reductive dechlorinators/genes were generally more uniform. Abundances in PEW 02 well water were similar or less than multi-level well abundances and in some cases were absent (*Dehalobacter* and *Desulfuromonas*). PEW 02 Biotrap abundances were variable; in some cases they were greater and in others less than PEW 02 well water and seemed unrelated to SMLS 4 well water (**Figure 5.27**). Abundances measured by HRPP micro-biotraps were generally lower than well Biotraps or well water at both sites. However, at both sites abundances of *Dehalobacter*, *Desulfitobacterium* , and *Desulfuromonas* abundances measured by HRPP micro-biotraps were roughly equal or greater than well water or well Biotraps. The inconsistencies in relative abundances between measurement methods may reflect differences in microbial lifestyles. Some species may be more biofilm dependent while others may be more planktonic, or some species may be better able to colonize the Biosep beads. In any case, there does appear to be biases for certain species/genes.

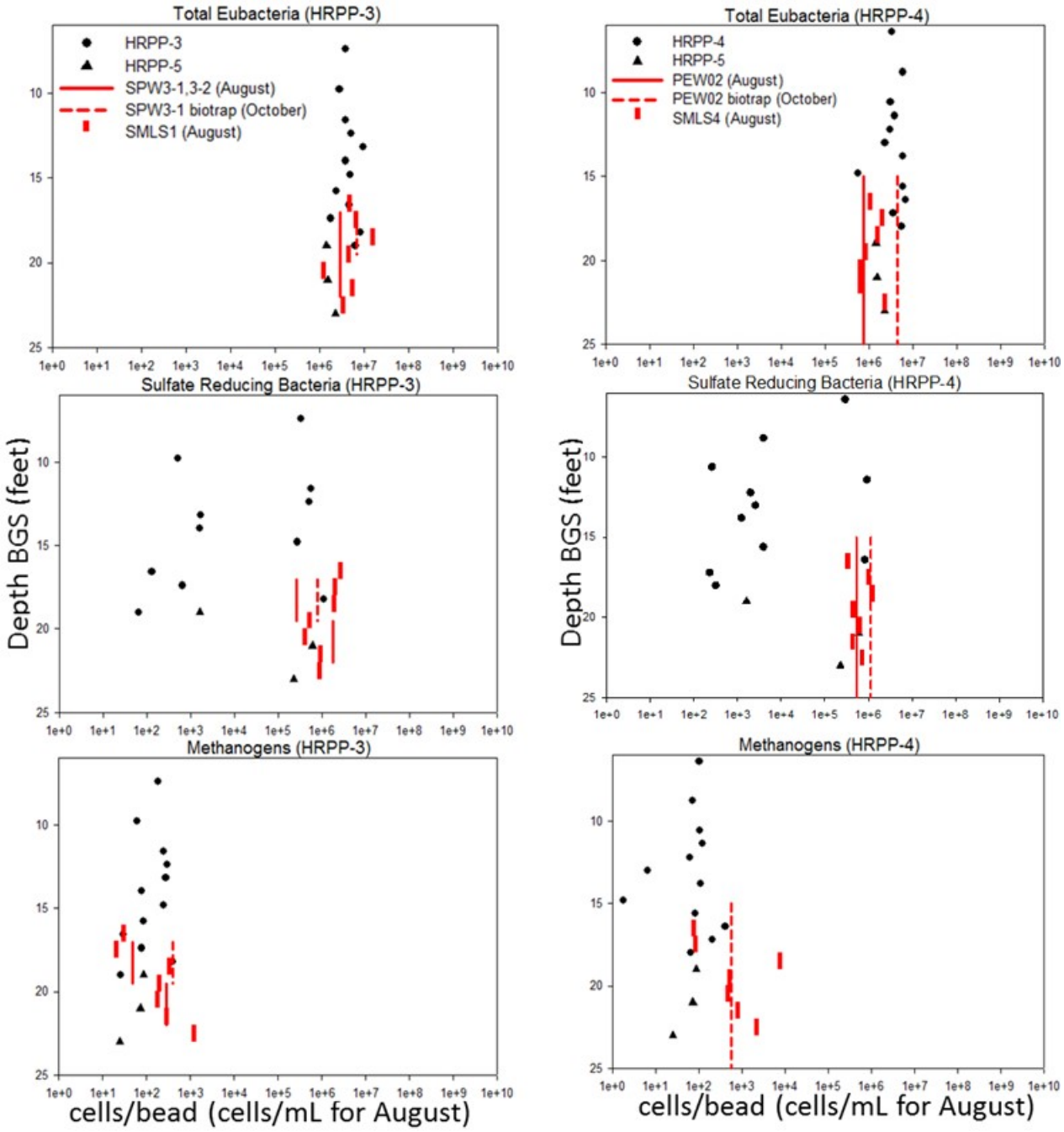

Figure 5.25. Alameda HRPP-3 and HRPP-5 total eubacteria, sulfate-reducing bacteria, and methanogens compared to monitoring well water and Biotraps in wells.

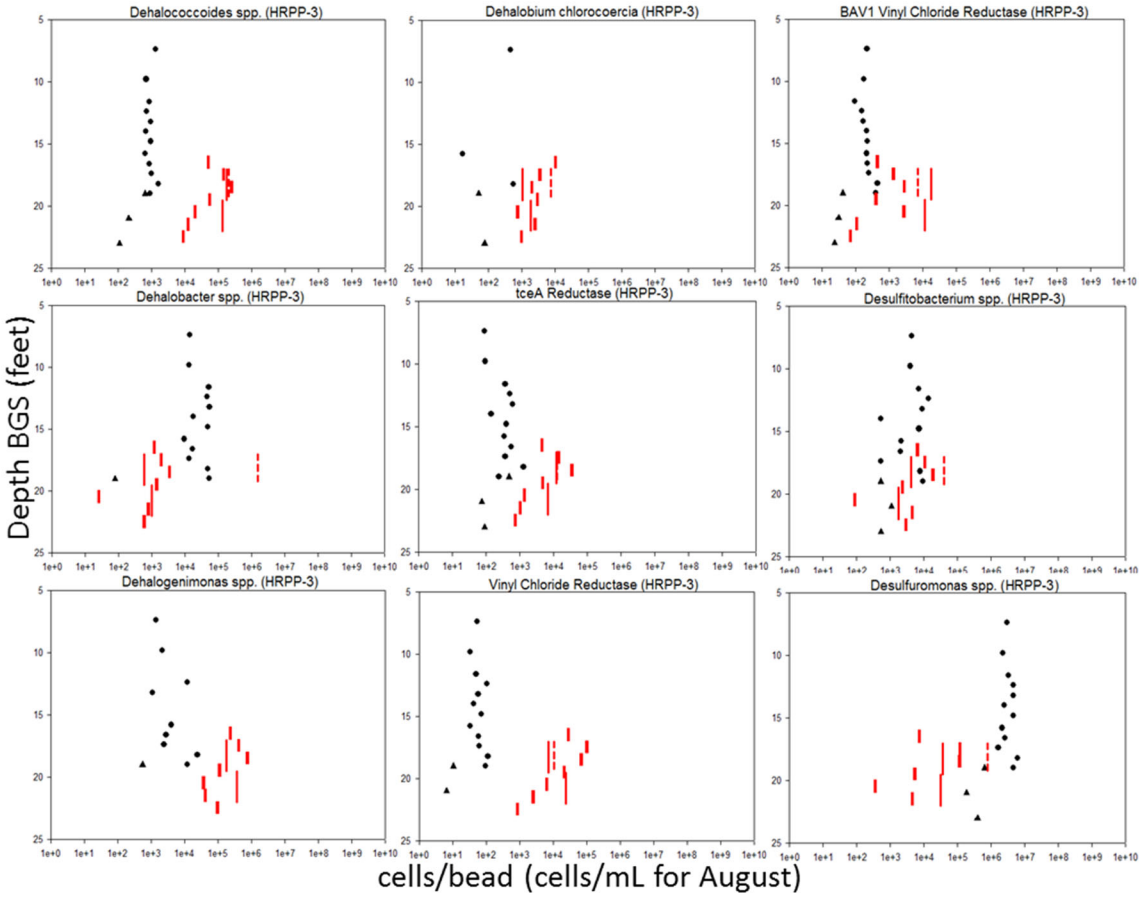

Figure 5.26. Alameda HRPP-3 and HRPP-5 reductive dechlorination microbial data compared to monitoring well water and Biotraps in wells.

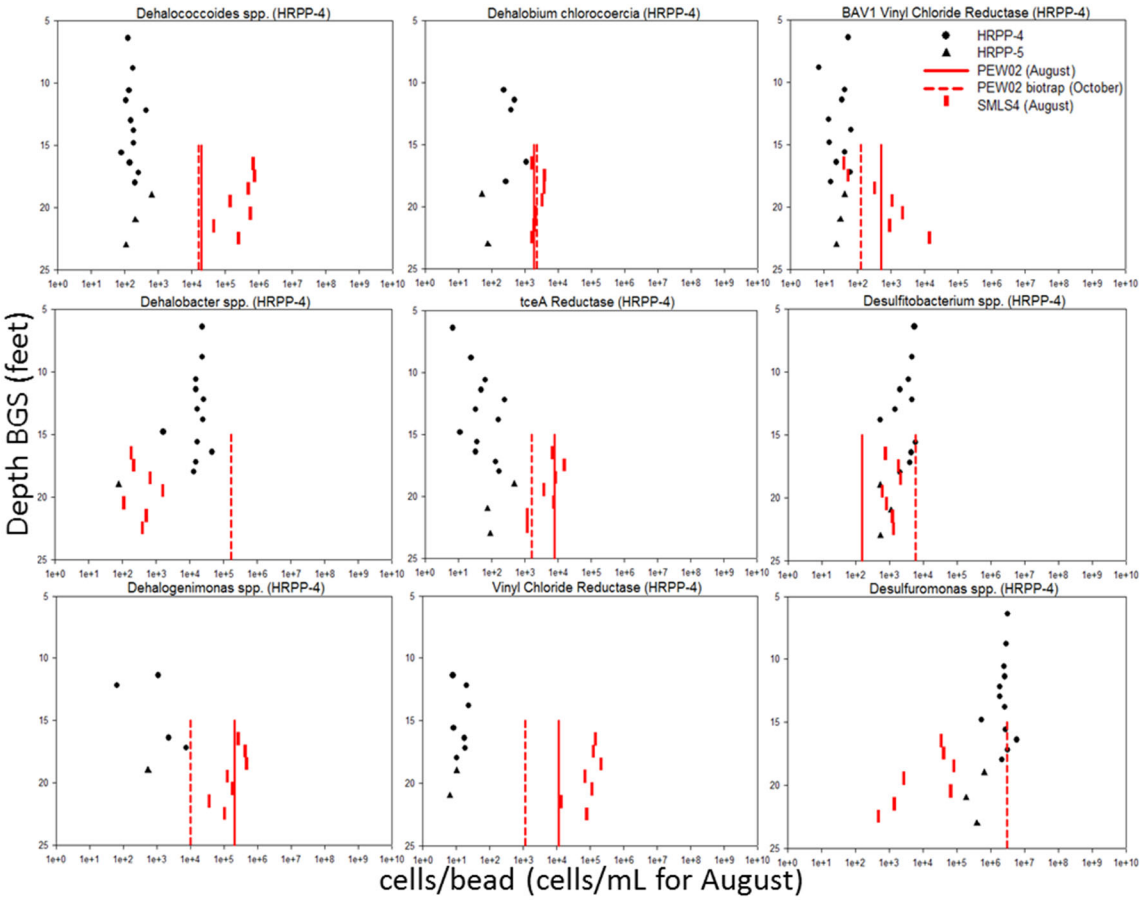

Figure 5.27. Alameda HRPP-4 and HRPP-5 reductive dechlorination microbial data compared to monitoring well water and Biotraps in wells.

5.3.2.4 CSIA of CVOCs

HRPP micro-biotraps in HRPP-3 and HRPP-4 and in well Biotraps SPW-3 and PEW 02 produced CSIA results that were very similar for *cis*-DCE but values were unrealistically negative and much lower than well water from these wells or in multilevel wells (**Figure 5.28**). Based on this, the data was considered circumspect and is not discussed further. CSIA of *cis*-DCE measured by micro-biotraps from HRPP-5 do generally match CSIA values for well water from multi-level wells. CSIA of well water from standard wells is more negative than multilevel wells at one HRPP location (HRPP-3), and intermediate at HRPP-4 location. CSIA of VC was consistent for all HRPP micro-biotrap samples. Values were generally consistent with well water, although values in well water were much more variable. CSIA of VC on Bio-traps from the standard monitoring wells at both sites could not be measured. Overall, well water from standard wells, multi-level wells, standard Bio-traps, and microbio-traps appears to produce variable results, particularly considering the extremely negative *cis*-DCE values measured. Excluding the anomalous *cis*-DCE data, HRPP-biotraps generally reflect $\delta^{13}C$ values of *cis*-DCE and VC near -20 and -25 to -30, respectively. Because CVOC concentration data from all methods show generally consistent ratios of *cis*-DCE to VC (~1:1) with depth, the very large changes (>25 ‰) multi-level CSIA data over <1 m are difficult to reconcile as our the trends in

changes for *cis*-DCE and VC appear random or counter to what should occur based on fractionation.

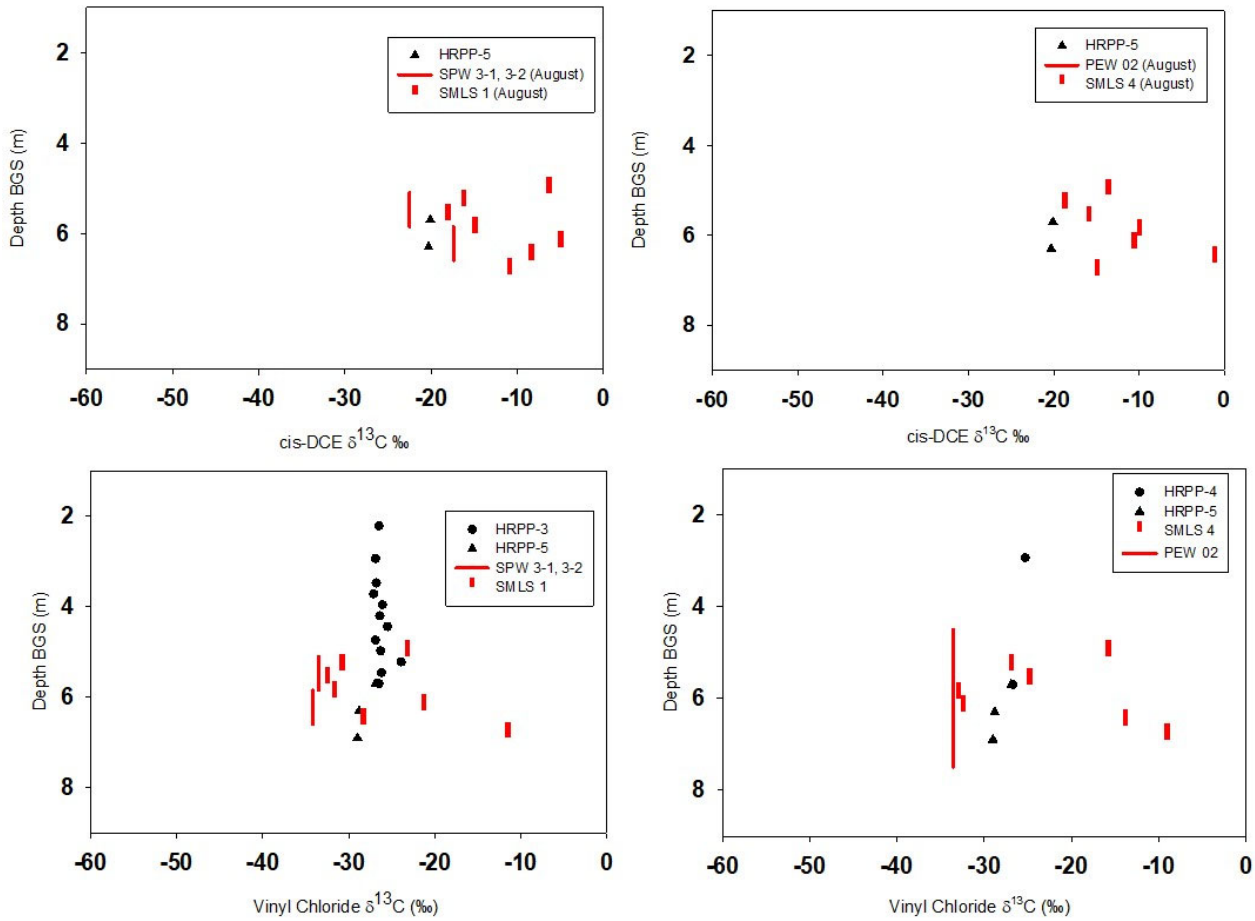

Figure 5.28. Alameda HRPP-3,4,5 CSIA for cis-DCE and vinyl chloride compared to monitoring well water and Biotraps in wells.

5.3.2.5 Velocity Results

Comparative velocity measurements at the Alameda site include an estimated average site velocity, MIP/HPT data, and passive flux meters installed in the standard monitoring wells. The MIP-EC measures electrical conductivity and the HPT measures hydraulic pressure; therefore, both tools are qualitative indicators of soil permeability changes with depth rather than direct measurements of velocity. The site average velocity based on hydraulic head difference is two cm/day. The passive flux meters in SPW 3-1 and SPW 3-2 (HRPP-3 location) detected velocities of four and three cm/day, respectively. HRPP-3 velocity estimates based on mass transfer of bromide range from one to five cm/day (**Figure 5.29**). In general, the HRPP-3 intervals with lower velocities (1 cm/day) occur at depths where the MIP/HPT indicates high pressure and high electrical conductivity, which both indicate a relatively low permeability soil.

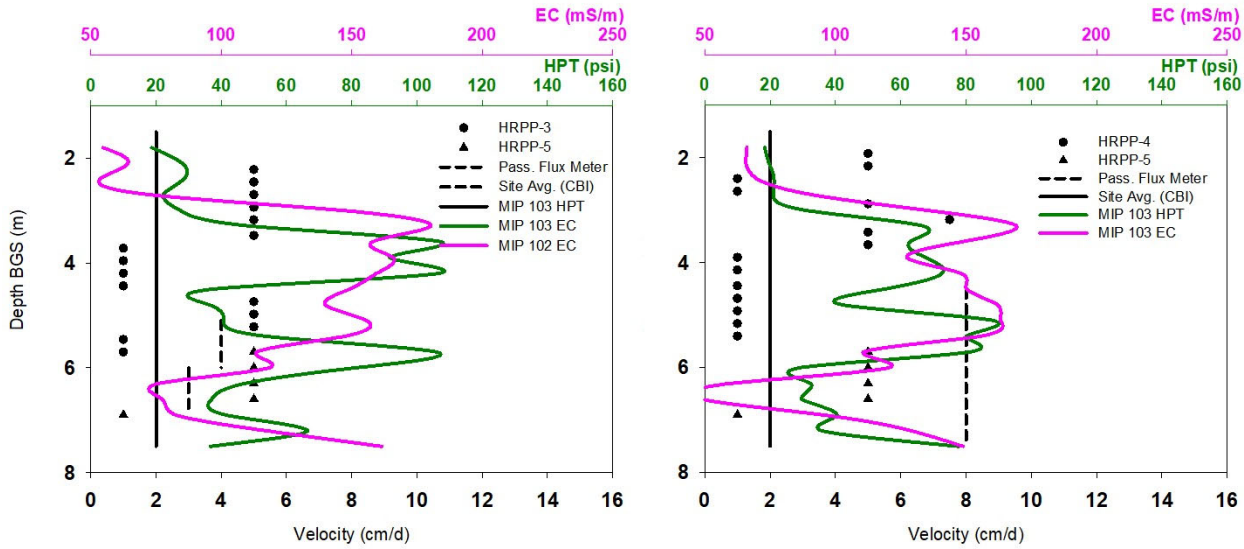

Figure 5.29. Alameda HRPP-3,4,5 velocity estimates based on mass transfer of a conservative tracer compared to passive flux meters in wells, hydraulic head site average, MIP-EC, and HPT.

The passive flux meter in PEW 02 (HRPP-4 location) detected a velocity of 8 cm/day. HRPP-4 velocity estimates based on mass transfer of bromide range from one to 7.5 cm/day. Similar to HRPP-3, the HRPP-4 intervals with lower velocities (1 cm/day) occurred at depths (4 to 5.5 meters BGS) where the MIP/HPT indicated relatively low permeability soil. HRPP-5 velocity estimates range from 1 to 5 cm/day, which makes HRPP-3, 4, and 5 velocity measurements within a reasonable deviation from the calculated site average and the passive flux meters in wells SPW 3-1, SPW 3-2, and PEW 02.

The HRPP velocity measurements are similar to those estimated by other methods (MIP/HPT, PFMs, etc.), whether qualitative or quantitative. The HRPP is not susceptible to interferences that can affect other methods of measuring velocity, such as high salinity for the MIP-EC probe or biased flow-through high permeability regions for PFMs in wells.

5.3.2.6 Conclusion

Similar to the Fort Dix field trial, the Alameda field trial demonstrated that the HRPP is capable of collecting data sets that are comparable to what is typically collected from monitoring wells, soil cores, and MIP/HPT profiles (groundwater velocity, contaminant concentrations, geochemistry, microbial community structure, and CSIA of CVOCs). HRPP duplicate depth samples for geochemistry and CVOC concentrations exhibit good reproducibility of HRPP data. The HRPPs once again captured concentration variability (of CVOCs, geochemical indicators, and microbial communities) that is not represented in broadly screened wells, and HRPP trends in geochemistry and CVOC concentrations matched trends in multilevel wells and soil cores. The Alameda field trial allowed us to test the physical design of the HRPP when three four-foot sections are coupled together. The new, longer HRPP resulted in more complete contaminant profiles up to approximately the same depth as the Fort Dix HRPPs (8 m BGS).

5.3.3 USDA BARC Site Field Evaluation

At the BARC site, HRPP samplers were used to evaluate a chlorinated solvent groundwater plume in a shallow heterogenous surficial aquifer. The site included a biowall installed to promote reductive dechlorination of CVOCs. A surface stream was located downgradient of the biowall. Strings of HRPP samplers were installed along a transect starting from an upgradient location with peak dissolved TCE concentrations (HRPP-MW6), within the biowall (HRPP-BW6), and downgradient of the biowall (HRPP-MW10). Each HRPP string was installed next (~3ft) to an existing monitoring well (MW6, BW6, and MW-10). In addition, single section HRPP samplers (1.33m) were installed between the biowall and well MW10 and immediately next to the stream. Wells were generally screened from ~1.5m BGS into the clay layer ~ 6-7m BGS. At the time of sampling, groundwater elevation was at or within ~0.3m of the ground surface at all locations. HRPP samples were used to established concentrations of cVOC with depth, changes in isotopic composition CVOCs, geochemical conditions (e.g. concentrations major dissolved redox sensitive species), microbial community abundance and composition, and pore velocity as discussed in detail below.

5.3.3.1 Groundwater Quality Comparisons Based on Well and HRPP Data at Co-Located Sites

5.3.3.1.1 Upgradient Site MW6 Location

MW6 was upgradient of the biowall in an area with elevated TCE concentrations based on previous sampling of well MW6. Well MW6 was screened from 1.5 to 5.9 m BGS. When the HRPP was installed, the groundwater elevation in the well was above the ground surface. The well was sampled from a depth of ~2.5 m BGS, near the mid-point of the HRPP installed depth. A Biotrap was also installed at a depth of 2.5 m BGS after well sampling. From in-field visual observations, the sediment varied from the surface consisting of layers of silt, silt/clay/sand, fine sand, and silt clay to ~ 3 m BGS. Below this depth was a uniform red clay.

5.3.3.1.1.1 Geochemistry

Well water sampled from MW6 was oxic (DO= 3.5 mg/l), had a positive ORP (+186 mV), and a pH of 4.8. Concentrations of Cl^-, SO_4^{-2}, Fe_T and methane were generally similar between depth discrete HRPP samples and well water with the exception of Fe_T, which was significantly lower than all HRPP samples. Chloride, a conservative species, increased slightly in concentration with depth, possibly due to infiltration of surface water. Concentrations in well water were near the average Cl^- concentration of depth discrete samples produced by the HRPP. Fe_T concentrations were generally quite elevated (>50 mg/l) for all depths and also increased slightly with depth similar to Cl^-. The cause of the very low concentration of Fe_T in MW6 well water is not clear but the concentration is also lower than all other sampled wells, suggesting that either a sampling or analysis error occurred, or that the Fe was being oxidized in the well. Oxidation of Fe in the well is possible given the presence of DO (3.5mg/l) and positive ORP in the well. Sulfate concentrations increased from ~70 to 150 mg/l with depth (0.6m to 1.2 m BGS) and remained constant (~150mg/l) down to 3.0 m, below which the concentration rapidly decreased (~60 mg/l). The concentration of SO_4^{-2} in well MW6 water was ~160 mg/l, which was very similar but at the upper end of concentrations measured by the HRPP for the mid depths 1.2-3.0 m BGS. The decrease in SO_4^{-2} near the surface is not likely due to dilution with surface water, as the

concentration of Cl^- and Fe_T do not decrease to such an extent nor SO_4^{-2} reduction due to the presence of O_2 in the well and positive ORP. The reduction in SO_4^{-2} at depth could be due to SO_4^{-2} reduction as the reduction in SO_4^{-2} at ~3m corresponds with the start of the clay layer and a peak in CH_4 concentrations. Methane concentrations increased to a peak (>200 ppmv) below 3 m. Concentrations of CH_4 in MW6 well water were at the low end (~50 mg/l) of concentrations measured for all depths by the HRPP.

5.3.3.1.1.2 VOC Concentrations

Only the presence of TCE (~430 µg/l) was detected in well water from MW6 (**Figure 5.30**). TCE was detected at all depths over which the HRPP was deployed. TCE concentrations generally increased from the top of the formation (~15 µg/l) to 3.5m (~800 µg/l), below which they remained constant. The peak TCE concentrations and generally similar concentrations below 3 m correspond to the presence of the clay layer, suggesting that it is acting as a continued source to the above layers. DCE was generally detected above 2.2 m BGS but at much lower concentrations (<20% of TCE), excluding one depth. Well water TCE concentration was near the average of concentrations measured over the whole depth interval by the HRPP, although it is unlikely that sampled water was equally soured over the whole well screen based on both formation characteristics (e.g. clay layer) and concentrations of Cl^- and SO_4^{-2}, which do not correspond to average concentrations over the whole depth interval.

In addition to CVOC concentrations, the stable isotopic composition was also evaluated for micro-biotraps from all HRPP sample depths, well water, a Biotrap placed in the well, and equilibrated pore water from one HRPP depth (~4.2 m BGS). The $\delta^{13}C$ of TCE from the well and biotrap in the well were nearly identical (-23 ‰) (**Figure 5.30**). The $\delta^{13}C$ of TCE in micro-biotraps were generally similar to the well water but varied from -18 to -23 ‰. The $\delta^{13}C$ value (-20‰) of equilibrated pore water from one HRPP sample cell (4.2 m BGS) was essentially identical to the value from the HRPP Biotraps at the same depth (-22 ‰). *Cis*-DCE $\delta^{13}C$ values (-25 to -26 ‰) were obtained from 3 HRPP micro-biotraps depths (1.5 to 2 m) and were lighter, as would be expected from biological fractionation during reduction of TCE in the absence of VC production.

5.3.3.1.1.3 Pore Velocity

Pore velocities measured using the HRPP ranged from 0 to 7 cm/d. Velocities <2 cm/d cannot be differentiated from the 0-velocity case (**Figure 5.30**). Lowest velocities were measured 3 m BGS, which corresponds to the start of the clay layer. Velocities increased from 3 to 2 m BGS and then varied with decreasing depth. Velocities > 2 cm/d were measured at depths 2, 1.1 and 0.4 m BGS, which could be consistent with the identified sand layers near those depths. Definitive correlation between depths and sediment characteristics cannot be accomplished due to both the relative thin nature of the sediment layers and incomplete capture in cores.

5.3.3.1.1.4 Microbial Community Analysis

The microbial community and capacity were compared using well water, in well Biotraps, and HRPP discrete depth microbio-traps (**Figure 5.31**). Only a small number of species or capacities

were detected. Abundances were lowest for well water in which only Total Eubacteria, and Sulfate Reducing bacteria were above the detection limit and abundances were generally an order of magnitude lower than in well Biotraps or HRPP microbio-traps. In well Biotraps only detected bacteria that were detected in well water, but abundances were similar between in well Biotraps and HRPP microbio-traps for those species/genes. The HRPP microbio-traps were able to detect a number of additional species or genes. Some detections were only at sporadic depths (e.g. reductases and co-metabolic processes) but abundances of others were generally constant with depth (e.g. *Dehalobacter, Desulfuromonas)*. Overall, it appears that the HRPP microbio-traps were better able to evaluate the sediment microbial composition and that well water was a poor predictor of microbial capacity. This is probably because the HRPP microbio-traps are in direct contact with sediment. The microbial distribution largely supports the observed dominance of TCE and lower concentrations of *cis*-DCE as well as sulfate reduction at depth. Four species of bacteria capable of reductive dechlorination were observed (*Desulfitobacterium, Desulfuromonas, Dehalobacter, and Dehalobium Chlorocoercia*) at reasonable abundances. These species are only capable of reducing TCE to *cis*-DCE.

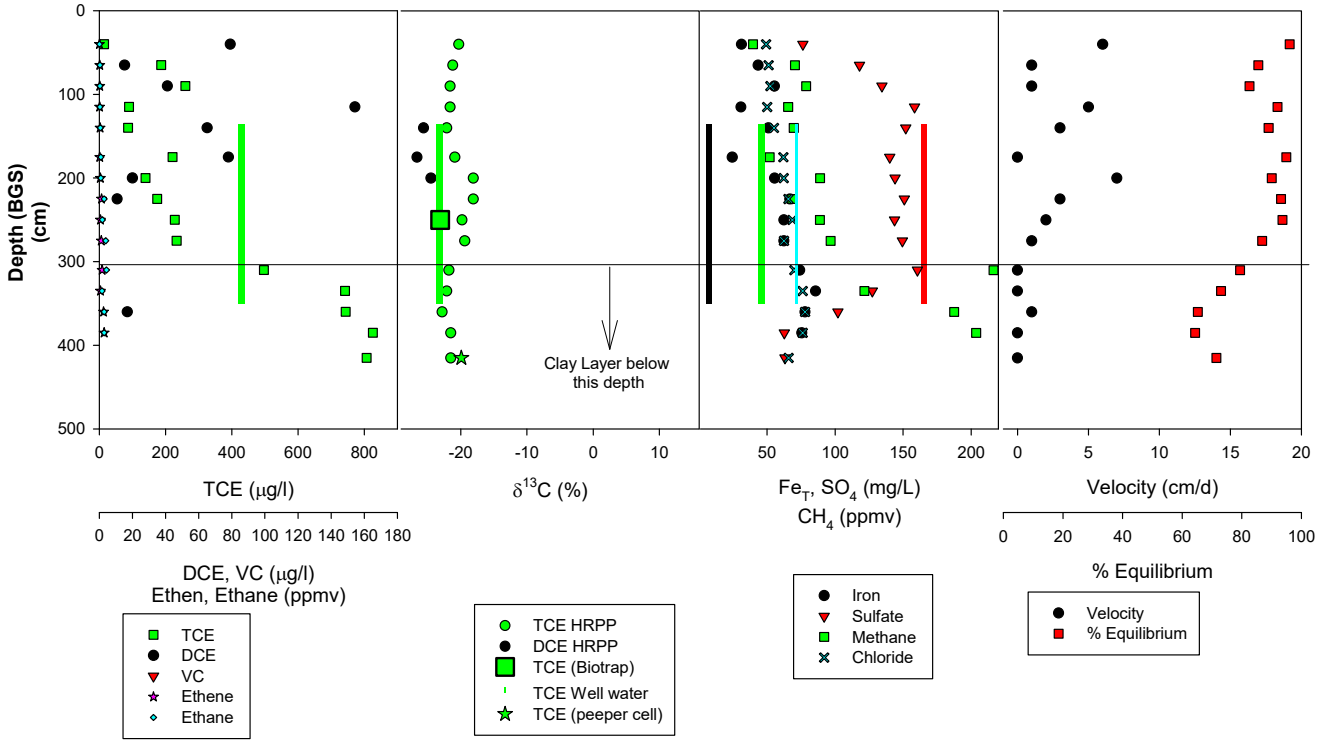

Figure 5.30. Concentration distributions of VOCs and geochemical indicators, CSIA of CVOCs, and pore velocity at location MW6, BARC site.

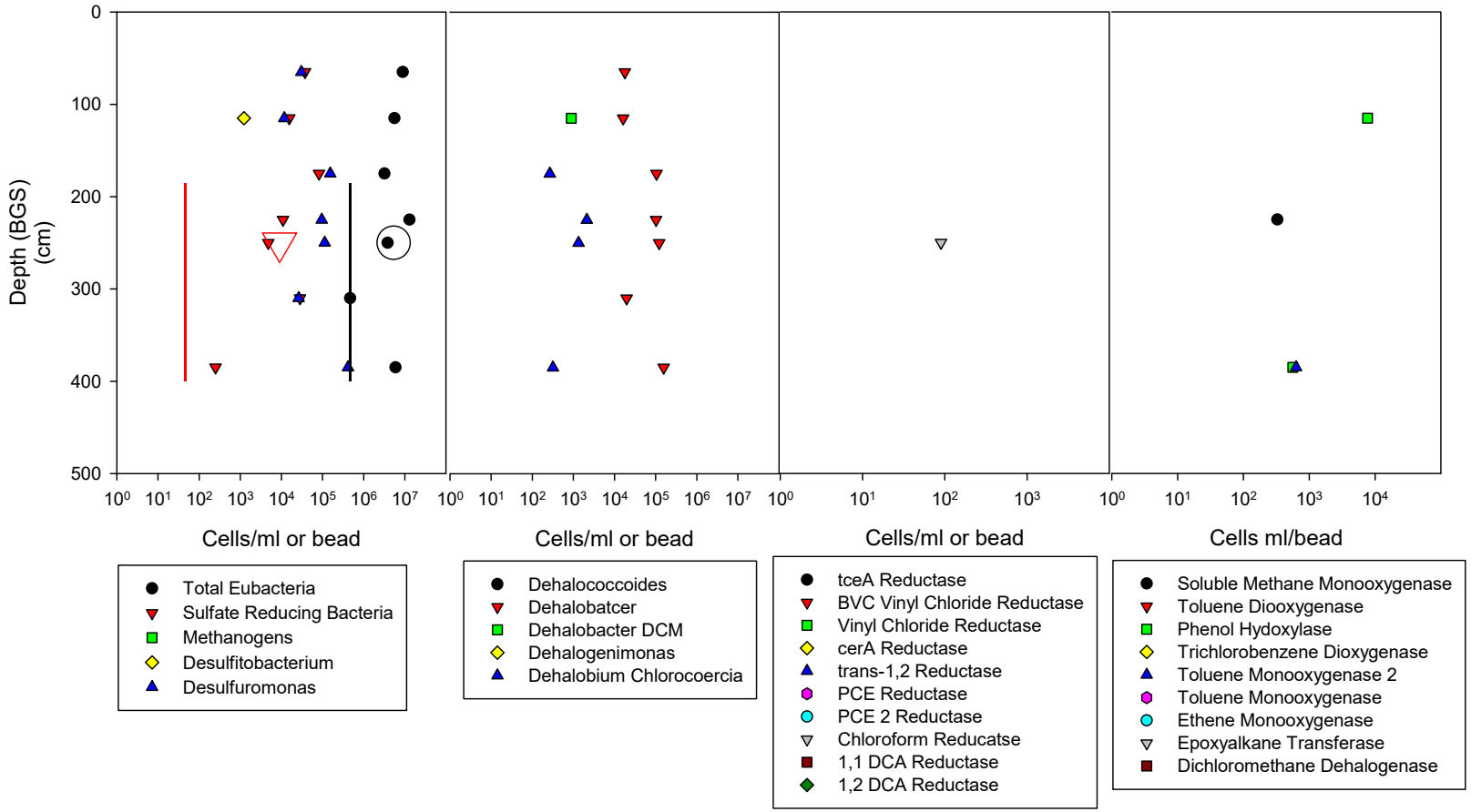

Figure 5.31. Microbial Distribution at the upgradient MW6 site. Small solid symbols represent HRPP micro-biotrap, large open symbols represent in well Bio-traps, and solid lines represent well water.

5.3.3.1.2 Biowall Location (BW6)

The BW6 location was within the biowall. Well BW6 was screened from 1.35 to 5.9 m BGS. When the HRPP was installed, the groundwater elevation in the well was 0.8 m BGS, equivalent to 0.2 m below the water table at MW6. The well was sampled from a depth of ~3.3 m BGS, near the mid-point of the HRPP installed depth (160cm-640cm BGS). The Biotrap was also installed at a depth of 3.3 m BGS after well sampling.

5.3.3.1.2.1 Geochemistry

Well water sampled from BW6 was anoxic based on ORP (-55mV) and had a pH of 6.3. The DO could not be determined due to interferences from the high concentrations of DOC from the biowall. Based on HRPP samples, Cl^-, a conservative species, increased in concentration from 1.5 to a peak at 3.5 m BGS and decreased slightly with increasing depth (**Figure 5.32**). Chloride in well water (~67 mg/l) was similar to the peak HRPP Cl^- concentration (~60 mg/l). HRPP Fe_T concentrations were generally quite elevated (~>50 mg/l) for all depths but were lowest at 3.5 m with increasing concentrations above and below this depth. Similar to Cl^-, Fe_T concentration in well water matched those in the HRPP at a depth of 3.5 m. Sulfate in HRPP samples was below detection except for two depths (3.5 and 3.7 m BG) where it increased to ~60 mg/l. The concentration of SO_4^{-2} in BW6 well water was ~160 mg/l. HRPP methane concentrations were very elevated (3500 to >20,000 ppmv) and generally followed a similar trend as SO_4^{-2}, with a low concentration at 3.5 m BGS and more elevated concentrations above and below this depth, although lowest concentrations occurred at a depth of ~1.8 m BGS. As with Cl^-, and Fe_T, CH_4 concentration in BW6 well water was very similar to that corresponding to concentrations from the HRPP at ~3.5 m.

5.3.3.1.2.2 VOCs

HRPP samples TCE, *cis*-DCE, VC, and ethene concentrations were at or below the detection limit, except at depths around 3.5 m BGS, where there was a sharp peak in concentrations (**Figure 5.32**). *Cis*-DCE and VC were the dominant VOCs, followed by ethene. VOC concentrations in well water were below peak concentrations for ethene and VC, and greater than peak concentrations of *Ccis*-DCE. Total VOCs for HRPP samples at 3.5 and 3.7 m BGS were similar to total VOC in well water, but the distribution was different with more lower chlorinated compounds in HRPP samples than in well water.

In addition to CVOC concentrations, the stable isotopic composition of CVOCs was also evaluated for micro-biotraps from select HRPP sample depths (those with detectable CVOCs), well water, and a Biotrap placed in the well (**Figure 5.32**). The $\delta^{13}C$ of TCE and *cis*-DCE from the well (+15 and -21‰, respectively) and Biotrap in the well (+15 and -20 ‰, respectively) were nearly identical. Only the $\delta^{13}C$ of *cis*-DCE was measurable in HRPP micro-biotraps. $\delta^{13}C$ values of *cis*-DCE were much more negative (-0.9 and -7.6 ‰, respectively) than those in well samples. CVOC $\delta^{13}C$ values for well water and Biotrap are consistent with nearly complete degradation of TCE to DCE and no further reduction to VC, consistent with the much larger concentrations of DCE (~130 µg/l) in well water than TCE (21 µg/l) or VC (26 µg/l) and lack of ethene. On the other hand, the more negative values of *cis*-DCE at HRPP depths 3.5 and 3.7 m BGS were also consistent with the relative ratios of DCE to VC and lack of TCE. For the sample at HRPP depth 3.5 m, VC and ethene concentrations are approximately equal (~60 µg/l) and

exceed *cis*-DCE (45 µg/l). Compared to well water, total concentration of VOCs are the same (165 and 157 µg/l for HRPP-3.5 m and well water, respectively) but VOC distribution based on HRPP data clearly indicates more complete reduction of *cis*-DCE consistent with the much more negative measured $\delta^{13}C$ value (-0.9 ‰). For the HRPP sample at 3.7 m, total VOC concentrations were also close to those in well water (167 µg/l) but at this depth, while there is more VC and ethene (64 and 11 µg/l, respectively) than in well water, *cis*-DCE (95 µg/) is still the dominant VOC; this finding is consistent with the measured $\delta^{13}C$ value (-7.6 ‰) that is less negative than that at HRPP 3.5 m but more negative than well water.

5.3.3.1.2.3 Pore Velocity

Pore velocities measured using the HRPP ranged from 0 to 40 cm/d (**Figure 5.32**). Peak velocities were measured from 3.2 to 3.7 m BGS, with the peak at 3.7 m BGS. Velocities at all other depths were <3 cm/d, with one exception. Previously measured velocities at BW6 in the biowall were reported to range between 2 and 5 cm/d based on slug tests, pumping tests, and tracer tests.

5.3.3.1.2.4 Microbial Community Analysis

The microbial community and capacity were compared using well water, in well Biotraps, and HRPP discrete depth micro-biotraps (**Figure 5.33**). Generally, organisms or genes detected by one method were detected by all methods with a few exceptions. Abundances were also similar between methods although there were numerous cases where one method was higher or lower than others, but there was no consistent trend between methods. A number of bacteria capable of reductive dechlorination were observed (*Desulfitobacterium, Desulfuromonas, Dehalobacter, Dehalogenimonas, Dehalococcoides, and Dehalobium Chlorocoercia*) at reasonable abundances. The reductase tceA was measured in well water and well biotrap but not in HRPP samples, consistent with the lack of TCE in HRPP samples, while VCR reductase was measured in well water, in well Biotrap, and HRPP micro-biotraps.

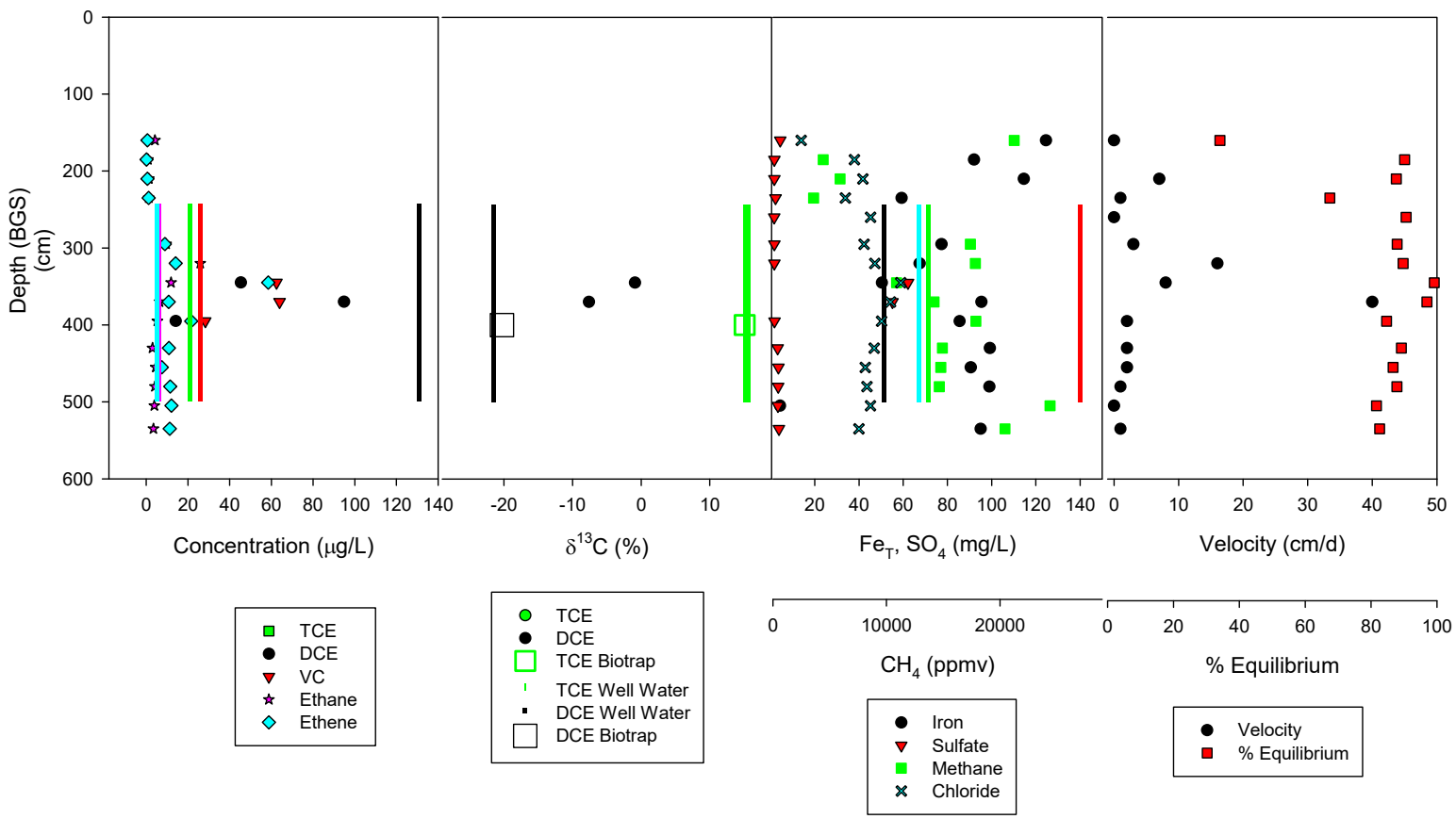

Figure 5.32 Concentration distributions of VOCs and geochemical indicators, CSIA of CVOCs, and pore velocity at location BW6, BARC site.

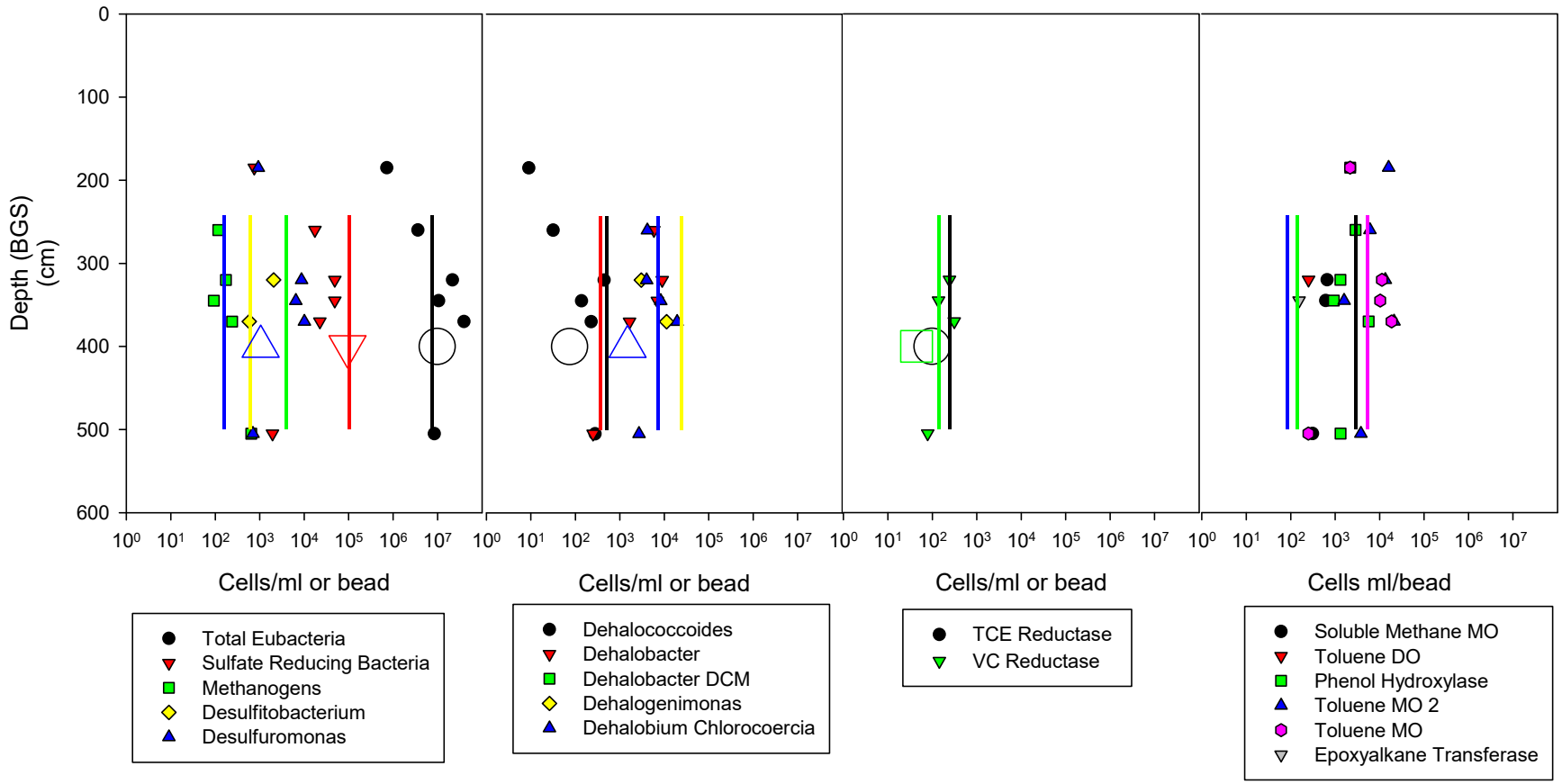

Figure 5.33. Microbial Distribution at the upgradient MW6 site. Small solid symbols represent HRPP microbio-trap, large open symbols represent in well Biotraps, and solid lines represent well water.

5.3.3.1.3 MW10 Location

The MW10 location was ~21m downgradient of location BW6. Well MW10 was screened from 1.8 to 4.8 m BGS. When the HRPP was installed, the groundwater elevation in the well was 0.56 m BGS equivalent to 1.46 m below the water table at MW6. The well was sampled from a depth of ~1.8 m BGS, near the mid-point of the HRPP installed depth (0.3 - 3.9 m BGS). No Biotrap was installed in this well. Based on coring, the clay layer was present below ~3.0 m, above which were layers of sand with and without gravel.

5.3.3.1.3.1 Geochemistry

Well water sampled from BW6 was anoxic based on ORP (-30 mV) and had a pH of 6.2. Chloride concentration remained < 10 mg/l from 0.3 to 1.5 m BGS, below which it generally increased before decreasing at the deepest sample depths (**Figure 5.34**). Chloride in well water (~50 mg/l) was greater than peak HRPP Cl^- concentrations (36 mg/l). Except at the shallowest depth, Fe_T concentrations were generally elevated for all depths (>35 mg/l) with highest concentrations between 1.8 and 3 m BGS. Fe_T concentration in well water (53 mg/l) was in the mid-range of concentrations measure by the HRPP. Sulfate in HRPP samples was generally low < 5 mg/l except near the surface and a small increase between 2.0 and 2.5 m BGS. The concentration of SO_4^{-2} in MW10 well water was ~53 mg/l much higher than any HRPP depth. Methane concentrations were ranged from below detection at the shallowest sampled depth (0.3 m BGS) to >2,000 ppmv at mid-depths before decreasing to a near constant concentration ~340 ppmv below 3.4 m BGS. Methane in well water was similar to peak concentrations measured by the HRPP at 2.0 and 2.75 m BGS.

5.3.3.1.3.2 VOCs

In both HRPP samples and well water, only *cis*-DCE was measurable. In HRPP samples, *cis*-DCE was present at only a few depths (~2 and 3 m BGS) and was <50 µg/l. Cis-DCE concentrations in well water was much higher ~130 mg/l (**Figure 5.34**). The $\delta^{13}C$ values of Cis-DCE were very similar (-21 and -19 ‰, respectively) for well water and HRPP micro-biotraps at ~2 m BGS (no well Biotrap was installed at this location due to the smaller well casing diameter). The values are near those of source TCE, suggesting near complete conversion of TCE to *cis*-DCE but little further transformation to VC.

5.3.3.1.3.3 Pore Velocity

Pore velocities measured using the HRPP were uniformly low (2cm/d) except at the two shallowest depths (<60cm BGS), at which they were higher (13-20 cm/d) (Figure 9.34).

5.3.3.1.3.4 Microbial Community Analysis

The microbial community and capacity were compared using well water, and HRPP discrete depth micro-biotraps (**Figure 5.35**). At this site, there were more discrepancies between organisms or genes with a number of organisms either not detected in well water (e.g. *Desulfitobacterium, Desulferomonas, and Dehalococcoides*) or where organisms were measured in much lower abundance in well water than those measured by HRPP microtraps (e.g. Sulfate reducers, Total Eubacteria, and *Dehalobacter*). Only a few reductive genes were measured and only for one depth, with none detected in well water. Cometabolic genes were highest in HRPP samples and significantly higher at the shallowest depth. A number of bacteria capable of reductive dechlorination were observed (*Desulfitobacterium, Desulfuromonas, Dehalobacter, Dehalogenimonas, Dehalococcoides, and Dehalobium Chlorocoercia*).

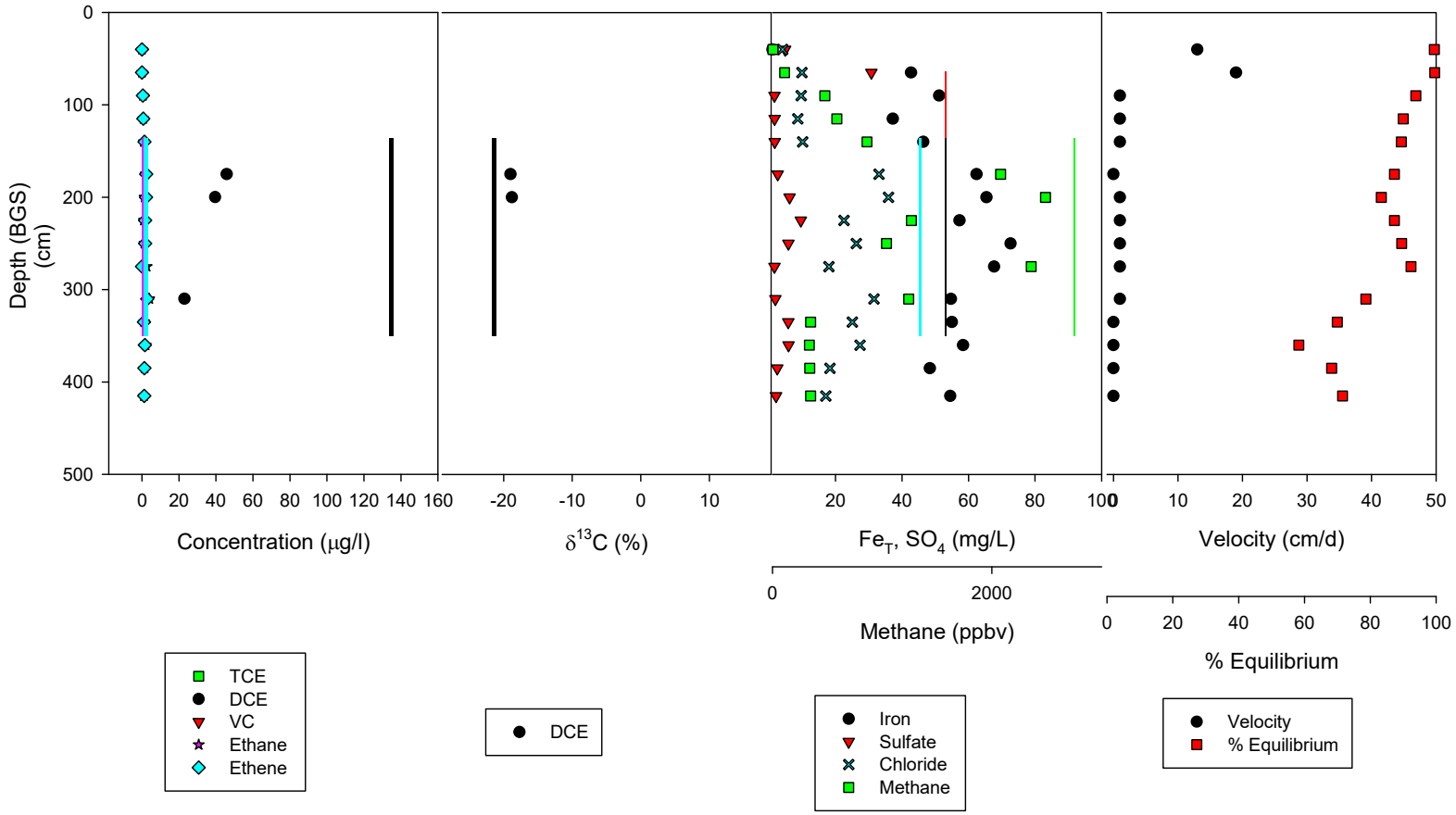

Figure 5.34. Concentration distributions of VOCs and geochemical indicators, CSIA of CVOCs, and pore velocity at location BW6, BARC site.

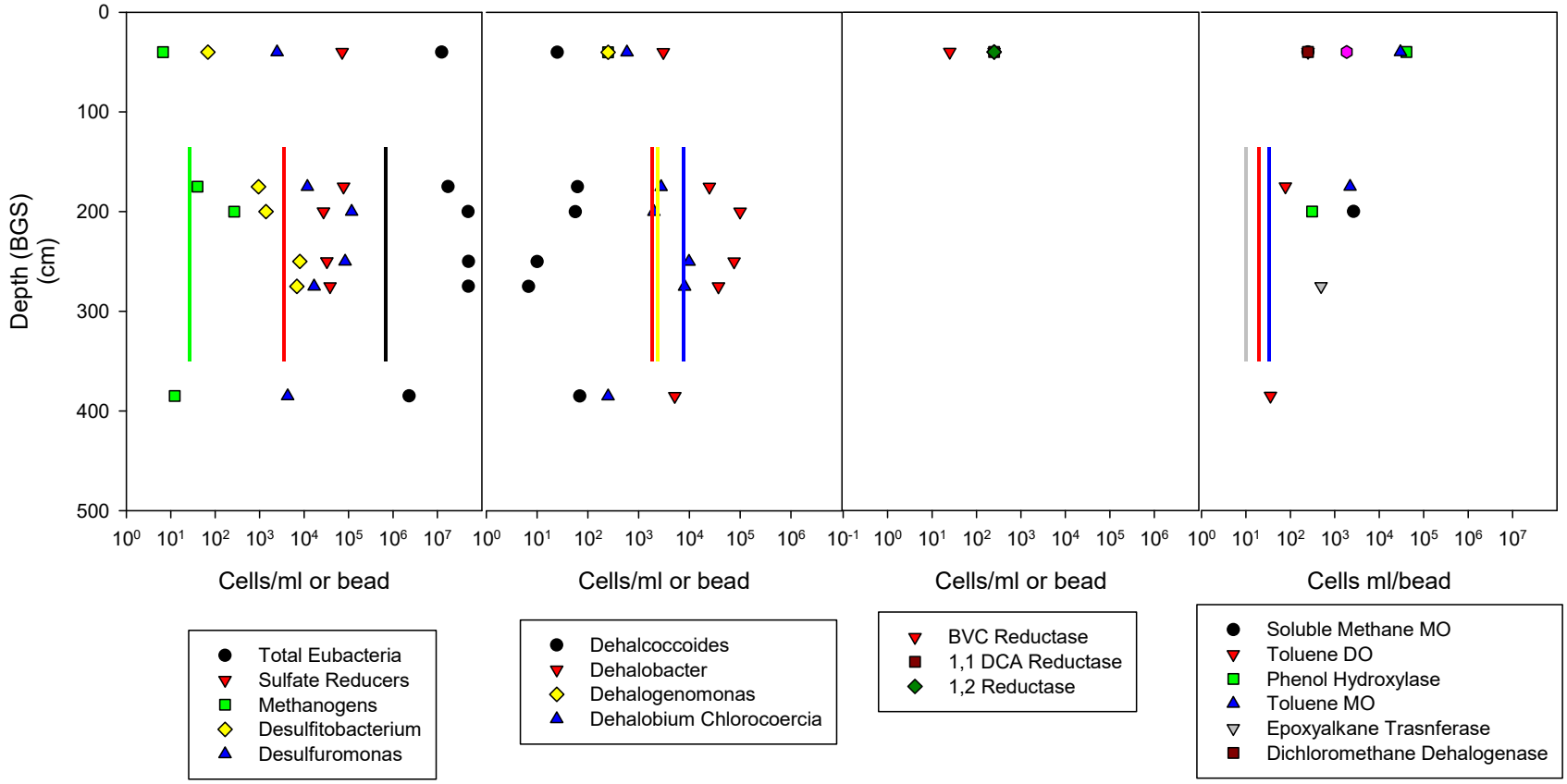

Figure 5.35. Microbial Distribution at the upgradient MW6 site. Small solid symbols represent HRPP microbio-trap, large open symbols represent in well Bio-traps, and solid lines represent well water.

5.3.3.2 Impacts of Site Evaluation as a function of Sampler Type

In general, at individual sites, data was generally similar between data obtained from wells (water and Bio-traps) and HRPP discrete depth samples, although some important differences were consistently observed as mentioned above. However, while using well data or HRPP data to assess the efficacy of the biowall on attenuation of CVOCs generally leads to similar gross conclusions there are a number of important differences.

Site Evaluation Based on Well Water-In well water Cl^- a conservative species decreased across the site (**Figure 5.36**). Based on changes in redox active species measured in wells, conditions in the biowall were more reducing than in the upgradient location based on increases in soluble total Fe and increases in CH_4 from the source to the biowall. Downgradient of the biowall, groundwater does not appear as reduced based on decreases in CH_4. Incongruently, in well water SO_4^{-2} is only slightly reduced in well BW6 compared to the source area (MW6) even though CH_4 in well BW6 is present at very high concentrations. These changes would in general be consistent with conditions conducive to TCE reduction in the biowall, with decreasing reduction potential downgradient of the wall. CVOCs in well water decrease from the source area to the biowall and then remain constant until the stream water, where no CVOCs were detected. Except for the source area, CVOC composition is dominated by *cis*-DCE in downgradient wells (**Figure 5.36A**). CVOC $\delta^{13}C$ values also support a near complete conversion of TCE to *cis*-DCE but no further reduction across the site based on $\delta^{13}C$ values of *cis*-DCE in well BW6 and MW10, which are similar to TCE in MW6. No reductive dechlorinating species were measured in well water or in well Biotraps in the source area supporting the lack of daughter products present, with higher concentrations of species capable of TCE transformation to *cis*-DCE in the biowall, but species capable of further reduction were not present. Downgradient of the biowall, ground water contains only a few species of bacteria capable for reductive dechlorination and at low relative numbers. Overall based only on data from well water samples (or Bio-traps in wells), the biowall would appear to only be reducing TCE to cis-DCE likely due to the absence of species capable of further reduction and down gradient of the biowall conditions generally unfavorable based on redox conditions and abundance of reductive dechlorinators. Finally, based on well screen intervals and well concentrations, it would appear that a significant flux of CVOCs is occurring due to the assumed presence of CVOCs across the whole screened interval and migration times (~ 1 year) to the stream based on site average ground water velocities (excluding sorption and dispersion).

Site Evaluation based on HRPP- Site evaluation based on HRPP data was compared using two approaches. For the first approach, the HRPP depth discrete data were averaged for each location and average depth concentration plotted over the sample transect, to make the comparison with well-derived data (single point per location) easier (**Figure 5.36B**). In addition, we also

compared the changes in constituent concentrations across the transect using maximum concentration from all depths (**Figure 5.36C**). While HRPP data is not intended to be in such a simple manner, the limitations of the well data make this the best comparison, keeping in mind that well water may only represent a small subset of depths. The second approach used the complete depth profiles across the transect, to highlight the advantages of high-resolution sampling. Site evaluation using the complete depth profiles is discussed later.

Using either the HRPP depth averaged or maximum concentrations of Cl^-, the overall trend in concentration change as well as concentration across the transect was very similar to well data. HRPP depth averaged or maximum SO_4^{-2} concentrations generally decline across the site, but the decrease is much more pronounced in HRPP samples for which SO_4^{-2} is almost completely reduced in samples from the biowall while in well water the concentrations are only slightly reduced. The larger reduction measured by HRPP samples is more consistent with the elevated concentrations in CH_4 in the biowall for both HRPP and well water. The average individual CVOC concentration across all HRPP sample depths at each sample location along the transect was compared to changes in well water CVOC concentration, and the trends are similar. This is also true of the maximum concentration of individual CVOC at each location across the transect compared to well water. Populations of bacteria capable of reductive dechlorination are generally higher and more species present across the transect, supporting the continued reduction in CVOCs and increased presence of VC and ethene in the biowall. Major differences include that cis-DCE concentrations are lower and continue to decline based on HRPP data. HRPP depth averaged porewater velocities ranged from 2 to 8 cm/d similar to estimates from well data (2 and 5 cm/d) based on slug tests, pumping tests, and tracer tests. Conclusions based on average or maximum HRPP values would be similar to those for well water except that CVOC degradation appears to be more complete and there appears to be continued loss of CVOCs downgradient of the biowall.

Overall, when using well water, depth averaged or maximum HRPP concentrations, the overall site assessment was very similar. However, if the complete HRPP profiles are used to assess the changes across the transect (**Figure 5.37, 5.38 and 5.39**), a number of important differences are evident as listed below.

1. At location MW6, TCE concentration increases with depth and peak concentrations are ~2X higher than in well water. Further, TCE penetrates and is highest in the clay layer present below 3m. This would suggest that higher concentrations in groundwater above this depth were present in the past and that the clay will act as a long-term source of TCE to downgradient areas.
2. At location BW6, based on HRPP data CVOCs are only present over a narrow depth range (3.2 – 3.9 m BGS). Based on HRPP data, CVOCs present are dominated by more reduced daughter products (VC and ethene) while well water is dominated by cis-DCE even though the sum of the CVOC concentrations measured by the HRPP equal the sum of the CVOCs measured in well water. Peak velocities occur at the same depths in which VOCs are present (3.2-3.7 m BGS) and suggest shorter residence times in this zone compared to residence time based on site average velocity. CH_4 is at a minimum and SO_4^{-2} is at a maximum and only present at 3.5-3.7 m BGS, congruent with the presence of reduced daughter products at those same depths. The $\delta^{13}C$ of cis-DCE is much more

enriched in HRPP samples (VC + ethene/Cis-DCE >1) than well water (VC + ethene/Cis-DCE <1). All of these observations support a conceptual model in which a highly permeable layer (<0.5m) exists near 3.7 m BGS in which reduction of *cis*-DCE and SO_4^{-2} occur along with CH_4 production. Well samples appear to both preferentially draw from this zone but also sample water originating outside the biowall.

3. The high velocity zone appears to exist across the transect downgradient of the biowall based on velocities with depth, profiles that largely overlap with presence of CVOCs downgradient of the biowall.
4. Although CVOCs are present at depths below the stream and in adjacent wells, no CVOCs appear to be upwelling into stream water; this observation could not be supported from well data alone, given the concentrations of *cis*-DCE in MW10.
5. Due to the assumption that well water represents the average concentration across the well scree, calculated fluxes at each location based on well water would be much higher than those based on depth discrete CVOC concentration and velocity profiles.
6. Based on HRPP microbial data, a large diverse set of organisms capable of reductive dechlorination is present, including those capable of complete reduction to ethene. Based on well water, it would appear there are only a few species present and at low abundance, and the microbes present are not capable of complete reduction.

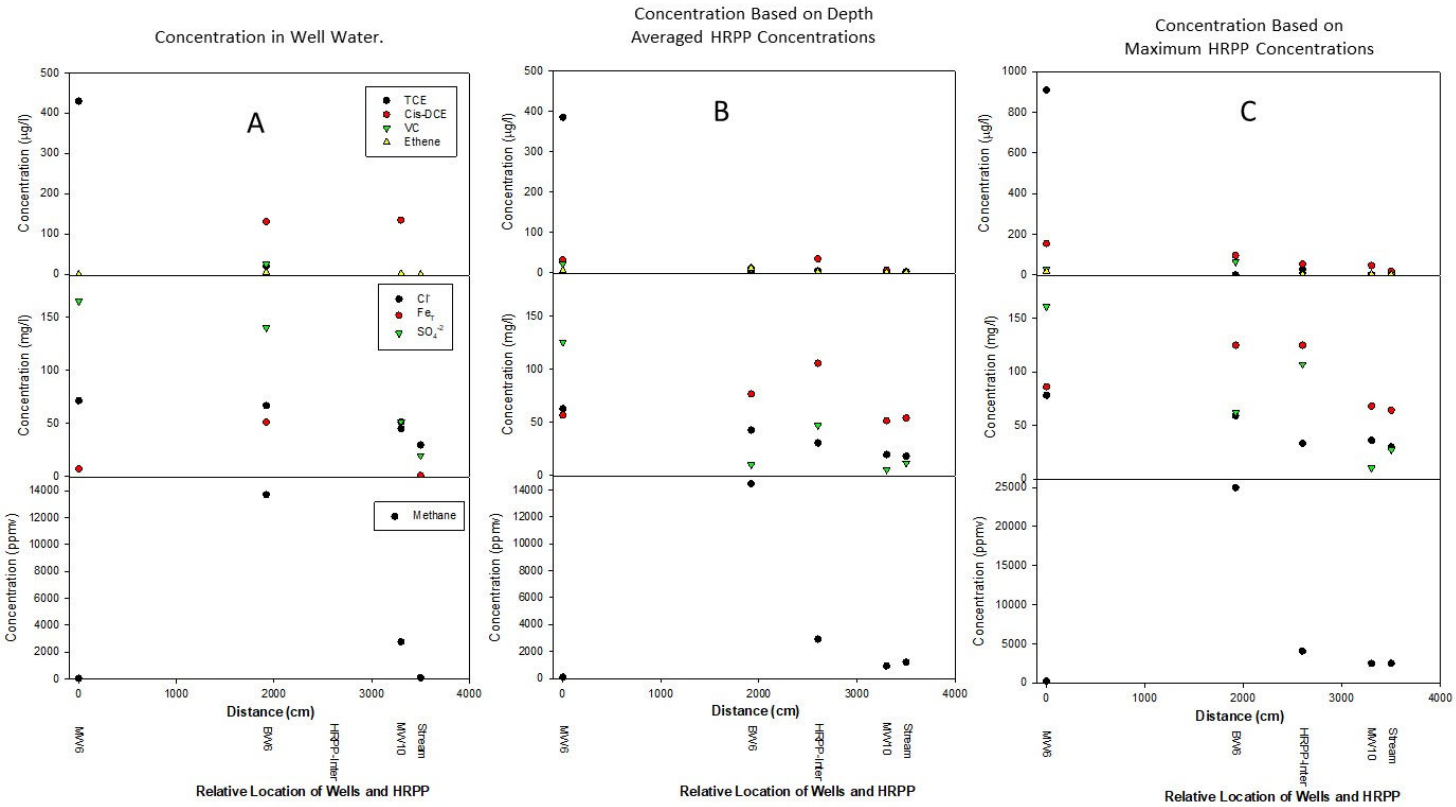

Figure 5.36. Concentration Distribution across groundwater transect. A) Concentrations based on sampled well water; B) Concentrations based on depth averaged HRPP concentrations; C) Concentrations based on maximum HRPP concentrations.

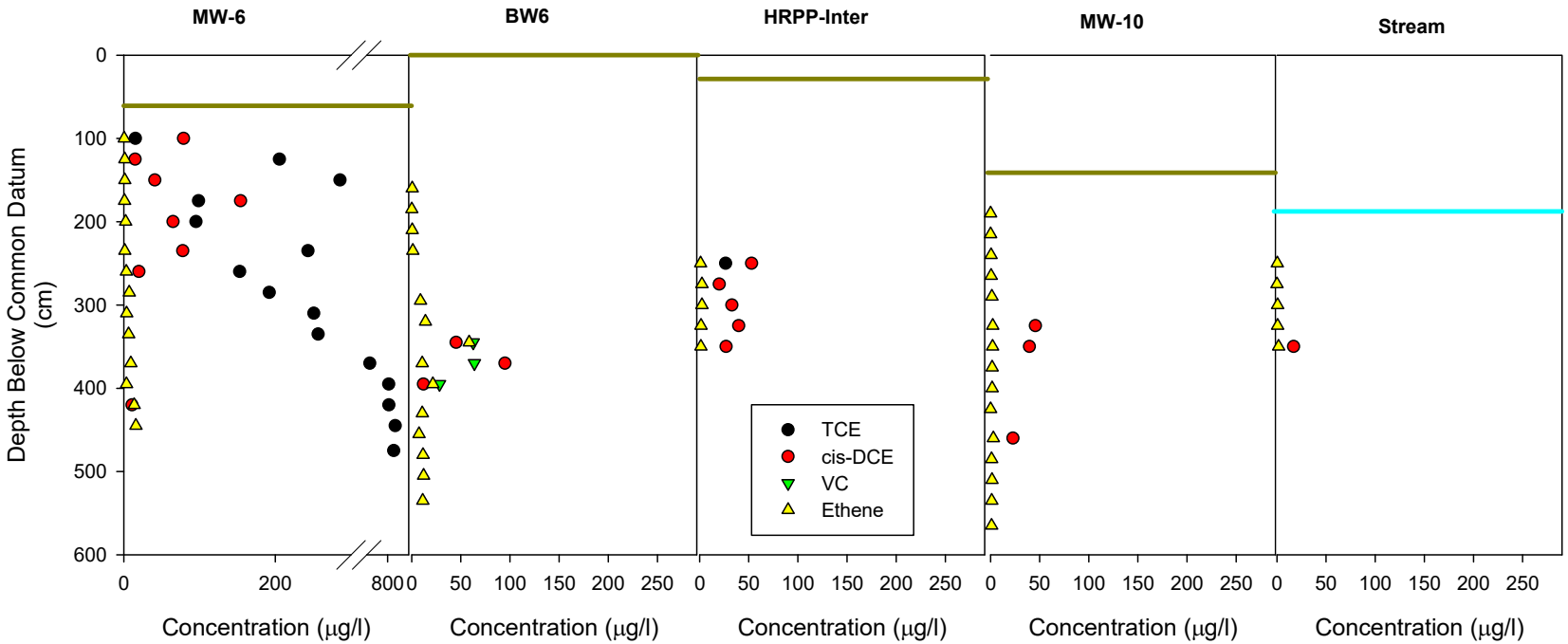

Figure 5.37. Concentration of CVOCs with depth based on HRPP samples across groundwater transect.

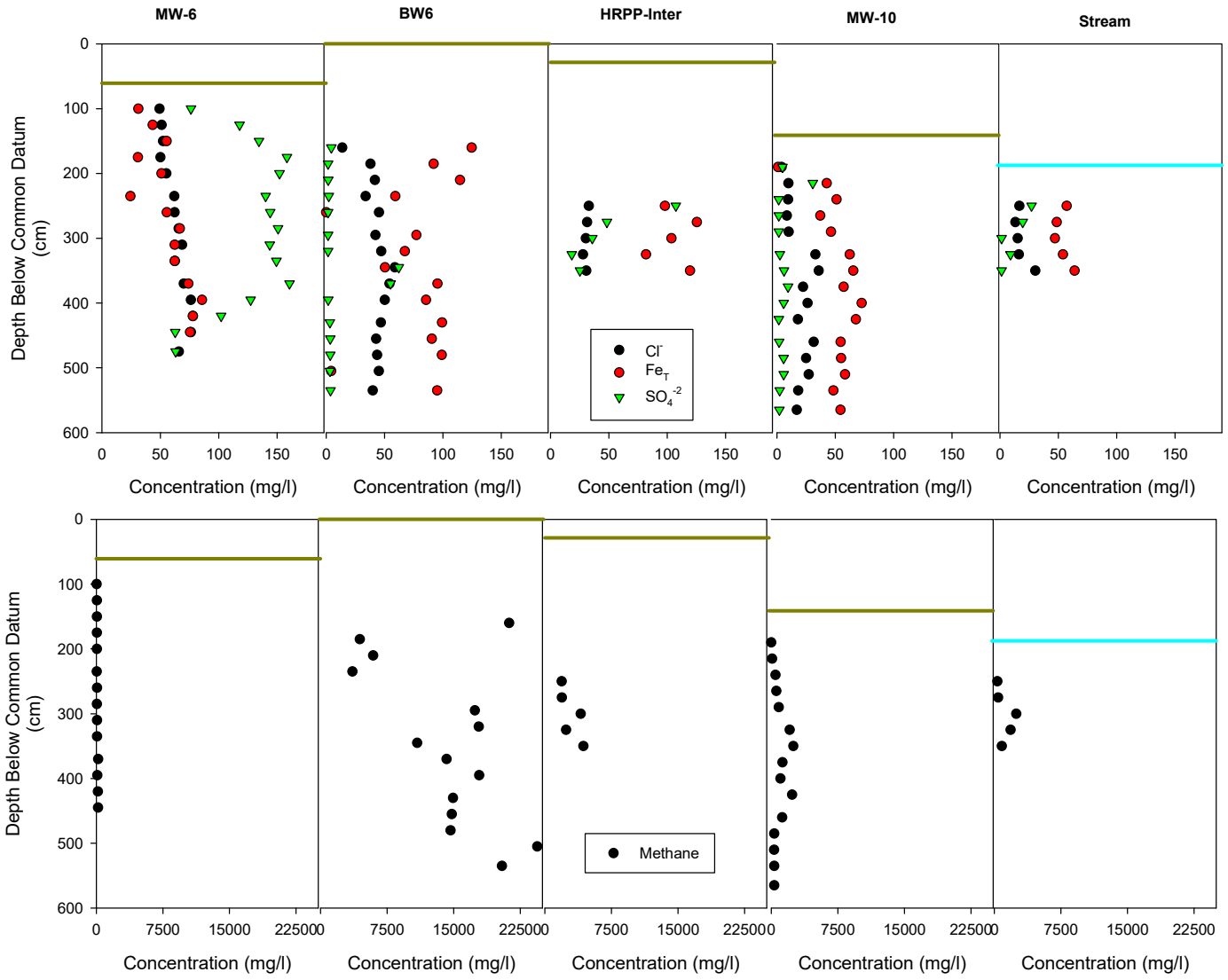

Figure 5.38. Concentration of geochemical indicators with depth based on HRPP samples across groundwater transect.

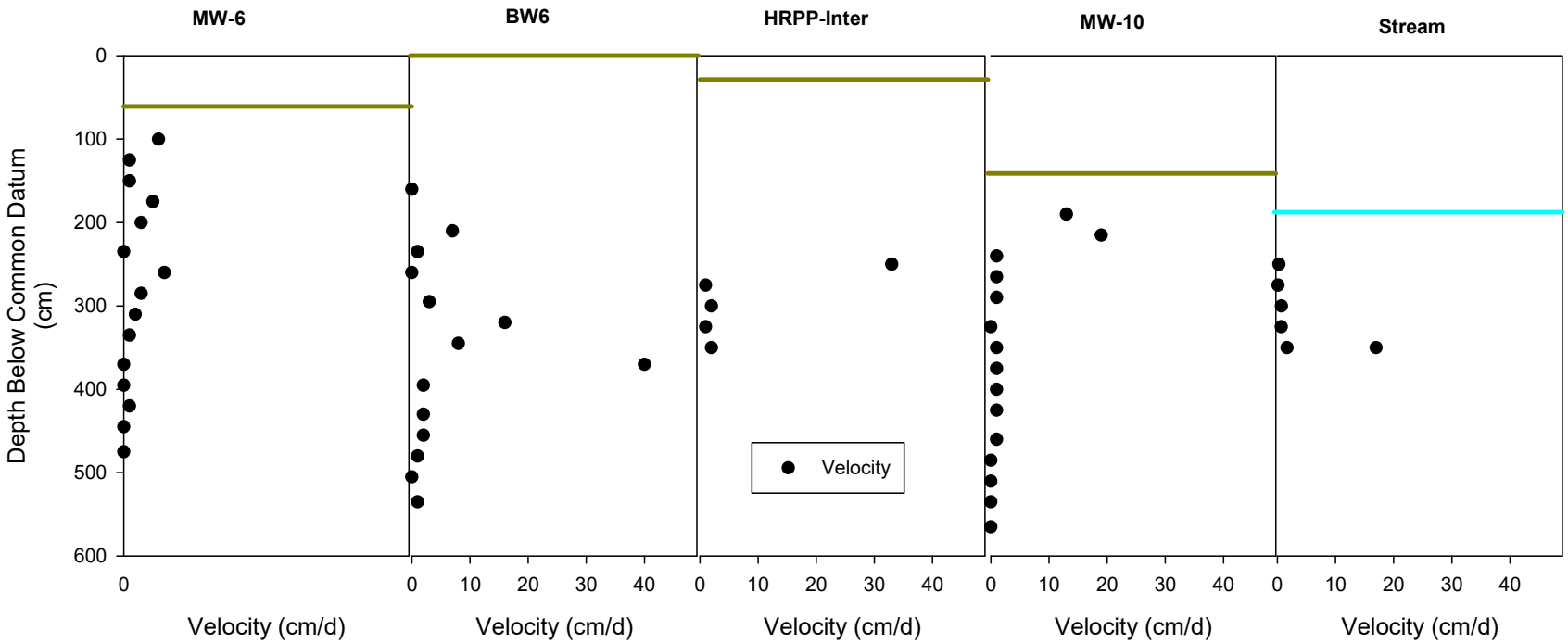

Figure 5.39. Pore Velocity with depth based on HRPP samples across groundwater transect.

6 CONCLUSIONS AND IMPLICATIONS FOR FUTURE RESEARCH/IMPLEMENTATION

During this SERDP project, we developed and validated a modified peeper design (HRPP) capable of providing information far beyond concentration data including: microbial numbers and activity, groundwater and contaminant flux, and contaminant degradation at dm-scale resolution. Multiple field deployments support the HRPPs ability to measure CVOC concentrations, geochemical parameters and CSIA with similar sensitivity as other methods and without the need to install wells while still providing speciation and high vertical spatial resolution. Field deployments also demonstrated that while HRPP microbio-traps, in well Biotraps, and well water reflect some differences in predicted microbial community abundances, the differences appear to be more due to differences in microbial populations than the sampling method. Finally, measurements of pore velocity at all three field sites were within the range of values based on other methods but with much higher spatial resolution and no need to install wells. Our research also demonstrates that while both HRPP and monitoring wells can lead to similar overall site assessments, the high resolution spatial data sets provide much more information that can significantly change the overall assessment of fate and transport, remedial activity success, and/or design. Samplers capable of producing such a holistic set of characterization parameters with this level of resolution will be an enormous advantage over existing methods and should lead to higher fidelity site models, more tailored design of remediation activities, and improved remedial performance evaluations. Further, the tool allows monitoring and assessment of difficult contaminated formations such as thin layers of high or low permeability and clay layers that cannot currently be adequately evaluated. The new tool can be relatively easily deployed similar to other direct drive tools and can provide data to guide source zone assessment, well placement, rebound potential from low permeability zones, homogeneity and extent of bioaugmentation/stimulation efforts, or other remedial activities.

There is an immediate opportunity to implement this technology at DoD sites, not only CVOC sites but any shallow groundwater site at total depths less than 10 m BGS contaminated with compounds with sufficient solubility to test with the HRPP sampler volumes. This would include energetics, explosives, fuels, pesticides, and PFAS. The HRPP would greatly increase initial site assessments by providing higher resolution vertical distributions of source zones. As the samplers can be readily deployed in about the same time as other direct drive devices, the samplers can be used to create a detailed 3D map of the source zone. This would allow better placement of monitoring wells, injection points/wells, better vertical control of screen intervals, as well as identification of low permeable regions that may act as long-term sources or impede remediation efforts and high permeability zones that can bias monitoring efforts. The sampler can also be used to provide coupled data sets that will allow for more constrained models and verification of transformation leading to more constrained remedial actions and more reliable

outcomes. Finally, the sampler can also be useful in cases where groundwater upwelling is suspected.

The HRPP tool is currently ready for commercialization. The application of the tool could easily be provided by any number of consultants or field service companies. Commercialization will most likely be dependent on establishing the benefits of the HRPP with site managers and regulators, who can then encourage its use to improve site characterization, site conceptual models and impact of remedial activities. At the time of this writing, the NAVY was further evaluating the tools capabilities, additional demonstrations through the ESTCP program would also facilitate its adoption by further demonstrating its utility.

7 LITERATURE CITATIONS

Albrechtsen, Hans-Jorgen, and Anne Winding. 1992. "Microbial biomass and activity in subsurface sediments from Vejen, Denmark." *Microbial Ecology 23* 303-317.

Amellal, N, J-M Portal, and J Berthelin. 2001. "Effect of soil structure on the bioavailability of polycyclic aromatic hydrocarbons within aggregates of a contaminated soil." *Applied Geochemistry 16* 1611-1619.

Annable, Michael D, Kirk Hatfield, Jaehyun Cho, Harald Klammler, Beth L Parker, John A Cherry, and P Suresh C Rao. 2005. "Field-scale evaluation of the passive flux meter for simultaneous measurement of groundwater and contaminant fluxes." *Environmental Science & Technology 39* 7194-7201.

Baas-Becking, LGM, IR Kaplan, and D Moore. 1960. "Limits of the natural environment in terms of pH and oxidation reduction-potential." *Journal of Geology* 243-248.

Beeman, Ralph, and Joseph Suflita. 1987. "Microbial ecology of a shallow unconfined ground water aquifer polluted by municipal landfill leachate." *Microbial Ecology* 39-54.

Berner, RA. 1980. *Early Diagenesis: a Theoretical Approach.* Princeton, NJ: Princeton University Press.

BMT, 2018. Beaver Dam Road Landfill: Interim Remedial Action Completion Report. Prepared by BMT Designers and Planners, Inc. for U.S. Department of Agriculture Agricultural Research Service, Beltsville, MD. Contract AG-3K06-B-06-0001. July, 2017, 268 pp.

Busch-Harris, Jennifer, Kerry Sublette, Kenneth P Roberts, Carla Landrum, Aaron D Peacock, Greg Davis, and Dora Ogles. 2008. "Bio-traps coupled with molecular biological methods and stable isotope probing demonstrate the in situ biodegradation potential of MTBE and TBA in gasoline-contaminated aquifers." *Groundwater Monitoring & Remediation 28* 47-62.

Carignan, R. 1984. "Interstitial water sampling by dialysis: Methodological notes." *Limnology and Oceanography* 667-670.

Cervini-Silva, J, JE Kostka, RA Larson, JW Stucki, and J Wu. 2003. "Dehydrochlorination of 1,1,1-trichloroethane and pentachloroethane by microbially reduced ferruginous smectite." *Environmental Toxicology and Chemistry* 1046-1050.

Chapman, Steven W, and Beth L Parker. 2005. "Plume persistence due to aquitard back diffusion following dense nonaqueous phase liquid source removal or isolation." *Water Resources Research 41.*

Choy, Bruce, and Danny D Reible. 1999. *Diffusion models of environmental transport.* CRC Press.

Cozzarelli, Isabelle M, Janet S Herman, Mary Jo Baedecker, and Jeffrey M Fischer. 1999. "Geochemical heterogeneity of a gasoline-contaminated aquifer." *Journal of Contaminant Hydrology 40* 261-284.

Dietrich, Peter, James J Butler, and Klaus Faiß. 2008. "A rapid method for hydraulic profiling in unconsolidated formations." *Groundwater 46* 323-328.

Dragun, J. 1988. *The Soil Chemistry of Hazardous Materials.* Silver Spring, MD: Hazardous Materials Control Research Institute.

EPA. 1991. *Seminar Publication: Site Characterization for Subsurface Remediation.* Washington, DC: EPA.

Feehley, C Erin, Chunmiao Zheng, and Fred J Molz. 2000. "A dual-domain mass transfer appraoch for modeling solute transport in heterogenous aquifers: Application to the Macrodispersion Experiment (MADE) site." *Water Resources Research 36* 2501-25115.

Ghiorse, WC, and DL Balkwill. 1983. "Enumeration and morphological characterization of bacteria indigenous to subsurface environments." *Developments in Industrial Microbiology 24* 213-224.

Haggerty, Roy, Charles F Harvey, Claudius Frieherr von Schwerin, and Lucy C Meigs. 2004. "What controls the apparent timescale of solute mass transfer in aquifers and soils? A comparison of experimental results." *Water Resources Research 40.*

Harper, MP, W Davison, and W Tych. 1997. "Temporal spatial and resolution constraints for in situ sampling devices using diffusion equilibration; Dialysis and DET." *Environmental Science & Technology 41* 3110-3119.

Hesslein, RH. 1976. "An in situ sampler for close interval pore water studies." *Limnology and Oceanography* 912-914.

Kunu, D, and M Suzuki. 1967. *Int J Heat Mass Transfer.*

Liu, Chongxuan, and William P Ball. 2002. "Back diffusion of chlorinated solvent contaminants from a natural aquitard to a remediated aquifer under well-controlled field conditions: Predictions and measurements." *Ground Water 40* 175-184.

Martin, Holger. 1978. "Low Peclet number particle-to-fluid heat and mass transfer in packed beds." *Chemical Engineering Science 33* 913-919.

Millington, RJ, and JP Quirk. 1961. "Permeability of porous solids." *Transactions of the Faraday Society 57* 1200-1207.

Musslewhite, Chris L, Don Swift, Johnnie Gilpen, and Michael J McInerney. 2007. "Spatial variability of sulfate reduction in a shallow aquifer." *Environmental Microbiology 9* 2810-2819.

Nzengung, Valentine A, Reyna M Castillo, Will P Gates, and Gary L Mills. 2001. "Abiotic transformation of perchloroethylene in homogenous dithionite solution and in suspensions of dithionite-treated clay minerals." *Environmental Science & Technology 35* 2244-2251.

Ranz, WE, and WR Marshall. 1952. "Evaporation from drops." *Chemical Engineering Progress 48.3.*

Rexwinkel, G, ABM Heesink, and WPM Van Swaaij. 1997. "Mass transfer in packed beds at low Peclet numbers--wrong experiments or wrong interpretations?" *Chemical Engineering Science 52* 3995-4003.

Sale, Tom C, Julio A Zimbron, and David S Dandy. 2008. "Effects of reduced contaminant loading on downgradient water quality in an idealized two-layer granular porous media." *Journal of Contaminant Hydrology 102* 72-85.

Schanzle, D. 2018. Using Chlorinated Ethenes as a Groundwater Tracer: A Field Experiment. Presented at Environmental Monitoring and Data Quality Workshop, April 2018, Orlando, FL.

Schneider, Haley A, W Andrew Jackson, Ken Rainwater, Danny Reible, Stephen Morse, Paul B Hatzinger, and Uriel Garza-Rubalcava. 2019. "Estimation of Interstitial Velocity Using a Direct Drive High Resolution Passive Profiler." *Groundwater 57* 915-924.

Stucki, JW. 2006. "Properties and Behavior of Iron in Clay Minerals." In *Developments in Clay Science, Vol 1, Handbook of Clay Science*, by F Bergaya, BKG Theng and G Lagaly, 423-475. Elsevier.

Vroblesky, DA. 2001. *User's Guide for Polyethylene-Based Passive Diffusion Bag Samplers to Obtain Volatile Organic Compound Concentrations in Wells, Part 1: Deployment, Recovery, Data Interpretation, and Quality Control and Assurance.* United States Geological Survey.

Webster, Ian T, Peter R Teasdale, and Nicola J Grigg. 1998. "Theoretical and experimental analysis of peeper equilibration dynamics." *Environmental Science & Technology 32* 1727-1733.

ZoBell, CE. 1946. *Marine Microbiology.* Waltham: Chronica Botanica Company.

8 APPENDICES

A. Supporting Data

None

B. List of Scientific/Technical Publications

Peer Reviewed Journals

1. Schneider, H., W.A. Jackson*, K. Rainwater, D. Reible, S. Morse, P. Hatzinger, U. Rubalcava. (2019) Estimation of Interstitial Velocity Using a Direct Drive High Resolution Passive Profiler. *Groundwate*r. 57:6 915-924
2. Schneider, H.*, W.A. Jackson, S. Morse, P. Hatzinger, and Shaeffer, C. (In Review) High-Resolution Characterization of a Chlorinated Solvent Impacted Aquifer Using a Passive Profiler. Submitted to Groundwater Monitoring and Remediation
3. Rubalcava, U., P. Hatzinger, and W.A. Jackson*. (In preparation) Using High Resolution Passive Sampling to evaluate the efficacy of a biowall treating a groundwater plume.

Conference Abstracts

1. Jackson, W.A., Garza-Rubalcava, U., Hatzinger, P., Lavorgna, G., and Schanzle, D. (2020) High Resolution Passive Sampling to Characterize Heterogenous Chlorinated Solvent Sites. *Battelle Twelth International Conference on Remediation of Chlorinated and Recalcitrant Compounds. Portland, Oregon.*

2. W.A. Jackson, Schneider, H., Hatzinger, P. B., Morse, S, Reible, D. and U. Rubalcava. Spatially Discrete Passive Samplers to Evaluate Contaminant Transport, Fate, and Impacts in Dynamic Systems. *Environmental Monitoring and Data Quality Workshop; 2018 April 11; Orlando, Fl. 4-19-2017.*
3. Jackson, W. A., Hatzinger, P. B., Reible, D. D., Schneider, H. High Resolution Delineation of Chlorinated Solvent Concentrations, Biogeochemical Processes, and Microbial Communities in Saturated Subsurface Environments. In *Battelle Eleventh International Conference on Remediation of Chlorinated and Recalcitrant Compounds; 2018 April 8-12; Palm Springs, California. Abstract H3-321. 4-11-2018.*
4. Jackson, W. A. High Resolution Delineation of Chlorinated Solvent Concentrations, Biogeochemical Processes, and Microbial Communities in Saturated Subsurface Environments. In *Battelle Fourth International Symposium on Bioremediation and Sustainable Environmental Technologies; 2017 May 22-25; Miami, Florida. Abstract C5-269. 5-24-2017.*
5. W. Andrew Jackson, H. Schneider, B. Rao, and D. Reible. The Use of Spatially Discrete Passive Sampler to Simultaneously Evaluate Contaminant Transport and Impacts of Biogeochemical Processes in Dynamic Systems. University Consortium for Field-Focused Groundwater Contaminant Research 2017. University of Guelph
6. *W. Andrew Jackson. High Resolution Delineation of Chlorinated Solvent Concentrations, Biogeochemical Processes, and Microbial Communities in Saturated Subsurface, SERDP-ESTCP Webinar May 2017

7. Schneider[s], H., Hatzinger, P. B., Jackson, W. A. High Resolution Delineation of Chlorinated Solvent Concentrations, Biogeochemical Processes, and Microbial Communities in Saturated Subsurface Environments. In *Environmental Monitoring and Data Quality Workshop; 2017 April 18-20; Phoenix, Arizona. Session 3: SERDP-ESTCP. 4-19-2017.*
8. Schneider, H[s]., Jackson, W. A., Hatzinger, P. B., Koster van Groos, P. G., High Resolution Delineation of Chlorinated Solvent Concentrations, Biogeochemical Processes, and Microbial Communities in Saturated Subsurface Environments. In Battelle Tenth International Conference on Remediation of Chlorinated and Recalcitrant Compounds; 2016 May 22-26; Palm Springs, California. Abstract G3-352. 5-24-2016
9. *W. Andrew Jackson, Haley Schneider, and Stephen Morse. (2016) High Resolution Delineation of Chlorinated Solvent Concentrations, Biogeochemical Processes, and Microbial Communities in Saturated Subsurface Environments. Environmental Monitoring and Data Quality Workshop. St Louis MS.